CANMET

Canada Centre for
Mineral and Energy
Technology

Centre canadien de la
technologie des
minéraux et de l'énergie

**Efficiency
and Alternative
Energy
Technology
Branch**

**Direction de la
technologie de
l'efficacité énergétique
et des énergies
de remplacement**

Energy, Mines and
Resources Canada

Énergie, Mines et
Ressources Canada

Canada

THE ENERGY OF OUR RESOURCES - THE POWER OF OUR IDEAS

L'ENERGIE DE NOS RESSOURCES - NOTRE FORCE CREATRICE

ELECTROCHROMIC MATERIALS AND DEVICES FOR SWITCHABLE WINDOW APPLICATIONS

PREPARED FOR:

Efficiency and Alternative Energy Technology Branch
Energy, Mines and Resources Canada
Ottawa, Ont.
DSS Contract No. 23283-8-6052/01-SZ
May, 1990

PREPARED BY:

University of Moncton
Moncton, New Brunswick
E1A 3E9

SCIENTIFIC AUTHORITY:

Joel Allarie
Efficiency and Alternative Energy Technology Branch
Energy, Mines and Resources Canada
580 Booth Street
Ottawa, Ont.
K1A 0E4

160 pp

MICROMEDIA

91-01238/

CITATION

Truong, V., P.V. Ashrit, G. Bader and F.E. Girouard, University of Moncton. Electrochromic Materials and Devices for Switchable Window Applications. DSS Contract No. 23283-8-6052/01-SZ. Efficiency and Alternative Energy Technology Branch, Energy, Mines and Resources Canada, Ottawa, Ontario. 1990 (143 pp.)

Copies of this report may be obtained through the following:

Efficiency and Alternative Energy Technology Branch
CANMET
Energy, Mines and Resources Canada
580 Booth Street, 7th Floor
Ottawa, Ont.
K1A 0E4

or

Document Delivery Service
Library and Documentation Services Division
CANMET
Energy, Mines and Resources Canada
562 Booth Street
Ottawa, Ont.
K1A 0G1

DISCLAIMER

This report is distributed for informational purposes and does not necessarily reflect the views of the Government of Canada nor constitute any endorsement of any commercial product or person. Neither Canada nor its ministries, officers, employees or agents makes any warranty in respect of this report or assumes any liability arising out of this report.

© Minister of Supply & Services Canada 1990
Catalogue No. M91-7/97-1990E
ISBN. 0-662-18035-6

ACKNOWLEDGMENTS

The authors of the report acknowledge the support and encouragement of Energy, Mines and Resources during the whole duration of this contract work. In particular, we are grateful to Tim Mayo and Joel Allarie for their positive approach to the conducting of this work.

We would like also to express our deep appreciation to Dr. Simona Badilescu for her contribution in the water content study of WO_3 and to Mrs. Suzie Paulin of Ecole Polytechnique de Montréal for her help in the XPS study.

ABSTRACT

The present report lays a basis for developing electrochromic (EC) materials and devices for switchable window (SW) applications. First, there are the tools for studying the individual layers composing the system and the final EC system. Structure, composition as well as water content studies are necessary to obtain accurate information regarding the EC materials. The most interesting final properties are the optical properties (transmittance and reflectance characteristics in the visible and near infra-red) and the electrical properties (electronic and ionic conductivities). In particular, the optical constants of materials can be derived in a very accurate manner by an original method based on the simultaneous angular scanning of reflectance and transmittance. The stringent condition requiring all components of the EC device to be optically transmissive is addressed in detail, and the numerous potential material candidates are listed. Some ways of designing new EC materials are also discussed. Finally a device prototype has been thoroughly studied, showing very promising characteristics for SW application. This prototype is an all-solid-state system, operating with WO_3 as the EC material and lithium borate as the ionic conductor for lithium ions. An original method is proposed for storing ions in the counter electrode.

RÉSUMÉ

Le présent rapport jette les bases du développement de matériaux et de dispositifs électrochromes pouvant s'appliquer aux fenêtres commutables. Le rapport traite d'abord des outils servant à étudier chacune des couches qui forment le système ainsi que le système électrochrome lui-même. Des études sur la structure, la composition et la teneur en eau sont nécessaires pour obtenir des renseignements précis sur les matériaux électrochrome. Les propriétés les plus intéressantes du produit fini sont les propriétés optiques (caractéristiques de transmittance et de réflectance dans le spectre visible et près de l'infra-rouge) et les propriétés électriques (conductivités électronique et ionique). Notamment, les constantes optiques des matériaux peuvent être calculées d'une manière très précise grâce à une nouvelle méthode basée sur le balayage angulaire simultané de la réflectance et de la transmittance. Le rapport traite en détail de la condition qui veut que tous les composants du dispositif électrochrome soient optotransmetteurs et énumère les différents matériaux potentiels. Il est aussi question de différentes façons de concevoir les nouveaux matériaux électrochromes. Le rapport traite enfin d'une étude approfondie d'une prototype du dispositif qui a permis de faire ressortir des caractéristiques très prometteuses pour application aux fenêtres commutables. Ce prototype est un système à semiconducteurs fonctionnant avec du WO_3 comme matériaux électrochrome et du borate de lithium comme conducteur pour les ions de lithium. Une

méthode innovatrice est aussi proposée pour emmagasiner les ions dans une contre électrode.

CONTENTS

1. Introduction.. 1

2. Organization of this report.......................... 6

3. Electrochromic materials and devices................. 8
    - 3.1 EC materials.................................. 8
    - 3.2 EC devices.................................... 9
    - 3.3 General requirements for SWs.................. 11
    - 3.4 The transparent electrode..................... 12

4. Structure and composition studies.................... 14
    - 4.1 Structure studies............................. 14
    - 4.2 Composition studies........................... 20

5. Water adsorption behaviour of WO_3 thin films........... 22
    - 5.1 Experimental.................................. 23
    - 5.2 Results and discussions....................... 25
    - 5.3 Conclusion.................................... 37

6. Determination of the optical constants............... 38
    - 6.1 Theoretical formulaes and methods............. 39
    - 6.2 Experimental procedure........................ 42

7. Properties of the electrochromic (WO_y) layer........... 46
    - 7.1 Optical and electrical properties of WO_y..... 46
    - 7.2 Lithiation of WO_3 samples.................... 51
        - 7.2.1 High density coloration of WO_3........ 51
        - 7.2.2 Vacuum lithiation of WO_3.............. 54
    - 7.3 Optical and electrochromic properties of Au:WO_3, Ag:WO_3 and S_n:WO_3 cermets......... 58

8. Inorganic ion conductors............................. 84
    - 8.1 General consideration......................... 85
    - 8.2 H^+ ion conductors.............................. 88
    - 8.3 Li^+ ion conductors............................. 92
    - 8.4 Potassium and sodium ion conductors........... 97
    - 8.5 Silver ion conductors......................... 99
    - 8.6 Fluorine ion conductors....................... 99
    - 8.7 Conclusion.................................... 101

9. Ion conducting and ion storage layers and the prototype EC system.................................. 103
    - 9.1 Ionic conductors.............................. 103
    - 9.2 Counter electrode (CE) or ion storage......... 108
    - 9.3 All-solid-state prototype EC system and performance characteristics............. 117

10. Concluding remarks.................................. 129

Appendix

References

1. INTRODUCTION

Smart windows? Switchable glass? These terms are perhaps not well-known to the public but there exist now intense activities going on around the world to make them a reality. When we look at buildings, atria covered by large areas of glass windows, we cannot prevent ourselves from wondering about the large amount of radiating energy going in and out of those transparent panels. First, there is the sun that sends us its rays, from the ultraviolet (high-energy radiation) to the infrared (low-energy radiation) and then, there is also the radiation (infrared) coming from objects or persons inside the buildings. If this latter radiation was totally reflected by the glass, preventing it from being "leaked" to the outside, we would have the perfect "greenhouse effect", and energy losses by radiation would be practically nil.

But can we maximize, reduce or eliminate this greenhouse effect according to our needs? Can we have the options of letting sunlight going through or blocking it with the same windows? Those questions have been asked for some time by people working in the building industry and now, a number of researchers from different backgrounds are trying to produce those windows, or those "smart windows", as first coined by a Swedish research team. A more modest term to describe them is "switchable windows" because in the present devices, light transmission through the window can be controlled by the simple flick of a switch. With both terms however, the abbreviation SW is equally applicable.

There are of course conventional options such as mechanical blinds installed near the glass windows but they are not the best ones, due to problems related to energy control efficiency, maintenance and aesthetic considerations. The SWs being developed now in many laboratories are primarily based on electrochromic materials, or materials that change color upon application of a low electric field. Liquid crystals are also used and large area blinds are presently produced commercially by a few companies.

The first area of application obviously is related to the controlling of glare and light transmission for comfort and privacy purposes. Any window in houses or buildings in principle can have a switchable glazing incorporated in order to control light transmission (doors, skylights, sloped glazings...). The SWs however become more attractive when we consider their potential in energy management for houses and buildings. With their adjustable optical properties, one can effectively use incident solar radiation for heating and lighting, thus reducing the net energy consumption in buildings, especially in winter time. When the climate is warm, the cooling load can be substantially reduced if incident solar radiation is rejected instead. According to many building research studies[1-3], the use of properly designed switchable windows would indeed constitute the best strategy for saving energy. The amount of savings of course will vary with different seasons. A recent study[4] by Lawrence Berkeley Laboratory has also pointed out that other benefits include large savings in cooling equipment, with a cost savings that may offset the added cost of glazing and the daylighting control system. The use of switchable windows can moreover contribute to reducing peak electric demand connected with cooling loads.

As SWs are still in the development stage, it is difficult to establish exactly how they cost when they will be actually produced in a high volume. Cost studies have however been performed by groups at SERI (Solar Energy Research Institute/USA) and EIC Laboratories (USA) and the cost to produce electrochromic switchable glass would be in a range of $ 1.90 to $4.40 per square foot (1989 figures). The general conclusion is that as compared to other options, these SWs are economically attractive.

It is precisely this potential of realizing energy management with SWs that has revived interest in electrochromic materials in the early 80's. Before that time, different laboratories were interested in those materials mostly for application in display device technology[5]. Research on displays in many groups was however discontinued in the late 70's because electrochromic materials could not provide fast response times necessary for display application, and because liquid crystals were a more viable alternative. As response time is no longer an issue in energy management application (response times up to 300s can be easily tolerated), electrochromic materials have become very attractive. Their optical properties, among other qualities, are superior to those of many other materials, including liquid crystals[5].

Research and development of SWs are performed in many countries. In the US, the Solar Energy Research Institute, EIC Laboratories, the Lawrence Berkeley Laboratory and Tufts University are the driving forces. In Japan many research projects are conducted at Asahi Glass and Nissan Glass. Asahi Glass, for example, have already installed large windows in a museum for demonstration purpose. Windows having dimensions as large as 0,8 x 0.4 m have been tested in laboratories but according to Asahi representatives, very soon 30 x 30 cm windows will be commercially available. These windows are based on injection of lithium ions and the ion conductor used is a laminated polymer layer. Many European groups are also involved, among them Chalmers University of Technology (Sweden), the Imperial College of Science and Technology (Great Britain) and the Academy of Mining and Metallurgy (Poland). In Canada there are at least 5 groups which have done work on EC systems. A group at the former Ontario Research Foundation has developed a solid state optical shutter using crystalline WO_3 (Ref. 6). In Quebec, L'Institut National de la Recherche Scientifique (INRS) is currently working on relatively large windows (30 x 30 cm) made with organic materials[7,8]. A group at Simon Fraser University has prepared thin films of WO_3 by pyrolytic spray deposition, a simple and inexpensive way to produce large area electrochromic devices[9]. A researcher at Guelph University is developing new polymeric ion conductors which can be used in switchable window fabrication[10]. At l'Université de Moncton, the Thin Films Research Group has been working on all-solid-state devices based either on protons or lithium ions[11,12]. Recent results are the basis of this report.

As mentioned earlier, beside electrochromic materials, liquid crystals are also used to fabricate large area blinds[13]. Those blinds can for example prevent people from outside to view through some retail displays, for security reasons as well as for the simple purpose of attracting attention, when the blinds are switched back and forth from the transparent to the opaque states. The blinds can also be used for instant privacy, as recently advertised by a company in Ontario (Haworth Office Systems, Ltd). Thus partitions in office areas, conference rooms, stores can effectively have these liquid crystal blinds incorporated. These blends consist of a coated plastic film sandwiched between two glass panels and they will become transparent when low-voltage electricity is applied. When the power is turned off, it returns to the original state which is opaque. Compared to electrochromic materials, however, liquid crystals are less attractive as SW. Preliminary testing done at our laboratories with commercial samples, along with measurements done by a number of participants in Task X of the International Energy Agency, have shown that only small changes occur in the solar transmittance between the bleached and colored states, thus making liquid crystals samples not yet proper for energy management purposes.

2. ORGANIZATION OF THIS REPORT

This report, after a brief introduction to electrochromic (EC) materials (section 3), is focussed on two main divisions, one dealing with the intrinsic properties of the components of the SW and the tools that are used for their studies, and another presenting the performance of all-solid-state devices fabricated in our laboratories.

The structures and composition influence very much the properties of EC materials. They are discussed in section 4 and the characteristics of the film studied are presented, following electron microscopy work and XPS analysis. As the water content of WO_3 films also can affect strongly their behavior, a method for determining this content is presented in section 5 and applied to the analysis of the EC films.

Measurements of the optical properties of individual layers in a device configuration often are problematic and section 6 presents a method for doing so. An automatic reflection and transmission goniometer has been constructed and determination of the optical constants can be performed in a very satisfactory way, giving for example characteristics of ion conductors used in device fabrication.

Section 7 deals with the electro-optical characteristics of the main EC material used in our devices, i.e. WO_3. When the material is doped with metals such as Au, Ag and Sn, it can show interesting optical properties. The modification of WO_3 behavior by doping can be used in device fabrication, depending on the characteristics and performance sought for the SWs.

As the ionic conductors in SWs are the less researched materials until now, there is a special section (section 8) devoted to a general discussion on this crucial component of SWs. For transmissive devices, the ionic conductors have to be conducting for ions and should also be a transparent material. These two characteristics normally do not go hand in hand and a general discussion is needed in order to choose the proper materials for SWs fabrication.

In section 9 are presented the characteristics and performance of the most promising all-solid-state devices that were fabricated in our laboratory. A discussion on their qualities and shortcoming is made.

Finally, section 10 gives the concluding remarks of the report.

3. ELECTROCHROMIC MATERIALS AND DEVICES

3.1 EC materials

Review of EC materials and devices have been made by a number of authors[5,14,15]. The materials can be classified in three categories: the inorganic EC materials, the organic and the intercalated ones. The optical properties of the intercalated materials are not proper for transmission devices and therefore, the intercalated materials do not represent an interesting class for window applications. The organic materials, such as viologens, diphthalocyanines complexes and anthraquinoids, are not the objects of the present study. Their merits in SWs application have been discussed in previous works but in general, organic materials require liquid electrolytes for operation and they may present thermal degradation and freezing problems. The durability of the edge-sealing for organic devices and environmental problems associated with leaking of the devices may be serious issues to deal with.

The inorganic EC materials can be divided into two main categories: the anodic EC materials (e.g., iridium oxide, nickel oxide) and the cathodic EC materials (e.g., tungsten oxide, molybdenum oxide, vanadium oxide). Amongst these, WO_3 is largely recognized as the leading candidate for EC devices, due mostly to the easiness of preparation by different methods, the availability and relative low cost of the material and very good reproducible optical properties. The material, upon injection of positive ions (such as H^+, Li^+, Na^+) will become a bronze which exhibits radically different optical properties from WO_3. The generalized ion-insertion EC mechanism for cathodic materials is written as:

$$AB_n + xC^{m+} + mxe^- = C_x\,AB_n$$

where AB_n (e.g. WO_3) and $C_x\,AB_n$ (e.g. $H_x\,WO_3$) have totally different optical characteristics, m is a small positive integer and x generally comprised between 0 and 1.

Another most promising cathodic material is molybdenum oxide, due to qualities similar to the ones cited for WO_3. The study of molybdenum oxide is however outside the scope of the present work.

3.2 EC devices

To allow transport of the involved charges, EC materials must be conductive both for ions and electrons. An EC device may have the following configuration:

TC/ EC/ FIC/ CE/ TC

where TC represents a transparent conductor used as an electrode, EC is the electrochromic material, FIC is the fast ion conductor, and a CE is the counterelectrode.

In this configuration, CE, which must be a mixed ionic and electronic conductor, acts as an ion storage medium during the erase cycle (bleaching cycle). For cathodic EC materials, during the coloration cycle, positive ions go from CE to the FIC/ EC interface. The reverse evolution is observed in the bleaching process.

The above configuration is by no means the only possiblity.

An earlier version of EC device is the so-called water-dependent devices which has the following configuration:

TC/ EC/ Oxide layer/ Au electrode

with the oxide layer being mostly SiO_x (Ref. 16) or Ta_2O_5 (Ref. 17). Some other designs used solid electrolytes such as LiF (Refs. 12,18) or MgF_2 (Ref. 19). The main drawback of this type of device is its dependence upon ambiant humidity. Unless there is a way to eliminate this dependence, the device does not present a good potential for SWs application.

A most interesting device is the so-called complimentary type device. It consists of:

TC/ First EC/ Electrolyte/ Second EC/ TC

with one of the EC material being colored by reduction and the other by oxidation.

In principle, no component in such a device is consumed during its use. The so-called trapped-water device is a particular case of the complimentary type. An example is given by[20]

TC/ WO_3/ Cr_2O_3/ TC

In the above device, the water is believed to be tightly trapped by Cr_2O_3. In such a case, not only WO_3 (cathodic EC material) experiences a color change, but Cr_2O_3, an anodic EC material, also changes color when a voltage is applied. The water molecule inside the device, upon application of a voltage, dissociates into H^+ and OH^- driven respectively to WO_3 and Cr_2O_3. These ions then serve to color the EC materials. When a bleaching voltage is applied, OH^- and H^+ are driven back to the WO_3/ Cr_2O_3 interface to recombine into H_2O.

Another example of complimentary type device is[21]

$TC/\ WO_3/\ Ta_2O_5/\ IrO_x/\ TC$

where IrO_x is the anodic EC material. The main drawback of such a device is the high cost of IrO_x.

When a film acts both as an EC material and a solid electrolyte as in the case of phosphotungestic (PWA) and phosphomobybdic (PMA) acids[22], the device configuration becomes much simpler:

TC/ PWA or PMA/ CE

Each type of device has its merits and inconvenience, depending on the availability, stability and suitability of the device components.

3.3 General requirements for SWs

In order to be efficient in energy management of buildings there are a number of requirements to be met by SWs. When SWs are only used for glare control the requirements differ. Those different characteristics are shown in Table 3-1, following a work by Lampert (1988) for Task 10 of the International Energy Agency.

The characteristics listed in Table 3.1 reflect the overall performance of the EC device. T_s denotes the solar transmission, T_p the photopic transmission and R_{nir} the reflection in the near infrared spectrum. Besides the EC materials, it is important that components such as the transparent electrode (TC) and the fast-ion-conductor (FIC) discussed earlier exhibit fairly high transmission properties without losing their required electrical properties.

Table 3.1 Performance criteria for SWs

SPECTRAL RESPONSE	T_s (Bleached) = 50-70%
Solar Control	T_s (Colored) = 10-20%
Visible Control	T_p (Bleached) = 50-70%
	T_p (Colored) = < 10-20%
NEAR-IR CONTROL	R_{nir} (Bleached) = 10-20%
(reflective device)	R_{nir} (Colored) = > 70%
SWITCHING VOLTAGE	1-3 Volts (Small Device) 10-24 Volts (Large Device)
MEMORY	1-12 Hours
CYCLIC LIFETIME	> 10K-1M Cycles
LIFETIME	5-20 Years
OPERATING TEMPERATURE	-30 to 70°C 0-70°C, If Protected

3.4 The transparent electrode

The most commonly used transparent electrode is indium-tin-oxide (ITO) which has a high visible transmission and a low resistivity of the order of 2×10^{-4} Ω -cm. ITO can be prepared in different ways, either by evaporation from an oxide source or by sputtering[23]. They can also be prepared by electron enhanced ion plating based on electron-beam evaporation, chemical vapor deposition and oxidation of an In metal film[24]. An exhaustive review of ITO properties was made by Hamburg and Granqvist[25], giving extensive details on film preparation techniques and conditions.

A recent work by Nanto et al.[26] has established that with the rf magnetron sputtering technique, the use of a 95 wt.% In_2O_3 -5 wt.% SnO_2 target leads to ITO films with low resistivity. Such films in effect exhibit a resistivity as low as 2×10^{-4} Ω-cm and a transmittance above 85% in the visible spectral region. This is precisely the method which has been used for preparing our ITO films.

Other materials that can serve as TC include tin oxide, doped tin oxide, ZnO (Ref. 27) and $CdIn_2O_4$ (Ref. 28). Semi-transparent Au films are also used, mostly for research purpose and as the top electrode of the device.

4. STRUCTURE AND COMPOSITION STUDIES

The behavior of electrochromic materials depend very much on their microstructure and composition. Many studies for example, have established that porous films of amorphous WO_3 seemed to exhibit better coloration characteristics than well-packed films. We have thus used the replica technique to observe the surface of WO_3 deposited either on ITO-coated glasses or on plain glass (BK7) slides to see whether the type of substrate would influence the film's micro-structure. Composition studies also have been carried out in order to establish the elements forming the electrochromic film used in our devices. All the films studied in this section were formed by thermal evaporation (at the rate of 0.2-0.4 nm/s) on substrates maintained at 200°C and in a vacuum of 10^{-5} torr.

4.1 Structure studies

The replica technique with a transmission electron microscope (Hitachi EMV-IIC model) was the method used for inspecting WO_3 surfaces. The description of this technique can be found in standard litterature on electron microscopy (see for example, Guenther and Pulker[29]). The WO_3 film thickness was varied from 100 nm to 500 nm, i.e. in the range of thickness used for device fabrication.

Fig. 4.1 shows the WO_3 surface for films of different thicknesses deposited on ITO-coated glasses as supplied by Donnelly Corporation. As the thickness increases from 100 to 300 nm, the

Figure 4.1

Electron micrographs of WO_3 film surfaces

(a) thickness = 100 nm

(b) thickness = 200 nm

(c) thickness = 300 nm

(d) thickness = 400 nm

(e) thickness = 500 nm

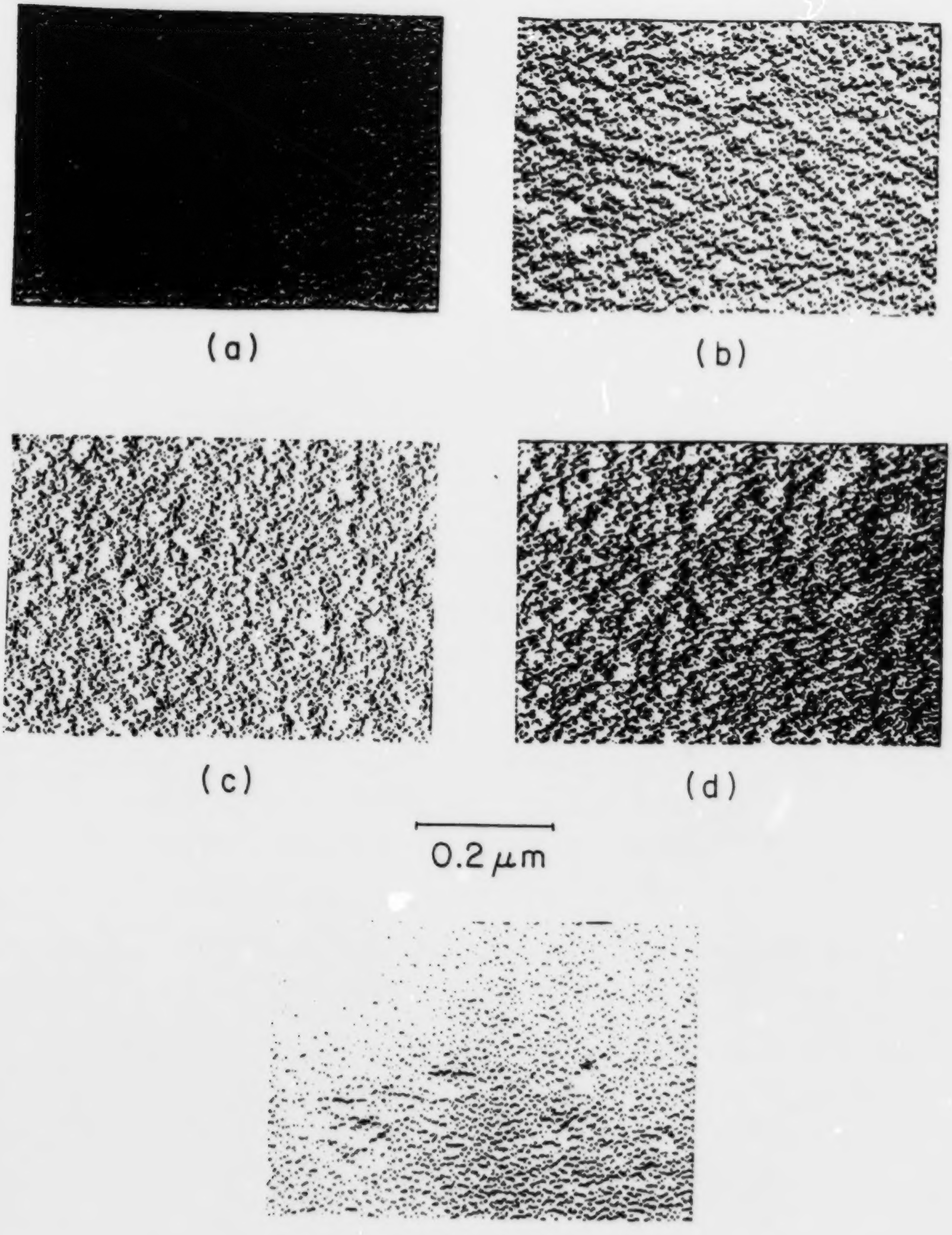
(a)
(b)
(c)
(d)
0.2 μm
(e)

trend is toward rougher surfaces. At 100 nm, many of the grain sizes are of the order of 10 nm whereas at 300 nm thickness for example, the agglomerates are about 3 times larger. Interestingly, when the thickness was increased to 500 nm, the surface became smoother, but at certain spots there were larger imperfections. Basically, the same type of microstructure evolution with thickness was found with WO_3 deposited on a plain BK7 substrate (microscope slides have a rougher surface than ITO films). This was reflected somewhat in the microstructure of WO_3 films. The most striking differences were found between the 500 nm WO_3 film deposited on ITO-coated glass and the 500 nm film deposited on the plain microscope slide (Fig. 4.2). Imperfections in this latter film were larger in number and in size. Although the 300 nm WO_3 film deposited on a glass slide had a rougher surface, its microstructure was however more comparable to the one for the 300 nm film deposited on ITO-coated glass (See Fig. 4.2).

From observations of the WO_3 film surface, it appears that a film with a large thickness (i.e. thicker than 500 nm) may not present good coloration characteristics because of its well-packed structure. The overall uniformity of the substrate is however essential for preparing WO_3 films showing an acceptable uniformity over a large surface. Such a quality should be achieved for large-area devices or windows.

Figure 4.2

Electron micrographs of WO_3 film surfaces

(a) 300 nm film deposited on ITO-coated glass

(b) 300 nm film deposited on glass slide

(c) 500 nm film deposited on ITO-coated glass

(d) 500 nm film deposited on glass slide

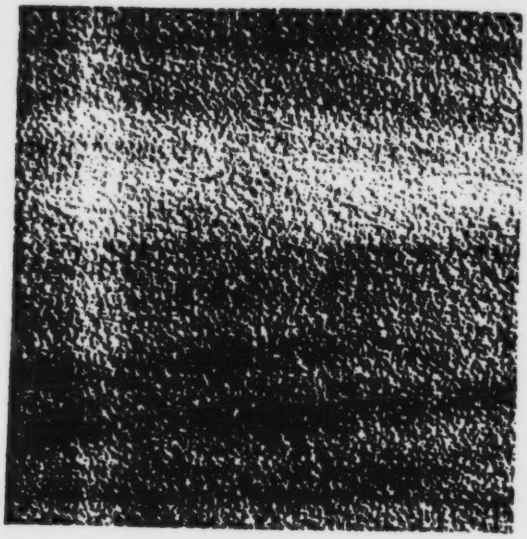

(a)

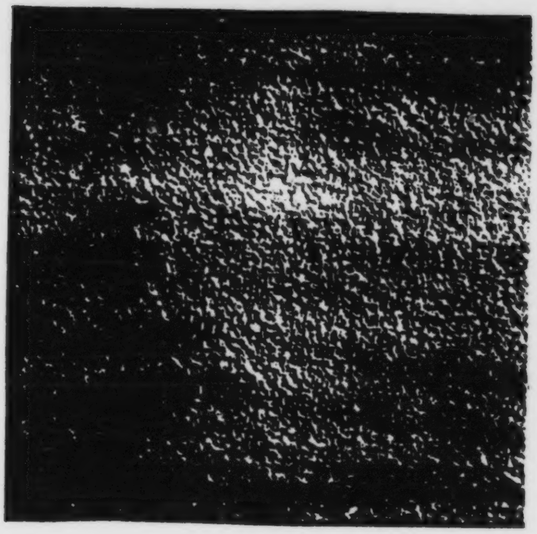

(b)

0.6 μm

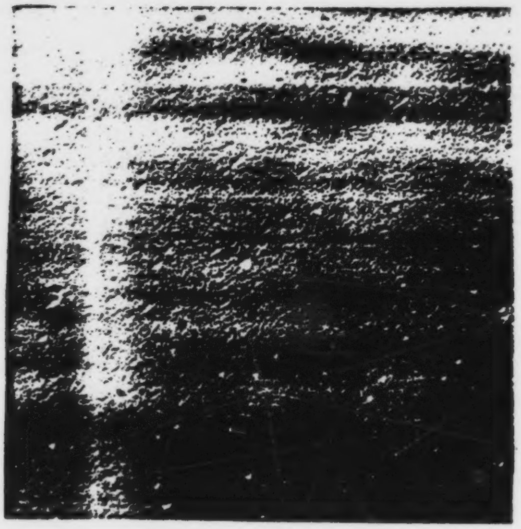

(c)

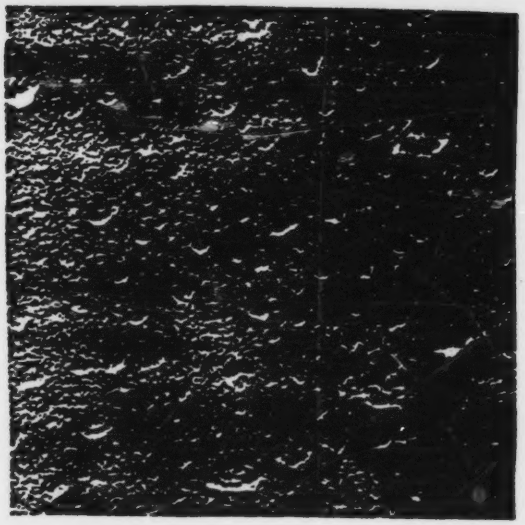

(d)

4.2 Composition studies

X-ray Photoelectron Spectroscopy (XPS), or Electron Spectroscopy for Chemical Analysis (ESCA), has been used for the determination of the chemical composition of samples used in our devices. Description of XPS can be found in many references (see for example, Martensson[30]). Samples of $W0_3$ thermally deposited have been characterized by this technique in the following manner.

A first quick scanning was made from 0 to -1000 eV (in binding energy), permitting the identification of the chemical elements that were present. A second spectrum at high resolution for each of the elements, i.e. C(-274 to -294 eV), 0(-521 to -541 eV) and W(-24 to -44 eV) was used to show the different chemical bonds and a third spectrum (curfit) served for analysis of different peaks for each element. Finally different parameters, i.e. the peak height and position, the full width at half maximum (FWHM) and the area under the curve, were derived and presented in a table. Also shown in the table is the ratio between the Gaussian and Lorentzian factors used to establish the peak shape.

The quick scanning spectrum showed the presence of C, N, O and W. The carbon high resolution spectrum presented 3 peaks: C - C bond at -284.9 eV, C-O bond at -286.5 eV and C-! bond at -288.8 eV. This latter peak was difficult to identify but it represented only 8% of the total carbon content. The oxygen high resolution spectrum had 3 peaks, the O-W bond at -533/eV. The tungsten high resolution spectrum on the other hand, showed 2 double peaks, respectively for W-0 bond ($W0_3$ bonding) at -35.64 eV and -37.75 eV and for W-0 bond ($W0_2$ bonding) at -34.10 and -35.97 eV.

The details of this composition studies are shown in Appendix I.

5. WATER ABSORPTION BEHAVIOR OF WO_3 THIN FILMS

Amorphous thin films of tungsten oxide have been shown to be of the form of $WO_{3-x}.yH_2O$ where x and y are dependent on the preparation conditions of the film[31]. The substrate temperature and the base pressure deposition are but some of the parameters that influence the structure and the hydration of the film[32,33]. The water concentration in the film may also be modified by exposing the film to atmospheres of different relative humidity[34].

The properties (electrical conductivity, optical density and rate of coloration) of an electrochromic system have been shown to be strongly influenced by the porosity and the water content of the amorphous WO_3 devices[18,35]. Although many investigators have recognized the importance of water content, only recently has the relationship between the structure and the EC properties of $WO_{3-x}.yH_2O$ been studied. Yoshiike and Kondo[36] pointed out that water absorbed in the material reacts with tungsten oxide, giving a hydroxylated film with a weak EC coloration as per the following reaction

$$\underset{\text{(transparent)}}{WO_{3-x}.yH_2O + xH^+ + xe} = \underset{\text{(colored)}}{WO_{3-x}(OH).yH_2O}$$

This dissolution initially improves the systems performance with respect to speed and optical density but its lifetime is also influenced by it.

Several techniques and models have been used to characterize the water concentration in such films. These include thermogravimetric and thermal differential analysis[37], IR absorption[31] and indirectly the Rutherford backscattering technique[39]. In this work the sensitivity of the attenuated total reflection (ATR) technique in the infrared[10] is investigated for the determination of water content in thin WO_3 films, and the technique is used to study the spectroscopic properties of these hydrated films. In the IR-ATR method, films are deposited on both sides of an IR transparent KRS-5 or ZnSe crystals. The multiple reflections (Fig. 5.1) from the dielectric coatings thus increases the sensitivity of the measurements. As in previous studies with IR-ATR, silver under and overlayers have been used with WO_3 thin films to enhance the sensitivity of the method.

5.1 Experimental

IR-ATR spectra of amorphous WO_3 films deposited on KRS-5 and ZnSe crystals were recorded on a Philips Pye Unicam SP3-200 spectrophotometer using a Model 300 ATR attachment (Barnes Analytical). These films were deposited by thermal evaporation on both sides of the crystal and the film thickness was monitored by quartz crystal method. A vacuum of 5×10^{-6} torr was maintained during deposition of the films and the composition of the gases present was analyzed by a mass analyzer. Films with different thicknesses ranging from 50 nm to 300 nm were deposited at various substrate temperatures. The deposition rate was maintained around 0.2nm/s. For the study of the effect of metal over-or-underlayers,

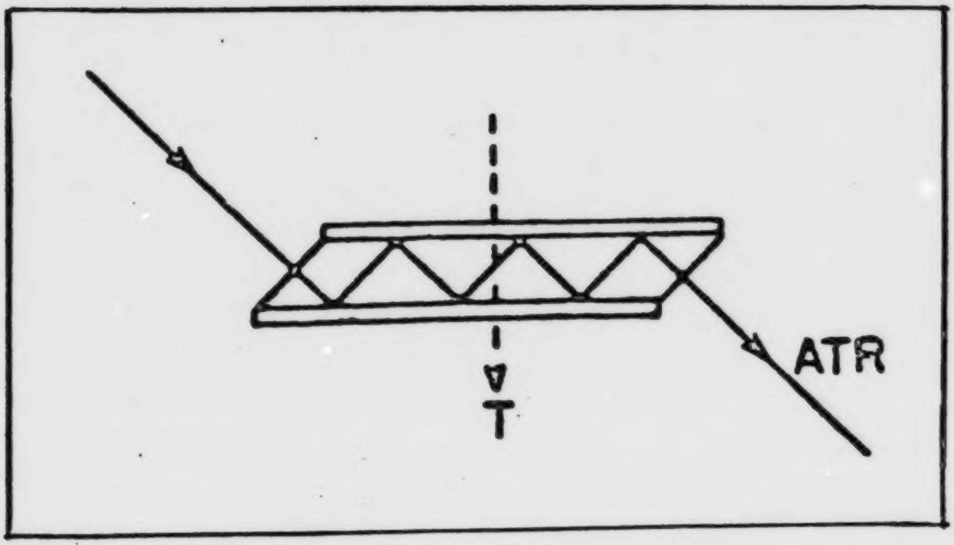

Fig. 5.1: Schematic diagram of attenuated total reflection (ATR) and transmission (T) modes of measurement with a KRS-5 crystal. The film under study is coated on both the sides of the crystal.

silver films of 2.5 nm were deposited before or after WO_3 coating.

The ATR crystals with the film were hydrated in an atmosphere of constant relative humidity (r.h) by keeping them in a glass dessicator. The constant r.h. was maintained by a saturated solution of an appropriate salt (ex. sodium nitrite for 66% r.h.). The volume percentage of water was calculated, as described in our previous work[40] with MgF_2 and Na_3AlF_6 films from the absorbance of the δ_{OH} band at 3400 cm^{-1} using the molar absorptivity ε of 69.6 x 10^3 cm^2/mole reported by Wyss and Falk[41]. Assuming Beer's law, the water concentration derived from absorbance data was converted into moles of water present in the total volume V_t . The volume V_{H_2O} occupied by the water molecules in the sample was expressed by

$$\frac{V_{H_2O}\,\%}{V_t} = \frac{100AM}{\varepsilon e}$$

where A is the measured absorbance, ε the molar absorptivity, M the molecular weight of water, and e the optical pathlength. The electrochromic coloration of these films on the crystal was achieved by proton injection using sulphuric acid (0.1N) and tin foil as a source of electrons. The EC coloration thus occurs without the application of any external potential[42].

5.2 Results and Discussion

In Figure 5.2 is given the water content dependence on the WO_3 film thickness, before and after hydration at a r.h. value of 66%. According to this figure, the volume percentage of water in the as

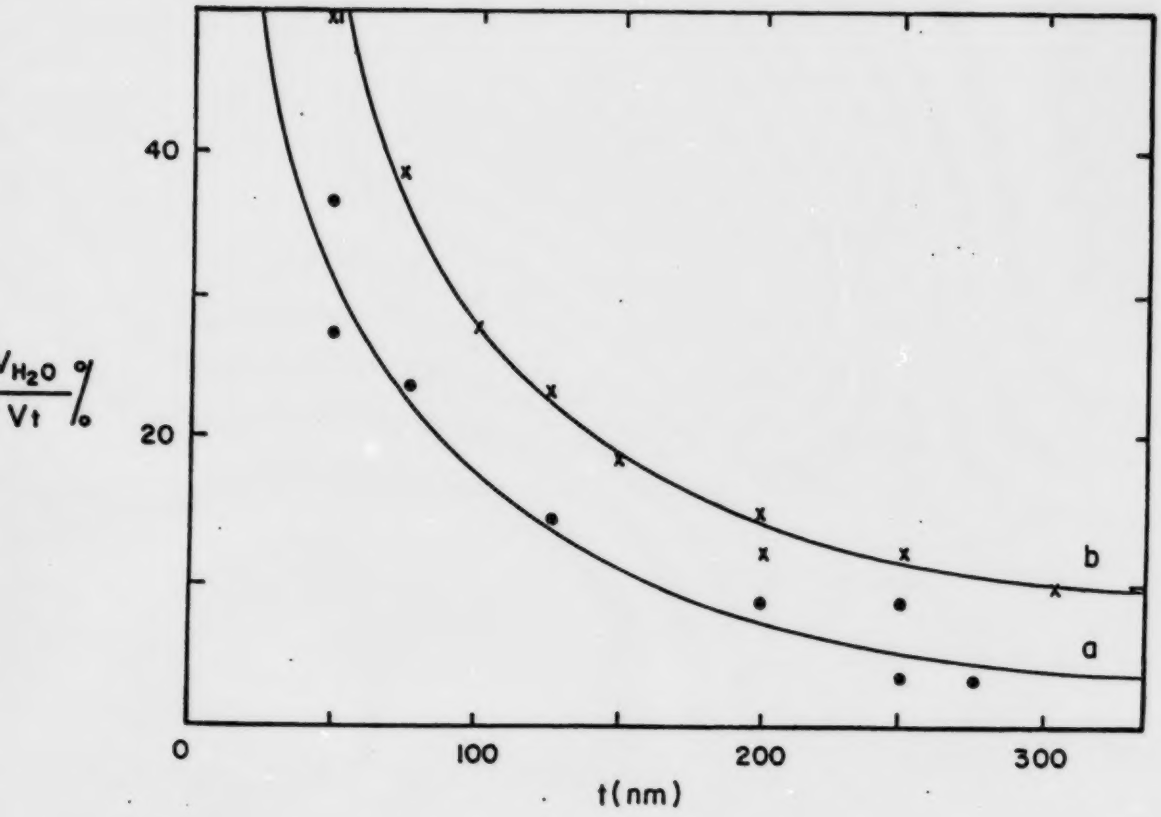

Fig. 5.2: Film thickness dependence of water content in tungsten oxide film, a) as deposited and b) after hydration at 66% r.h.

deposited WO_3 films decreases with increasing film thickness. The curve (a) falls from about 32% at 50 nm to 16% at 100 nm, and to 8% at 200 nm. This indicates that the actual amount of water in the films is almost the same at all the thicknesses studied. Representing this amount of water in terms of thickness, the water content through the thickness range studied corresponds to about 15 nm. Hence, it appears that all this water is present close to the crystal/film interface and is absorbed during deposition of the first 50 nm of film thickness. As the WO_3 film thickness increases, hardly any water is absorbed during deposition. The films might be highly porous at lower thickness and hence prone to large amounts of water absorption during deposition. This behavior is similar to our observations with cryolite films[40]. However, compared to cryolite films the amount of water present in WO_3 films is higher. Upon hydration in an atmosphere of 66% r.h. for a day the films show a higher water content at all the thicknesses studied (Fig. 5.2(b)). As per the report of Yoshiike and Kondo[36] the hydration of WO_3 films is complete within 24 hours.

Figure 5.3 shows the water concentration dependence on the substrate temperature during deposition for 50 nm thick WO_3 films, before and after hydration at 66% r.h. For films deposited at room temperature the water concentration is as high as 40% but decreases linearly with increase in the substrate temperature, (Fig 5.3(a)). For a substrate temperature of 300°C there seems to be hardly any water in the film. These films show a fixed increase in water concentration after hydration for all the substrate temperatures studied (Fig 5.2(b)). Our results in the case of

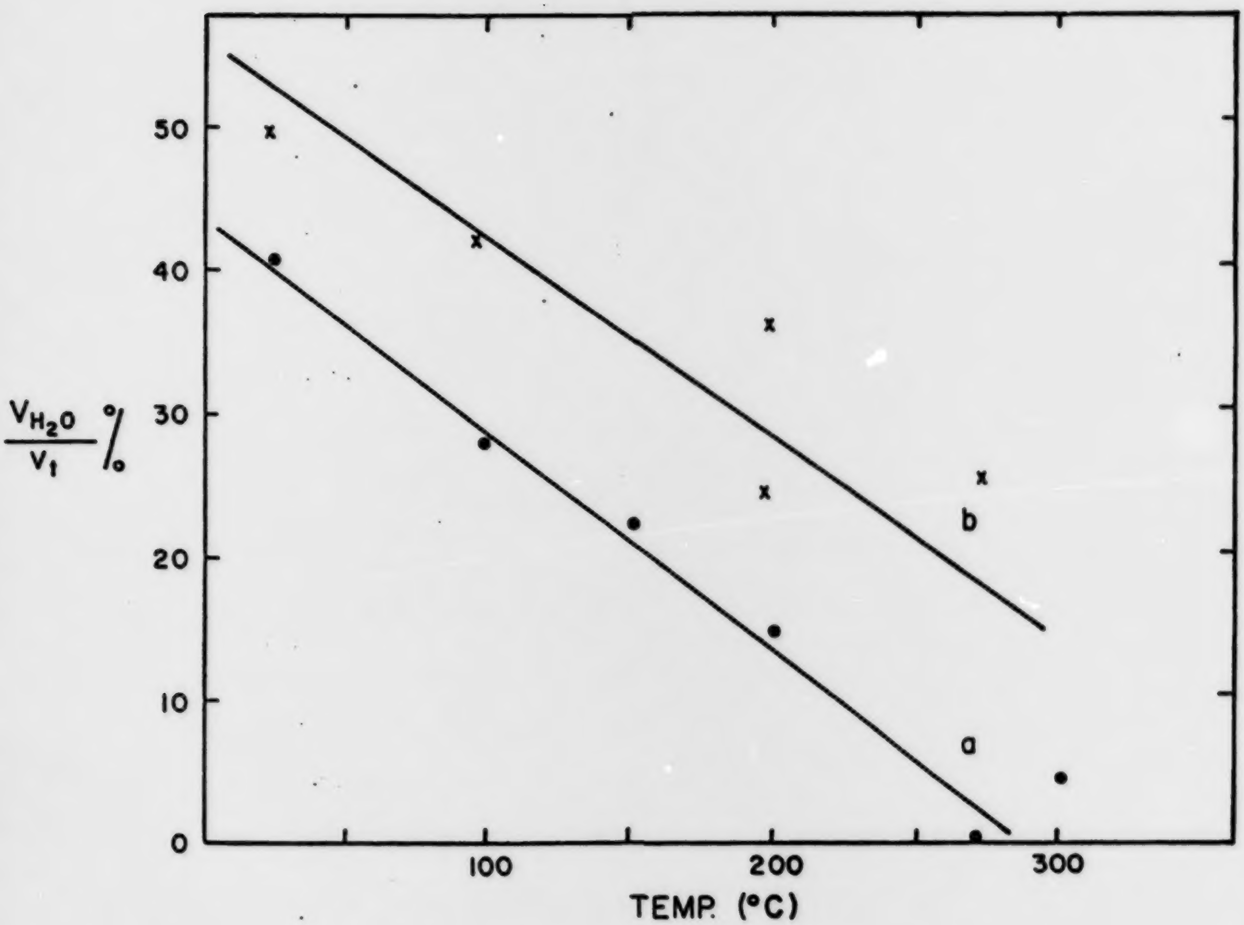

Fig. 5.3: Variation of water content with substrate temperature of a 50 nm-thick tungsten oxide film, a) as deposited and b) after hydration at 66% r.h.

hydrated films are scattered, perhaps due to some contribution from loosely bound water molecules at the samples' surfaces. The extent of this contribution however was not quantitatively estimated.

The ATR spectrum of a 50 nm WO_3 film deposited on a KRS-5 crystal at room temperature recorded immediately after deposition is shown in Fig. 5.4. In the high frequency region δ_{OH} stretching band of water molecules can be clearly seen as a broad band centered around 3400 cm^{-1}. The corresponding water bending band is present at 1600 cm^{-1}. The broad band beginning at 900 cm^{-1} corresponds to the different kinds of W-O stretching vibrations. Similar spectra of the 50 nm thick colored bronze (H_xWO_3) film is shown in Fig. 5.5, for different hydration conditions. For this film before hydration (Fig. 5.5(a)), the high frequency region corresponding to stretching vibrations of water molecules shows only a weak stretching (ν_{OH}) band corresponding to a water content of 15%. The weak band at 1630 cm^{-1} (δ_{OH}) is in agreement with this quite low amount of water. Comparing this with the spectrum of WO_3 (Fig. 5.4), it can be seen that in the case of the bronze film, in addition to the water bands, the spectrum shows a broad band centered around 1170 cm^{-1}, a narrow one at 1030 cm^{-1} and two shoulders at 930 and 870 cm^{-1}, respectively. Also most of these spectra display weak bands around 1430 cm^{-1} probably due to the first overtone of the strong ν_{W-O} stretching band.

When the crystal holding the blue tungsten bronze is kept in an atmosphere of 66%r.h., the volume percentage of absorbed water reaches 36% after 12 hours (Fig. 5.5(b)) and 50% after 36 hours (Fig. 5.5(c)). At the same time, the coloration of the film

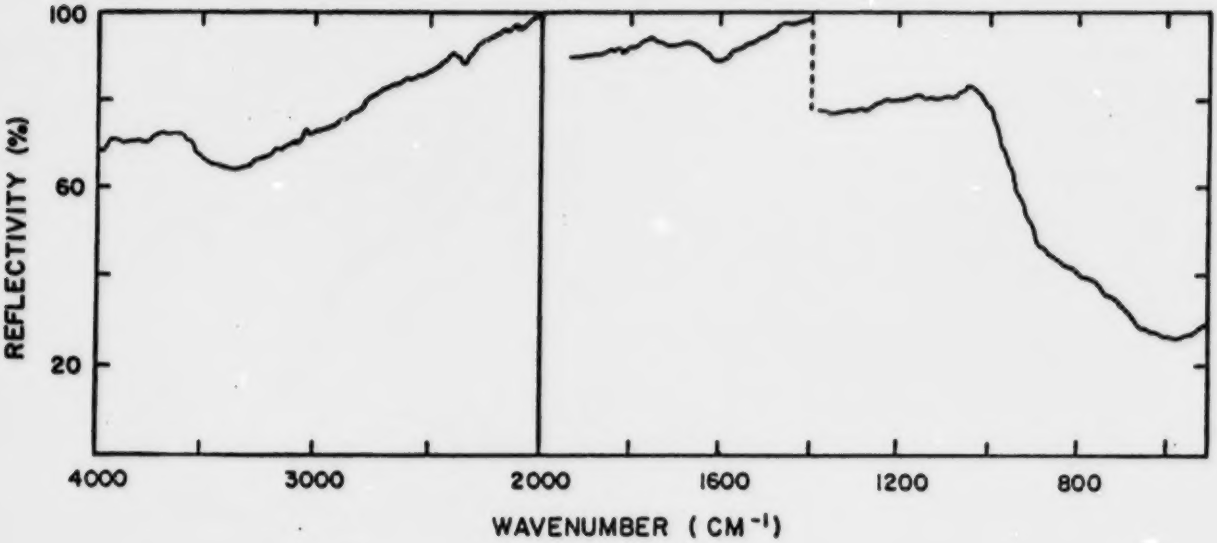

Fig. 5.4: IR-ATR spectrum of a 50 nm-thick WO_3 film immediately after deposition (the reflectivity unit is arbitrary in the wave number region between 1400 cm^{-1} and 600 cm^{-1}).

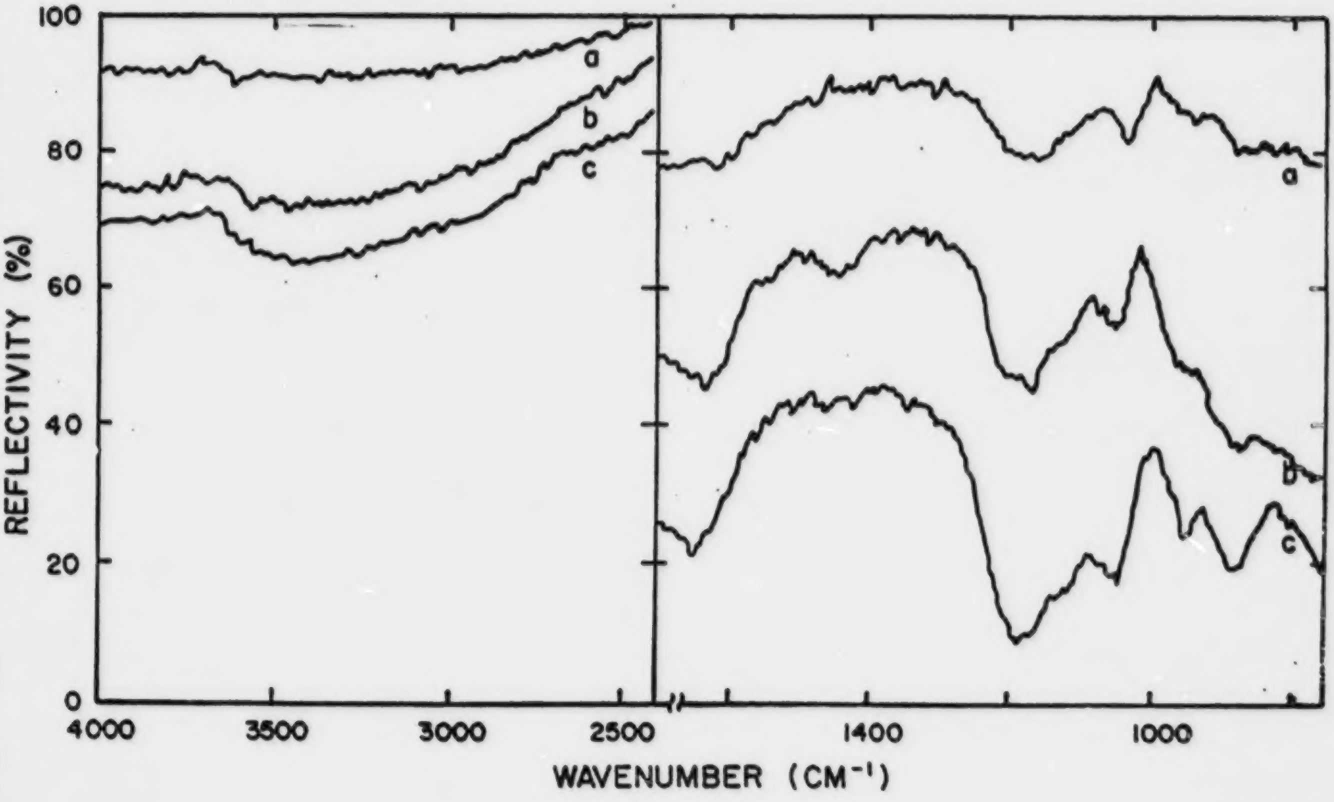

Fig. 5.5: IR-ATR spectra of colored 50 nm-thick WO_3 film, a) after coloration of the deposited film, b) after 12h of hydration, and c) after 36h of hydration.

gradually disappears. In the first stage of the hydration, the film is not continuous in appearance and the surface of the colored patches is reduced as the time of hydration increases. Fig. 5.5(b) and Fig. 5.5(c) corresponding to the hydrated films show well-defined bands at 880, 950, 1050, 1130 and 1180 cm^{-1}.

In order to increase the sensitivity of the ATR method in the study, thin silver films were used as underlayer or overlayer for a very thin WO_3 film. IR-absorption enhancements of a few orders of magnitude have been observed in ATR mode in films over- and undercoated with metal layers[39,43,44]. A 10 nm WO_3 film was evaporated on a 2.5 nm Ag film and the mechanism of the hydration was studied in the same way as in the previous experiment. The spectrum shown in Fig. 5.6b corresponds to the WO_3 deposited on Ag and hydrated for two days. In the same conditions, i.e. two days of hydration at 66% r.h., but using Ag as an overlayer, several strong bands are observed in the 800-1200 cm^{-1} region in the spectum 5.6c. Fig. 5.6a is the spectrum of a 10 nm WO_3 hydrated in the same conditions but without Ag. In this experiment WO_3 was evaporated on a ZnSe substrate but the same results with weaker bands have been observed with a KRS-5 substrate.

The results show some important differences between the underlayer (Fig. 5.6(b)) and overlayer (Fig. 5.6(c)) experiments. When Ag is an underlayer, the spectrum displays a broad absorption in the 1000-1100 cm^{-1} region with several bands at 1020,1045 and 1065 cm^{-1}, respectively. In the overlayer experiment, the single band at 1030 cm^{-1} is accompanied by a strong band at 1140 cm^{-1} present in the colored film as well (Fig. 5.5(c)). At the same

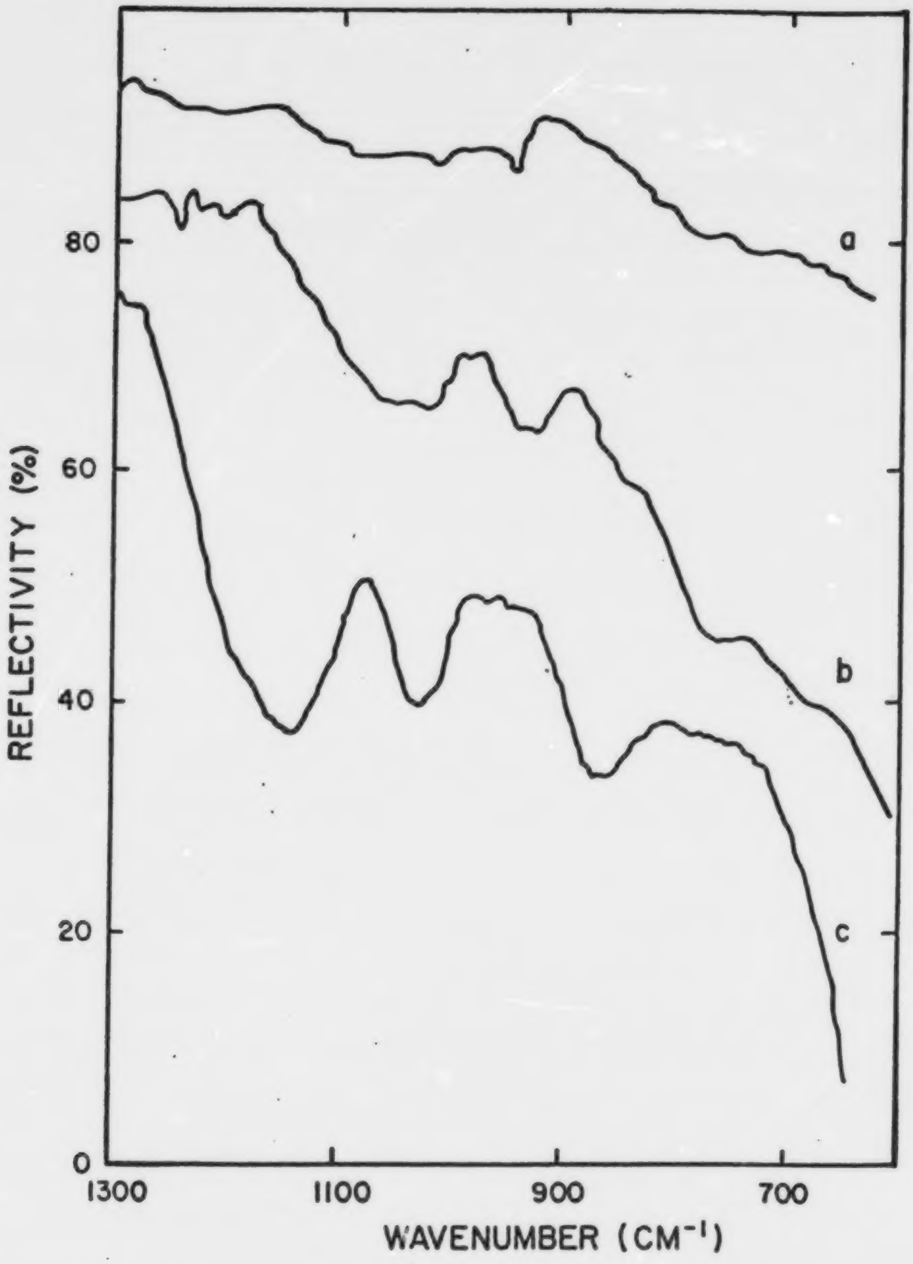

Fig. 5.6: IR-ATR spectra of a hydrated 10 nm-thick WO_3 film, a) without Ag, b) with a 2.5 nm underlayer, and c) with a 2.5 nm Ag overlayer.

time, in Fig. 5.5(c), the intensity of the broad band containing several W-O stretching modes decreases as those of 950-1250 cm^{-1} region increase, suggesting a structural change in the material during the hydration process. Comparing the spectra of colored hydrated tungsten bronze (i.e. Figs. 5.5(b) and (c)) with those of silver coated tungsten oxide films (i.e. Figs. 5.6(b) and (c)), we see that several bands not belonging to the W-O stretching vibrations appear in the region 950 cm^{-1} to 1200 cm^{-1}.

The high wavenumber region of the spectra given in Fig. 5.6(c) is shown in Fig. 5.7. The spectrum displays strong bands at 3400 cm^{-1} and 1630 cm^{-1} indicating a high percentage of absorbed water. However, in this experiment it is not possible to do any water concentration calculations because the absorption bands are obviously enhanced by the thin Ag film. The extension of the 1630 cm^{-1} δ_{OH} band towards the higher frequency region may come from an overtone vibration of the strong 865 cm^{-1} W-O stretching band enhanced by the Ag overlayer. In the high frequency region is an extension of the ν_{OH} band towards lower frequencies indicating different OH species in the silver coated WO_3 films. It is known from earlier studies[39,44] that Ag overlayers usually enhance the infrared absorption more than the underlayers of the same thickness. Thus, the stronger bands in Fig. 5.6(c) could be accounted for by an enhancement effect rather than by a stronger catalytic effect.

In order to find out whether the role of the silver is to catalyse the hydroxylation reaction or to enhance the weak bands, the overlayer effect of a 50 nm Ag layer has also been

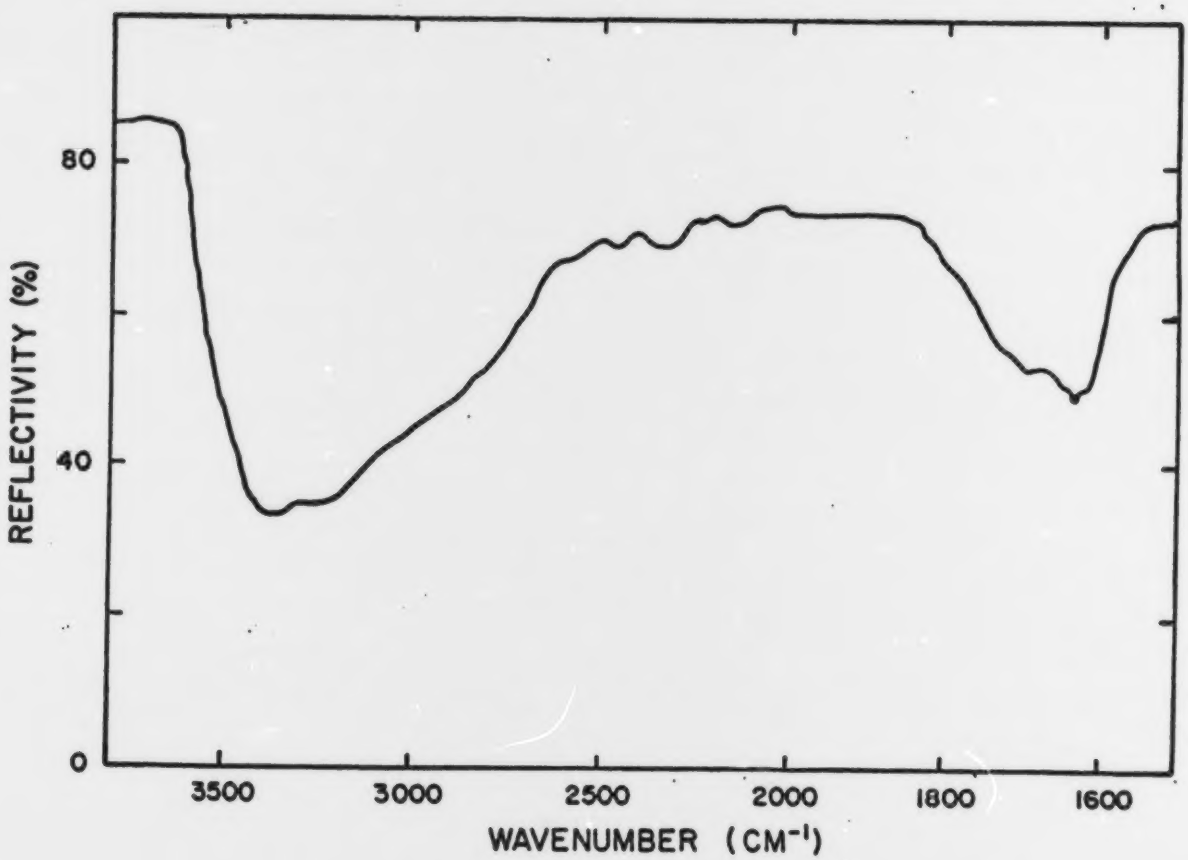

Fig. 5.7: The high-frequency region of the IR-ATR spectrum of hydrated 10 nm-thick WO_3 film with a 2.5 nm Ag overlayer.

studied. Keeping the crystal in the appropriate r.h. atmosphere for two days, the corresponding spectrum shows the same pattern but weaker bands than in Fig. 5.6(c) (2.5 nm Ag). It is apparent from these observations that the WO_3 film undergoes some chemical reactions during the hydration with the water molecules absorbed physically into the material. These reactions lead to a hydroxylated tungsten oxide surface layer displaying characteristic bands not only in the ν_{OH} stretching region but in the mid-infrared region as well.

The presence of a band at 950 cm^{-1} in the Raman spectrum of WO_3 has been related to the presence of the water molecules inserted in the film during the preparation[45]. The authors suggest the presence of hydrated species on the surface of the film, formed by the dissolution of WO_2 and W_2O_5 suboxides. According to the recent study of Yoshiike and Kondo[36] on the influence of water absorption and hydroxylation on the electrochromic properties of $WO_3 . \underline{x}\ H_2O$, the electrochromic reaction is accompanied by a hydroxylation and/or hydrolysis reaction. Comparing this behavior with those of other metal oxides, the authors have suggested that the hydroxylated surface layer has a complex structure having -O-W-OH and -W-O-W-O groups. ^{1}H-NMR data for WO_3 stored in air for several weeks showed a broad band assigned by the authors to the protons of the hydroxyl groups in $W(OH)_x$. The group of bands observed in Fig. 5.5 and 5.6 can be assigned to the W-O stretching and O-H bending modes in these complex structures. The OH groups are involved in hydrogen bonding with the absorbed water molecules and therefore their stretching vibrations are lowered and overlapped with the O-H stretching of water molecules.

The formation of these structures would be initiated and catalyzed by the small Ag particles. Very thin Ag films are generally known to form a granular structure[46] and may contribute to absorption enhancement. Ag is known as a very effective catalyst for many oxidation reactions[47,48].

5.3 Conclusion

The IR-ATR technique has been shown to be a sensitive and convenient method for studying the water absorption behavior in dielectric films such as WO_3. Thin films of WO_3 deposited at room temperature absorb fairly high amounts of water. With increasing substrate temperature during deposition there is a decrease in the water content. This behavior suggests that at higher substrate temperatures the films tend to be less porous.

The ATR spectra in the mid IR region of hydrated tungsten bronze and hydrated tungsten oxide with silver are found to be similar. The catalytic effect of the silver particles in the hydroxylation of the WO_3 surface has been suggested. At the same time, IR bands are enhanced by the thin Ag films increasing considerably the sensitivity of the method. It is the first attempt to enhance IR absorption bands corresponding to the vibrations of inorganic molecules and suggests that the IR absorption enhancement by Ag can be used to study the interface reactions in the electrochromic devices.

6. DETERMINATION OF THE OPTICAL CONSTANTS

There are many available methods for determining the optical constants n and k of thin films. Excellent reviews exist in the literature[49-51]. The measurements can be based on photometry, polarimetry or ellipsometry. In general, reflectance (R) and transmittance (T) are performed at normal-incidence but as discussed by Hansen[52], methods based on these measurements are not accurate, especially when k has large values. Oblique-incidence measurements also are used, with R measurements alone[53], or a combination of R and T (Ref. 54).

In the case of oblique-incidence, generally measurements of R and T are made at 3 or more incidence angles[53,55]. The equations for R and T are then inverted to derive n and k. The solutions are not always unique and suggestions have been made in order to circumvent this difficulty.

The accuracy in n and k determination increases with the number of measurements made at different angles[53,55]. It also depends on the values of the incidence angles chosen in the experiments. Inevitably, a measurement at a high angle of incidence is needed in order to enhance the accuracy in n and k values[55,56].

The method we propose in this work permits an unambiguous determination of n and K with a high degree of precision. R and T are measured simultaneously over a large interval of incidence angle, from near-normal incidence to 83°. The polarization of the incident light may be in the s or p state.

6.1 Theoretical formulaes and method

Fig. 6.1 shows a schematic representation of a multilayer system deposited on a thick substrate. If r_a and t_a are respectively the reflectance and transmittance of the m thin films when one passes from region (a) to region (b), and r_{a1} and t_{a1} respectively the reflectance and the transmittance of the m thin films when passing from region (c) to (a), then we have

$$r_a = \left| \frac{\eta_o B - C}{\eta_o B + C} \right|^2, \quad t_a = \frac{4\eta_o \operatorname{Re}(\eta_s)}{|\eta_o B + C|^2} \tag{1}$$

$$r_{a1} = \left| \frac{\eta_s B' - C'}{\eta_s B' + C'} \right|^2, \quad t_{a1} = \frac{4\eta_o \operatorname{Re}(\eta_s)}{|\eta_o B' + C'|^2} \tag{2}$$

with

$$\begin{bmatrix} B \\ C \end{bmatrix} = \begin{bmatrix} \prod_{i=1}^{m+1} (M_i) \end{bmatrix} \begin{bmatrix} 1 \\ \eta_s \end{bmatrix} \tag{3}$$

$$\begin{bmatrix} B' \\ C' \end{bmatrix} = \begin{bmatrix} \prod_{i=m}^{m+1} (M_i) \end{bmatrix} \begin{bmatrix} 1 \\ \eta_o \end{bmatrix} \tag{4}$$

where M_i = characteristic matrix for the i^{th} film

η = optical admittance of various media.

The reader is referred to Ref. 57 for the notations used.

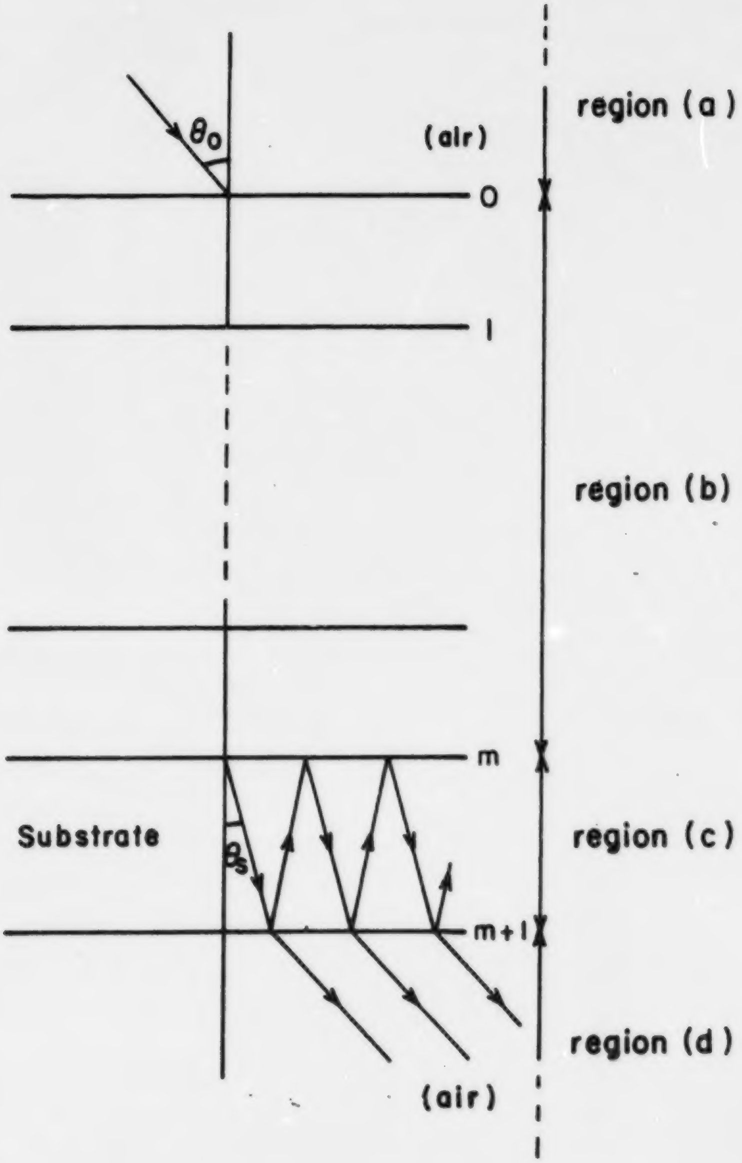

Fig. 6.1: Schematic representation of a thin film multilayer system on a thick substrate.

By summation of all the intensities transmitted to the final medium, we can show that the transmittance for the system, including the substrate, is

$$T = \frac{t_a\ t_v\ e^{-\alpha}}{1 - r_v\ r_{a1}\ e^{-2\alpha}} \tag{5}$$

where r_v = reflectance at the $(m + 1)^{th}$ interface

t_v = transmittance at the $(m + 1)^{th}$ interface

and

$$\alpha = \frac{4\pi d_s}{\lambda_o} \left| \text{Im}\ (N_s / \cos\theta_s) \right| \tag{6}$$

where d_s = substrate thickness

λ_o = light wavelength

N_s = substrate index of refraction

θ_s = refraction angle in the substrate

Similarly, we obtain for the reflectance:

$$R = r_a + \frac{t_a\ r_v\ t_{a1}\ e^{-2\alpha}}{1 - r_{a1}\ r_v\ e^{-2\alpha}} \tag{7}$$

If volume diffusion mechanisms in the substrate are included, the above expression for α is modified and we have[58]

$$\alpha = \frac{4\pi d_s}{\lambda_o} \left[\left|\text{Im}\ (N_s/\cos\theta_s)\right| + \frac{|\ k_{diff}\ |}{R_e\ (\cos\theta_s)} \right] \tag{8}$$

where k_{diff} is a phenomenological parameter which takes into account the diffusion process.

The problem is thus to find the set (n, k, d) from R and T with d representing the thickness for the film studied. Let's R_{exp} and T_{exp} be the values measured experimentally from 7° to 83° and R_{th} and T_{th} the corresponding theoretical values obtained from a given set of (n, k, d). We have to minimize the following function

$$F^2 = \sum_{\substack{\text{experimental} \\ \text{points}}} \left\{ \left[R_{exp} - R_{th}\right]^2 + \left[T_{exp} - T_{th}\right]^2 \right\} \qquad (9)$$

following a method proposed by Powell[59].

In general, for F of the order of 10^{-4}, only 5 to 8 iterations are needed to obtain a stationary minimum. The minimization procedure is enhanced in many cases by the introduction of the parameter k_{diff}.

6.2 Experimental procedure

The equipment used for simultaneous determination is shown in Fig. 6.2. The goniometer permits a scanning of the incidence angle from 7 to 84° with p or s-polarized light. The detector for R is positioned in an arm which rotates with the sample in such a way that the reflected beam is always detected.

The first step, at a given wavelength, consists of measuring the zero levels for the R, T and reference detectors, and establishing the sensibility ratio of the first two detectors with respect to the reference one. The second step is the simultaneous discrete angular scanning of R and T at this wavelength. The

Figure 6.2

A = Monochromator
B = Collimator
C = Polarizer (Glan-Taylor)
D = Filter
E = Beam splitter and mirror
F = Beam chopper (2 slits/2 frequencies)
G = Goniometer
H = Detector (Reference)
I = Detector (transmitted beam)
J = Power supply
K = Detector (Reflected beam)
L = Electronic controller for goniometer
M = Micro-computer
N = Coupler/intergrator
O = Reflection lock-in amplifier
P = Transmission lock-in amplifier
Q = Reference lock-in amplifier
R = Digital board
$V_{1,2}$ = Reference frequency

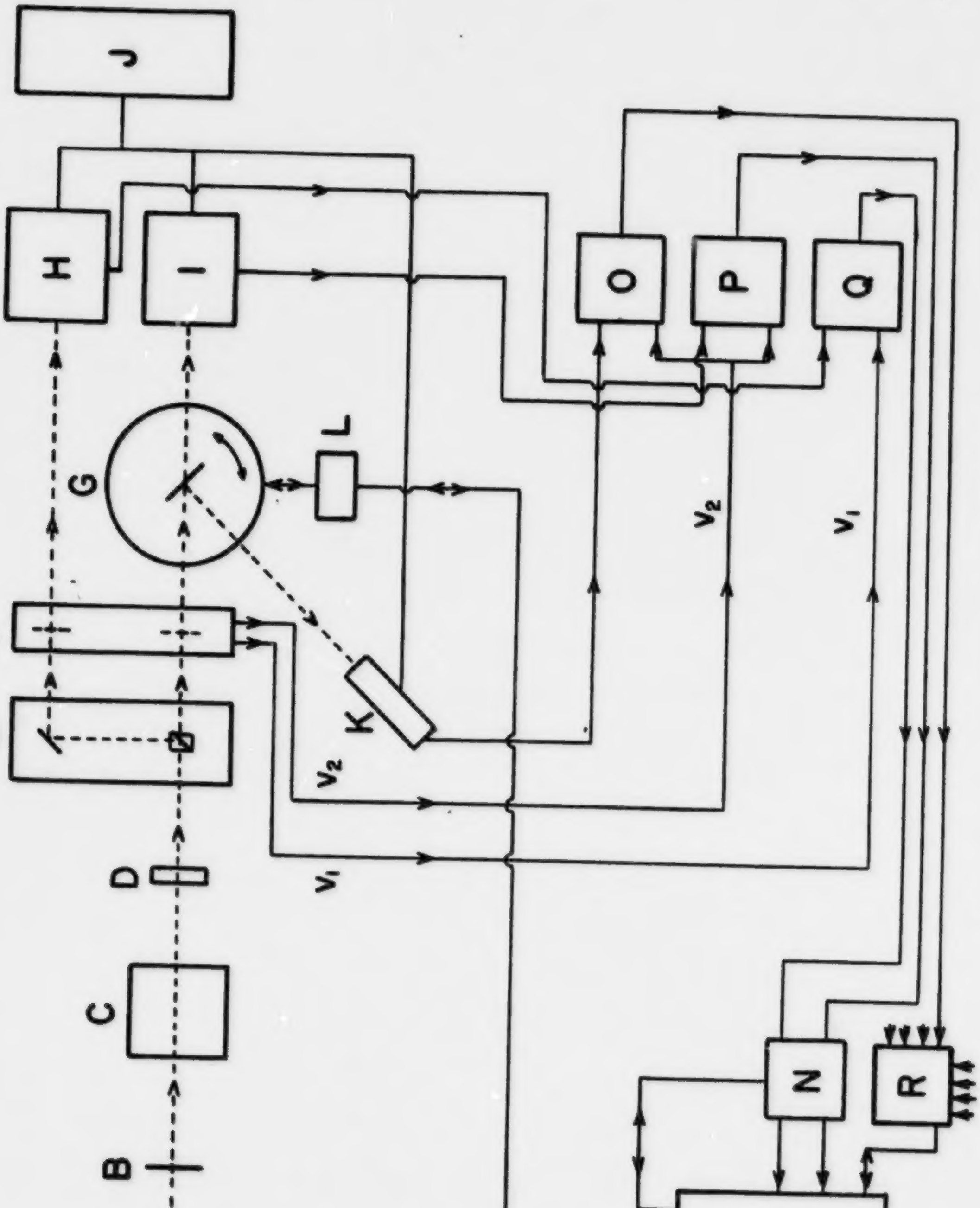
A
B
C
D
E
F
G
H
I
J
K
L
M
N
O
P
Q
R
V_1
V_2
V_2
V_1

angular variations are controlled automatically by a micro-computer.

The results for R and T are stored in a file and calculation for (n, k, d) can be performed thereafter with a program already installed in the computer.

7. PROPERTIES OF THE ELECTROCHROMIC (WO_y) LAYER

7.1 Optical and electrical properties of WO_y

In all the electrochromic (EC) systems the EC layer plays a pivotal role since this is the layer in which the actual change in optical properities occurs through the double insertion of electrons and ions. Transition metal oxides (TMO) are very well suited for this function amongst the inorganic materials. These TMO's exhibiting EC phenomenon can be divided into two categories: those coloring cathodically (e.g. WO_y, $y < 3$) and those coloring anodically (e.g. IrO_x). While the coloration in anodic type materials occurs through the removal of positive ions and electrons, as shown below,

$$\underset{\text{(colorless)}}{Ir(OH)_3} - H^+ - e = \underset{\text{(colored)}}{IrO_2, H_2O}$$

the cathodic coloration proceeds by the insertion of positive ions and electrons

$$\underset{\text{(colorless)}}{WO_y} + xM^+ + xe = \underset{\text{(colored)}}{M_x WO_y}$$

Tungsten oxide belonging to the second category of EC materials is found to be the most versatile material for EC layer for the following reasons:

1) Tungsten oxide exhibits EC behavior both in polycrystalline and amorphous forms, although the underlying mechanisms of coloration in the two forms is different. In polycrystalline

form the change in optical properties occurs through reflectance modulation. Here the reflectivity of the sample changes in accordance with the density of electrons and the ions inserted and the material behaves as a Drude metal. On the other hand, the change in the optical properties in amorphous WO_y occurs through absorption modulation. The degree of modulation is varied by the number of absorbers created through the insertion of positive ions and electrons.

2) The ionic and electronic conductivity of WO_y films is quite high even at room temperature and hence a fairly rapid electrochromic response can be expected.
3) It is very easy to prepare tungsten oxide films by different techniques (evaporation, chemical vapor deposition, sputtering, electron gun).
4) Tungsten oxide exhibits a fairly linear coloration response as a function of injected charge.
5) Quite high values of optical density change (ΔO.D) can be achieved under H^+ and Li^+ ion insertion. ΔO.D achievable in amorphous films is significantly higher than that in polycrystalline films.
6) Tungsten oxide is an inexpensive material as compared to others such as IrO_x etc.

In view of the above stated reasons most of the work carried out to date on EC system is based on WO_y films. We have used amorphous WO_3 films as the EC layer in the fabrication of the all-solid-state system. The WO_3 film for this purpose has been deposited by thermal evaporation. In addition to the qualities stated above, it is essential that the electrochromic coloration/bleaching cycles should be reversible. Hence, to examine the suitability of our WO_y samples for the EC mechanism we have studied in detail the various properties related to the EC performance of the film.

Optical properties:

The variation of optical transmission as a function of wavelength is given in Fig. 7.1 for three WO_y samples of film thickness of 200 nm. These samples were prepared at three different substrate temperatures of 100°C, 200°C and 300°C. Comparing the three curves it can be seen that the samples deposited at 100°C (curve a) and 200°C (curve b) exhibit a far superior transmission than that deposited at 300°C (curve c). This diminishing of the transmission in the case of film deposited at 300°C is due to its increased reflectance. That is, such a film deposited at high substrate temperature tends to be more crystalline than amorphous. The appearance of this film is slightly bluish. Such films have been reported to be having y values between 2.5 and 2.7(Ref.60). However, the other two samples deposited at 100°C and 200°C exhibit fairly high transmission values and no visible coloration except that due to interference.

Most of our study of the EC behavior and the fabrication of the all solid system has been carried out with the WO_3 film deposited at 200°C. This film in addition to exhibiting high

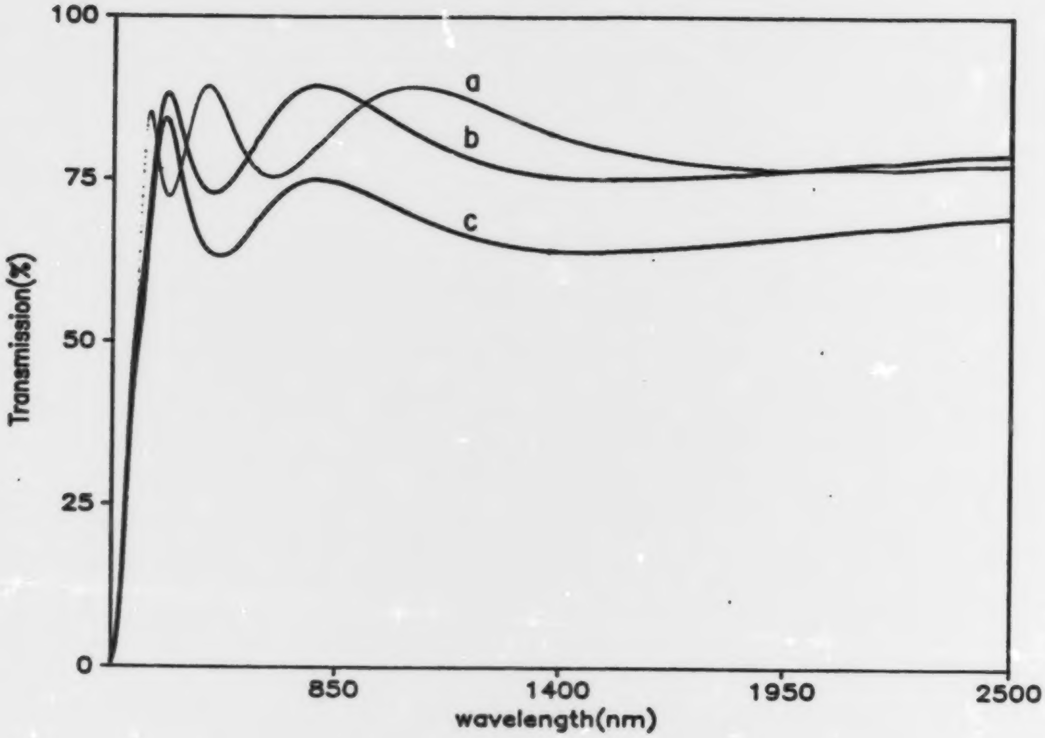

Fig. 7.1: Transmission spectra of 200 nm thick WO_3 film deposited on glass with substrate.

transmission in the visible and NIR region also has a higher physical stability on ITO than the film deposited at 100°C. The latter film on ITO when immersed in liquid electrolyte ($LiClO_4$ in propylene carbonate) peeled off the substrate. However, the film deposited at 200°C was found to be intact even after several cycles of such immersions in the liquid, washing with water and drying. Further, as discussed in section 5, the WO_3 films deposited at 200°C contain much less water (< 20%) as compared to those deposited at 100° C. Hence, for the fabrication and study of our Li^+ based electrochromic systems WO_3 films deposited at 200°C have been found to be suitable candidates.

Electrical resistivity:

The measurement of electrical resistance of the WO_y samples was carried out ex-situ using a Keithley electrometer (610 CR). These measurements were carried out after 24 hours of exposure of the films to air. The electrical resistivity values as calculated from the film geometry was found to be 1.93×10^2 Ω-cm, 6.71×10^5 Ω-cm and 3.184×10^6 Ω-cm, for the films deposited at 300°C, 200°C and 100°C respectively. As can be seen with these values there is a decrease in the film resistivity with increase in substrate temperature. This is due to the decreasing porosity and tending of the film towards crystallinity with increasing substrate temperature. In comparison with the other reported values of WO_y film resistivity (10^8 - 10^9 Ω-cm) (Refs. 60-62) in thermally deposited samples, our samples exhibit a rather low electrical resistivity. The origin of this could be the elevated substrate temperatures that we have used to deposit these films.

7.2 Lithiation of WO_3 samples

As discussed earlier one of the important characteristics of the EC layer is its ion intake capacity. Since it is the EC layer which brings about the optical modulation of the EC system it is extremely important to understand the nature of coloration mechanism. In this study of the WO_3 layer several important phenomena have been observed by us, as described in the following two sections.

7.2.1 High density coloration of WO_3

The dark blue coloration of WO_3 samples under double insertion of positive ions and electrons is very well known[63]. Several works have been reported on the linear dependance of the change in optical density (ΔO.D) on the injected charge, both upon proton and lithium ion injection[64,65]. However, under continued insertion of these ions beyond the normal limit of the formation of dark blue tungsten bronze an actual decrease in the ΔO.D occurs[66]. This leads to films with a brownish to almost transparent appearance. Although this seems to be an important phenomenon in evaluating the performance of the WO_3 samples, there is no work available in the literature about this anomalous behavior.

For a detailed study of this phenomenon our WO_3 samples were colored in an electrochemical cell containing a liquid electrolyte ($LiClO_4$ in propylene carbonate (PC)). WO_3 film on an ITO coated glass was one electrode while carbon served as the counter electrode. Lithium ion injection from the electrolyte into WO_3 was realized by applying a suitable potential between the electrodes. The charge density of the Li^+ ions injected was obtained by integrating the current through the system. The optical change was monitored at the wavelength of 632 nm. The film thickness of WO_3 was 200 nm.

Fig. 7.2 shows the dependence of ΔO.D on the injected charge density (Q). It can be seen that initially there is an almost linear dependence of ΔO.D on Q as reported by others[67,68]. However, under continued Li^+ ion injection there is a change in the slope of this curve gradually and ΔO.D saturates around 1.3. If further insertion of lithium is continued an actual decrease in ΔO.D can be clearly seen. It is also found that the EC behavior of the WO_3 films colored beyond this "reversal" point is irreversible. Hence, for our WO_3 sample, Fig. 7.2 clearly indicates that the maximum ΔO.D attainable is 1.3 and for a charge injection of around 50 mC/cm^2. This is the limit to which the sample can be colored without making the optical changes irreversible. In the range of charge density where the EC phenomenon is reversible the coloration occurs through the temporary formation of Li_xWO_3 ($0 \le x < 1$), the tungsten bronze. When this limit is surpassed, perhaps there is formation of lithium tungstate (Li_2WO_4). This change seems to be permanent with respect to EC bleaching. Li_2WO_4 is a transparent material unlike tungsten bronze (Li_xWO_3). Hence, this phenomenon

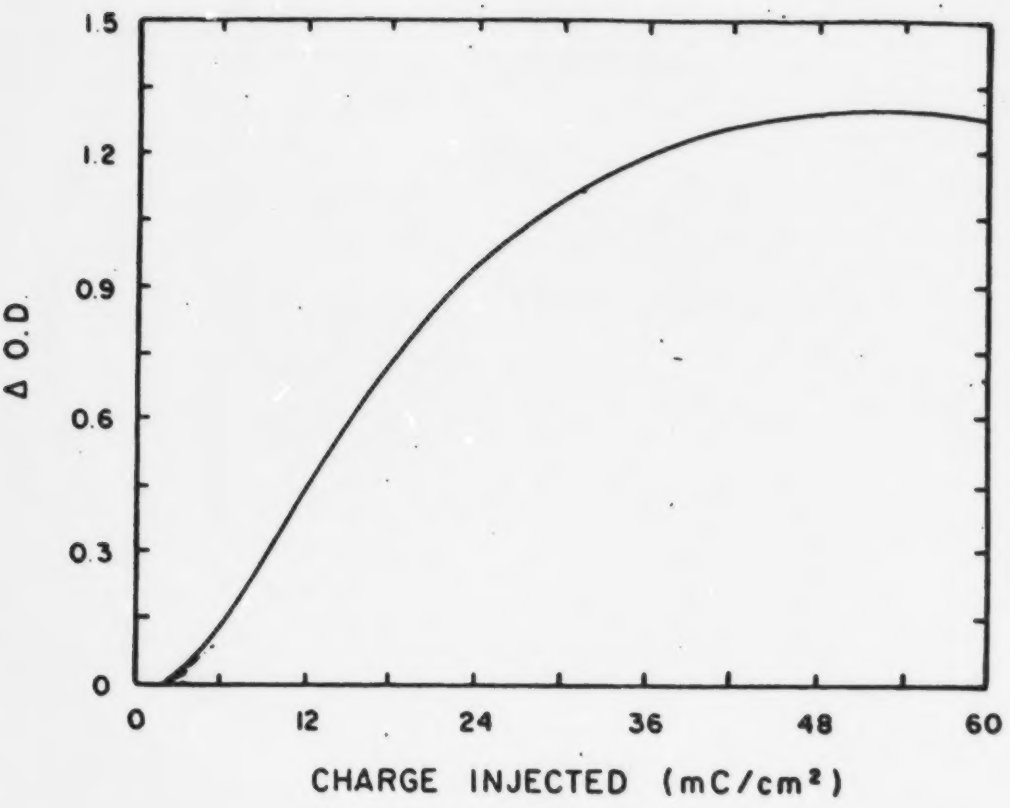

Fig. 7.2: Optical density change (Δ O. D.) as a function of the charge density injected in 200 nm thick WO_3 film.

serves as an important tool in evaluating the EC performance limit of the WO_3 samples. This limit, however, depends on the preparation conditions of the WO_3 film.

7.2.2 Vacuum lithiation of WO_3 films

The method of lithium insertion by using $LiClO_4$ in PC electrolyte, described in the last section is a convenient and most used method for studying the Li^+ based EC systems. Although it is a convenient method, the immersing of the sample in the liquid and the ensuing cleaning of the sample cause some problems. The colored sample of WO_3 is normally taken out of the electrochemical cell and rinsed in distilled running water. Then the sample is dried before making other measurements or depositing other films over it. This contact of the colored tungsten bronze (Li_xWO_3) film with water can sometimes lead to peeling of the film from the ITO surface. Hence, enormous care has to be taken to ensure stability and to avoid hydration of the film. Hence, a dry method of lithiation is preferable.

In our laboratory we have developed such a method of in-situ lithiation of the WO_3 samples. Lithium niobate ($LiNbO_3$) when heated in a vacuum chamber dissociates giving free lithium atoms. Exposing of a WO_3 sample in such an atmosphere leads to lithiation with the formation of Li_xWO_3. The WO_3 sample can be colored to any degree of optical density required. To illustrate the comparison between the lithiation using the liquid ($LiClO_4$ in PC) and the lithium niobate method, in Fig. 7.3 is given the dependence of ΔO.D

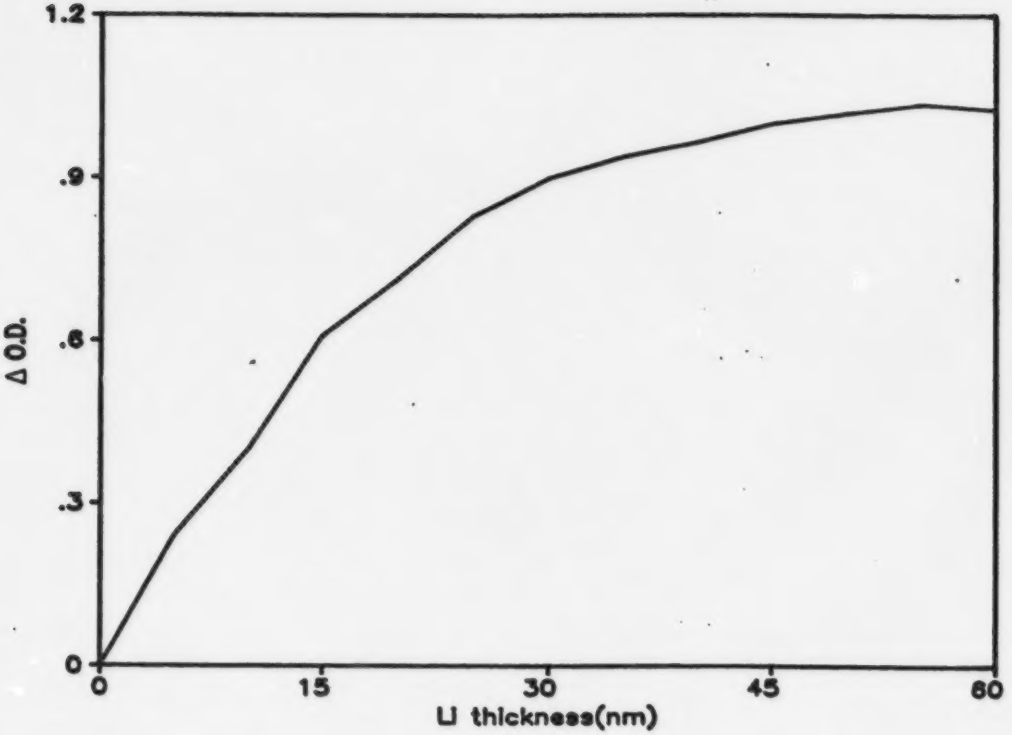

Fig. 7.3: Variation of Δ O.D. as a function of mass thickness of lithium deposited from lithium niobate ($LiNbO_3$).

on the mass thickness of lithium. The thickness shown here corresponds to the change noted on the quartz crystal (mass thickness) when $LiNbO_3$ was heated in a tungsten boat. Comparing Fig. 7.2 and Fig. 7.3 one can note that with increasing lithium mass thickness the change in optical density proceeds similar to that seen in liquid cell coloration. However the saturation ΔO.D attained in the thermal evaporation method around a thickness of 50 nm of lithium is 1 and not 1.3 as in the earlier method. However, using this method of lithium atom deposition, the required degree of optical density can be achieved rather easily. The method is clean and requires no subjecting of the WO_3 film to hydration.

This technique has been studied extensively and used in our laboratory for the characterization and fabrication of EC samples. To the best of our knowledge such a technique has not been used or reported by other workers in the field.

Fig. 7.4 gives the spectra of a WO_3 sample as deposited on a glass substrate and subsequently colored by the thermal evaporation of lithium atoms. The WO_3 sample was coated with mass thicknesses of 15, 30, 50 and 75 nm of lithium in different steps. The transmission changes rather drastically in each step. It can be seen clearly that the addition of lithium up to a thickness of 50 nm results in the overall diminishing of the transmission in the spectral range studied. However, with the addition of 75 nm of lithium, the transmission actually begins to increase overall. This is the indication of the "reversal" of optical density discussed earlier. The film coated with this thickness of lithium

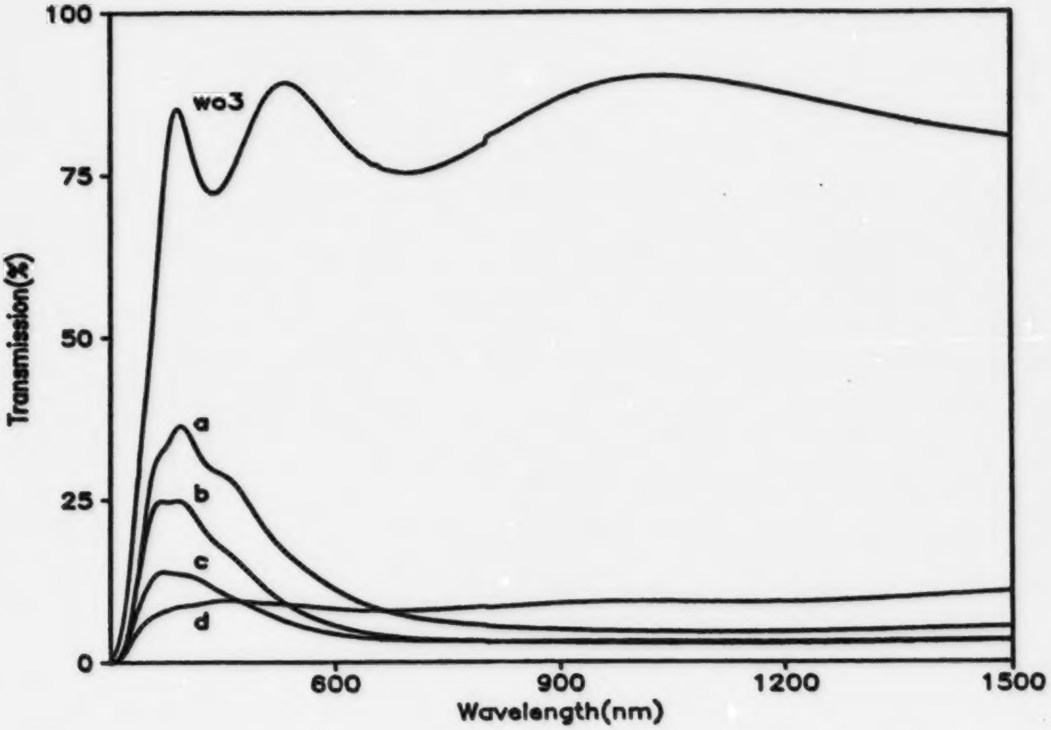

Fig. 7.4: Transmission spectra of 200 nm thick WO_3 film deposited with a) 15 nm, b) 30 nm, c) 50 nm and d) 70 nm of mass thickness of lithium.

begins to appear brownish. This once again proves the EC performance limit. Hence, our study and fabrication of the EC systems was carried out with a lithium mass thickness of around 50 nm for a 200 nm thick WO_3 film as EC layer giving us a optical density change (ΔO.D) value of 1 between the completely colored and bleached states.

7.3 Optical and electrochromic properties of Au: WO_3, Ag: WO_3 and Sn:WO_3 cermets

As discussed earlier, amorphous tungsten oxide films have been found to be very suitable for optical modulation through the reversible formation of tungsten bronze. However, it is well known that the absorption peak in the bronze lies in the near infrared region and only a tail of this absorption extends into the visible region[67]. This gives the characteristic blue coloration to these films. Hence, most of the optical modulation occurs in the NIR region. It is, however, desirable to extend the absorption to visible wavelengths for applications such as display devices etc. Several attempts have been made to achieve this absorption in the visible by mixing MoO_3 (Ref. 68), BaO (Ref. 69) or metal particles with WO_3 (Ref. 70). Our study of the metal particles doped WO_3 films for their optical and electrochromic properties was also intended at achieving this higher optical modulation in the visible region of the spectra. The three metals that we have used are Au, Ag and Sn since the free electron plasma absorption in these metals is located in the visible. The study of these three cermets revealed an interesting and characteristic optical and electrochromic behavior in each case.

Cermets with different compositions were prepared by alternate thermal evaporation of the metal and WO_3 film. These films were prepared at an elevated substrate temperature of 250°C. To ensure an even distribution of the metal in the WO_3 matrix, the metal film thickness was maintained at 1 nm and that of WO_3 film was varied to achieve different compositions. The total film thickness was kept around 200 nm in each case.

Au:WO_3:

Three compositions of the cermets studied are 2.4%, 5.8% and 8.7%. In Fig. 7.5 are given the transmission spectra of Au:WO_3 cermets with those Au filling factors. These curves are compared with that of pure WO_3 film (curve A). The transmission of the WO_3 film decreases rapidly with increasing Au filling factor. A clear transmission minimum develops around 600 nm attributable to the plasma resonance in gold particles. These films "as prepared" appeared light to dark blue depending on the Au filling factor. This behavior is similar to that reported earlier on Au-WO_3 (Ref. 71) and other Au containing cermet systems[72].

In order to understand this optical behavior qualitatively, we have used the simple Maxwell-Garnett (M-G) theory. The effective dielectric constant of a cermet system is given by

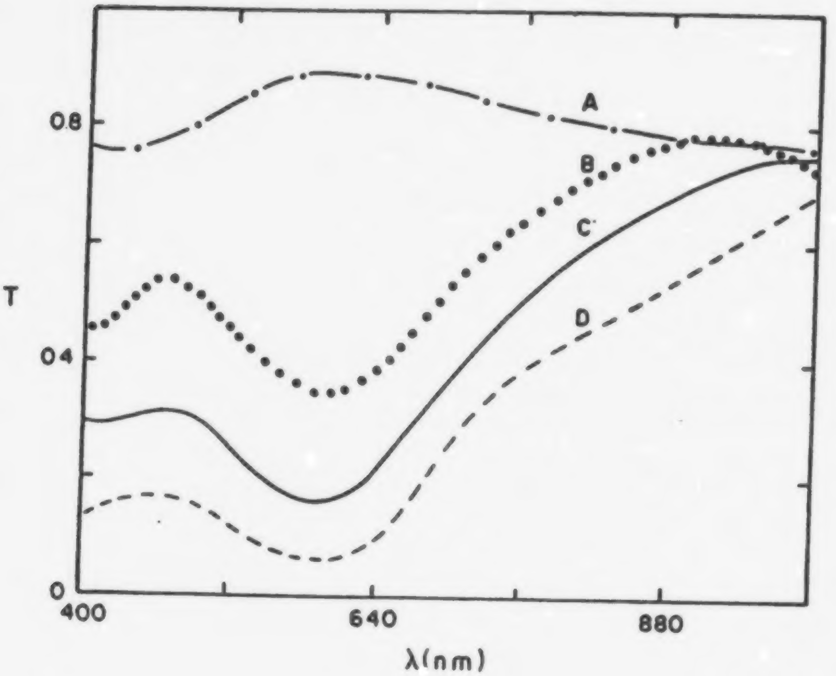

Fig. 7.5: Transmission spectra of Au-WO$_3$ films with different Au filling factor, Q; (a) 0%, (b) 2.4%, (c) 5.8% and (d) 8.7%

$$\epsilon = \epsilon_d + \frac{Q\epsilon_d}{(1-Q)/3 + \epsilon_d/(\epsilon_m - \epsilon_d)} \qquad (1)$$

where ϵ_d and ϵ_m are the dielectric constants of the host matrix WO_3 and the metal, Q is the volume filling factor of the metal. The metal filling factor is corrected for the classical size effect[73]. Using the M-G relation (Eq. 1) and a plasma energy of 9.1eV, a scattering energy of 0.026eV, a Fermi velocity of 1.4×10^6 m/s and a bulk mean free path of 35.4 nm, we have calculated the theoretical transmission. In Figs. 7.6(a) and 7.6(b) are given the comparisons between the M-G theoretical and the experimental transmission curves for Au:WO_3 cermets with respective Au compositions of 5.8% and 8.7%. We can see that for both these compositions there is a fairly good agreement between the experiment and the theory, especially at lower wavelengths. Towards higher wavelengths, the two curves show a deviation. This seems to be due to the variation in the optical properties of ITO film underneath the cermet during heating of the substrates. However, the close agreement in the nature of the two curves indicates that Au:WO_3 films prepared by alternate thermal evaporation have an optical behavior predicted by the simple Maxwell-Garnett theory.

The electrochromic coloration of these samples was carried out in an electrochemical cell containing $LiClO_4$ in PC. In Fig. 7.7(a), (b) and (c) are given the transmission curves of Au:WO_3 cermets before and after coloration, for the three compositions

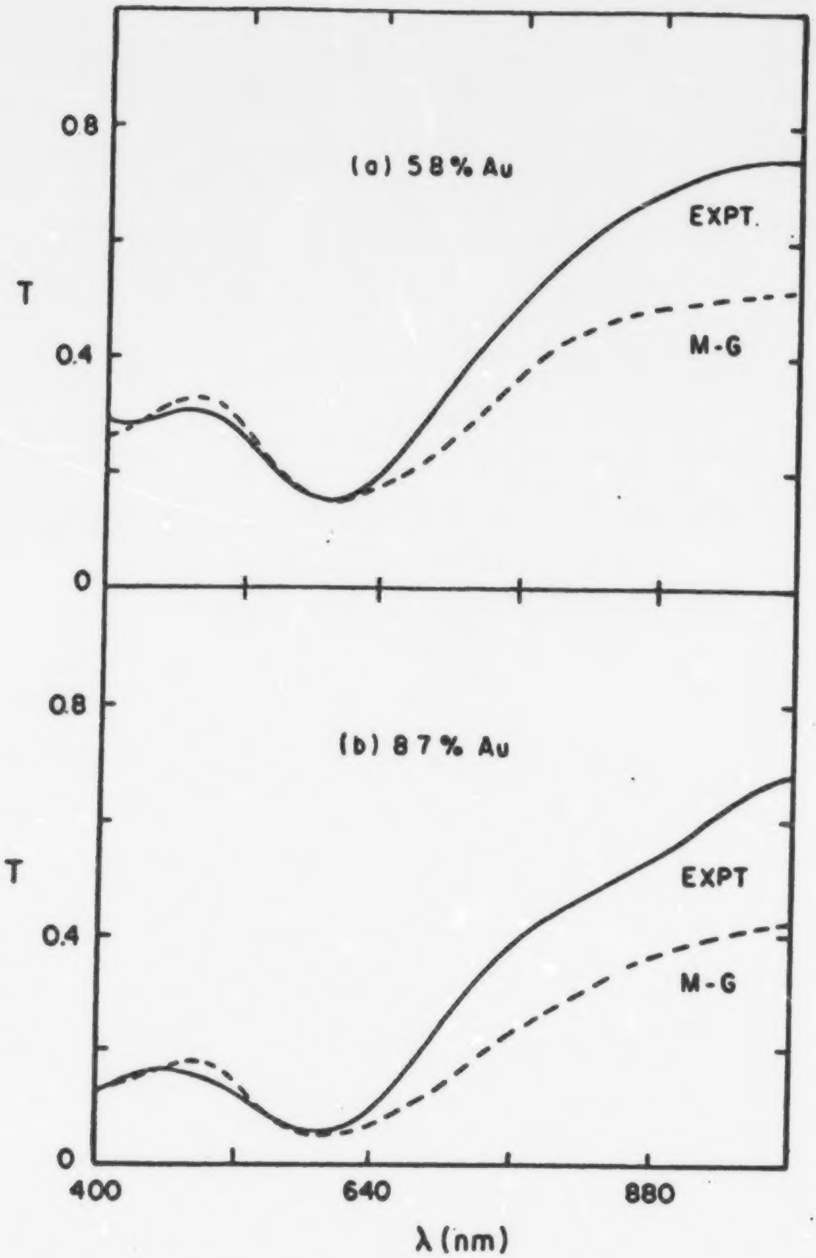

Fig. 7.6: M-G theoretical and experimental transmission curves in Au-WO_3 cermets, (a) Q = 5.8% Au and (b) Q = 8.7% Au.

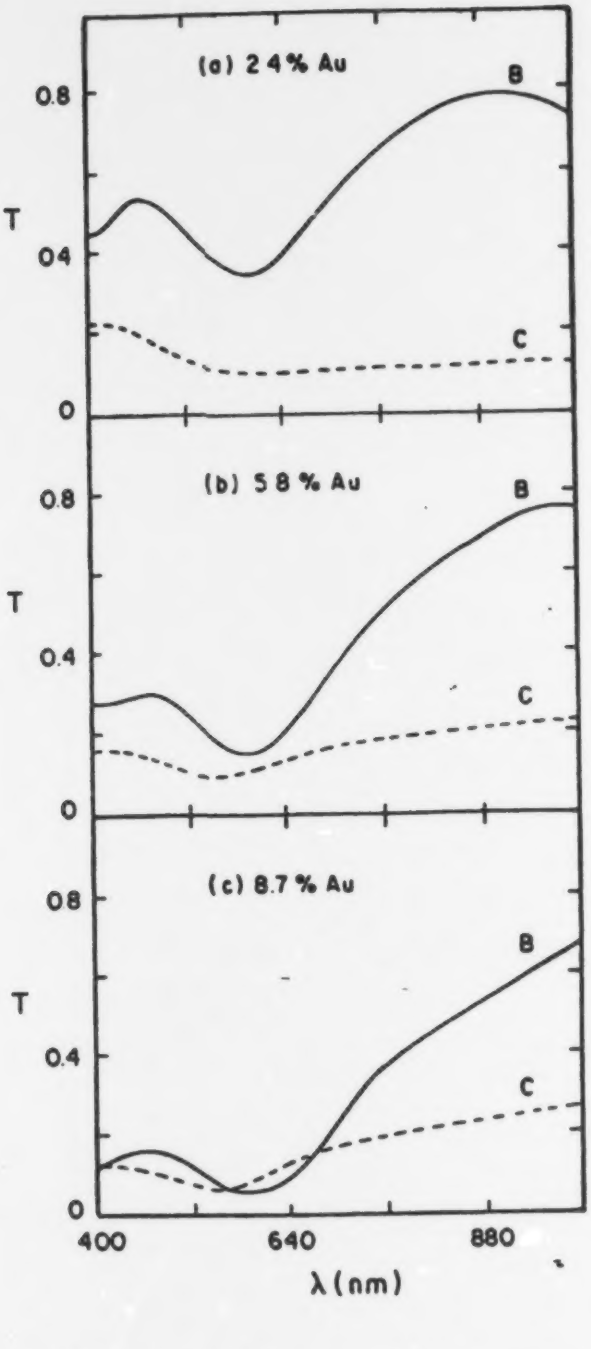

Fig. 7.7: Bleached (B) and colored (C) state transmission of Au-WO_3 cermets with (a) Q = 2.4%, (b) Q = 5.8% Au and (c) Q = 8.7% Au. Applied voltage = 2V.

studied.

In the film with 2.4% Au concentration we can see a large decrease in transmission throughout the spectral region examined. The transmission in the colored state is similar to that observed normally in pure WO_3, with increasing transmission towards lower wavelengths. The colored samples appeared dark blue. No minimum is apparent in these spectrum. However, with increasing Au concentration, (Fig. 7.7 (b) and (c)) a minimum in the colored state appears clearly. A shift of the minimum from around 600 nm to around 560 nm is evident. Due to further deepening of the bleached state minimum in the case of 8.7% Au this shift is even more distinct. In appearance the Au:WO_3 films with 2.4% of Au changed from light blue to dark blue while that of 8.7% changed from dark blue to light or deep pink. These observations are similar to those reported by Sichel and Gittleman[74].

Sichel and Gittleman[74], however, have tentatively attributed this sort of color change to the change of effective dielectric constant of colored WO_3 samples in the presence of Au particles. However, our detailed study of the WO_3 coloration has helped in understanding this anomaly. The observation of changing of the Au:WO_3 color from blue to pink under deep EC coloration is the same effect of "heavy" lithium ion injection discussed earlier. It is the irreversible formation of Li_2WO_4 that leads to such a color change. Under light coloration, it is the formation of Au:Li_xWO_3 ($0 \leq x \leq 1$) while deep coloration leads to Au:Li_2WO_4.

Ag:WO_3:

The optical behavior of Ag:WO_3 cermets are entirely different from those of Au:WO_3. In the case of Ag:WO_3, the compositions we have studied are 2.4%, 5.8% and 9.6% of Ag. The transmission spectra of these films is compared to that of pure WO_3 film in Fig. 7.8. With increasing Ag composition the overall transmission of the films decreases without exhibiting any structures. The transmission of the Ag:WO_3 cermets unlike those of Au:WO_3 is constant throughout the spectral region examined. Only in the case of 2.4% Ag composition we can notice an interference structure at lower wavelengths. With increasing metal composition and absorption, this structure disappears.

Such an absorptionless transmission in Ag:WO_3 is an unusual behavior as compared to other Ag containing cermets[13] in which the free electron plasma resonance of the Ag particles leads to a minimum in the transmission spectrum. For qualitatively understanding this behavior, the M-G theory (Eq. 1) was used. With a plasma energy of 9.15 eV, a scattering energy of 0.02eV, a Fermi velocity of 1.39 x 10^6 m/s and a bulk mean free path of 45.8 nm, the M-G theoretical transmission curve was obtained. In Fig. 7.9 is shown the comparison between M-G theoretical and experimental transmission curves for Ag compositions of 5.8% and 9.6%. We can see that there is a fairly good agreement between the theory and the experiment on using an extremely low value of 0.2 to 0.3 nm for Ag particle radius. This small value of particle radius perhaps indicates that Ag diffuses into the WO_3 host matrix in

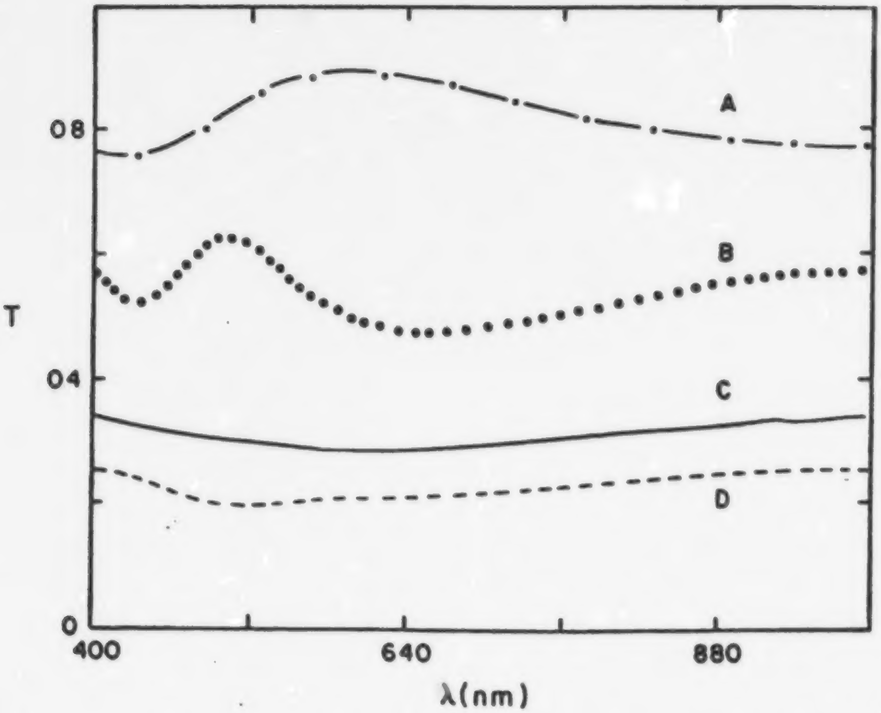

Fig. 7.8: Transmission spectra of Ag-WO_3 films with different Ag filling factor, Q; (a) 0%, (b) 2.4%, (c) 5.8% and (d) 9.6%.

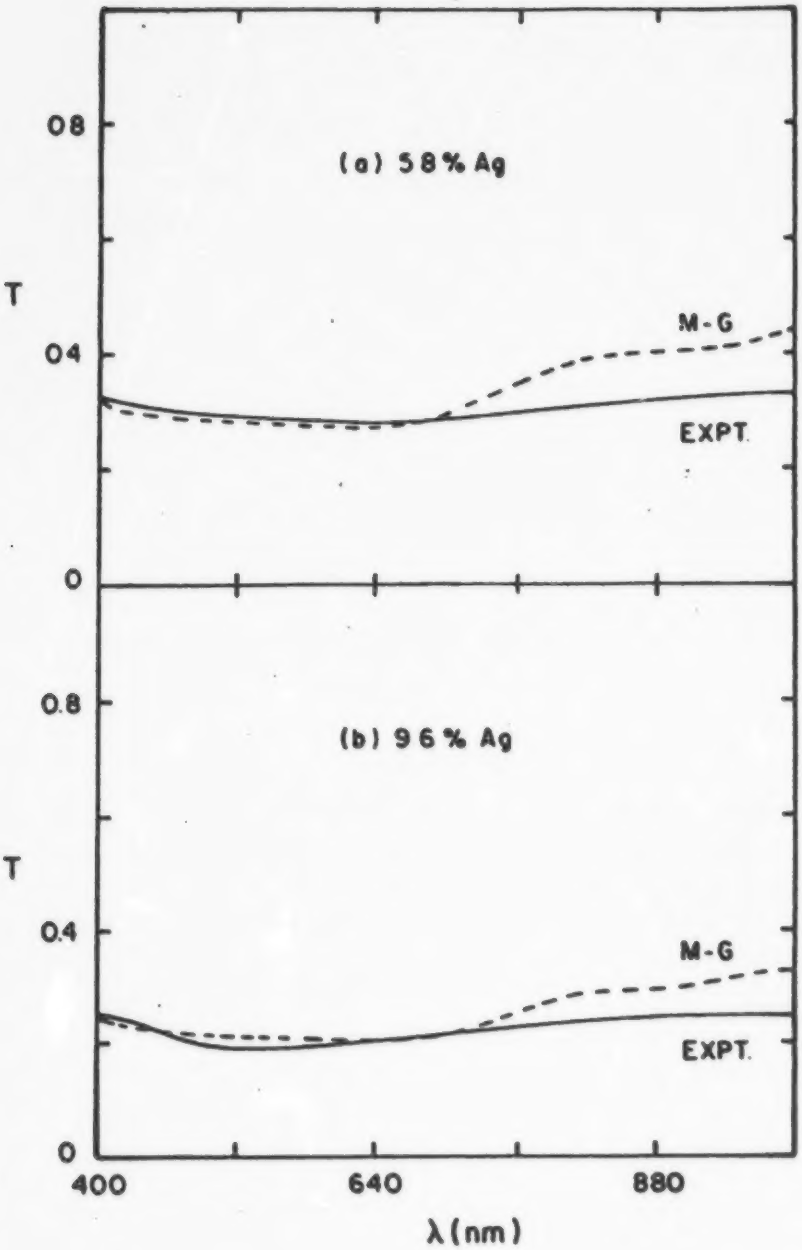

Fig. 7.9: M-G theoretical and experimental transmission curves in Ag-WO_3 cermets, (a) Q = 5.8% Ag and (b) Q = 9.6% Ag.

extremely small dimensions and does not granulate as in the case of Au particles. This changes the optical properties of $Ag:WO_3$ rather profoundly.

Electrochromic coloration of $Ag:WO_3$ cermets was also carried out under lithium injection in an $LiClO_4$ in PC containing electrochemical cell. Fig. 7.10 shows the transmission of the $Ag:WO_3$ cermets before and after EC coloration. In both the compositions shown there is a uniform decrease in transmission throughout the spectral range examined. Even in the case of $Ag:WO_3$ with a high value of 9.6%, no significant structure in the colored state is observed. This is perhaps due to the uniform and structurless transmission of $Ag:WO_3$ in the uncolored state, unlike the $Au:WO_3$ cermet in which due to the already existing minimum of the uncolored state, a shift is very clearly observed (Fig. 7.8). However, the same $Ag:WO_3$ film under prolonged injection of lithium ions begins to show a clear and broad minimum as shown in Fig. 7.12. In this heavily injected (HC) state the film begins to become more transparent than the lightly colored state, which is evident on comparing Fig. 7.10 and 7.11.

The transparency approaches almost that of the bleached state (B) in the higher visible and near infrared regions. This behavior once again is in accordance with our hypothesis of the formation of Li_2WO_4 under heavy lithium ion injection.

In Figs. 7.12 (a) and (b) are given the dependence of ΔO.D on the charge injected (Q) in both the cermet systems, $Au:WO_3$ and $Ag:WO_3$, respectively. It can be clearly seen in both the cases that compared to pure WO_3 film, the ΔO.D maximum achievable in

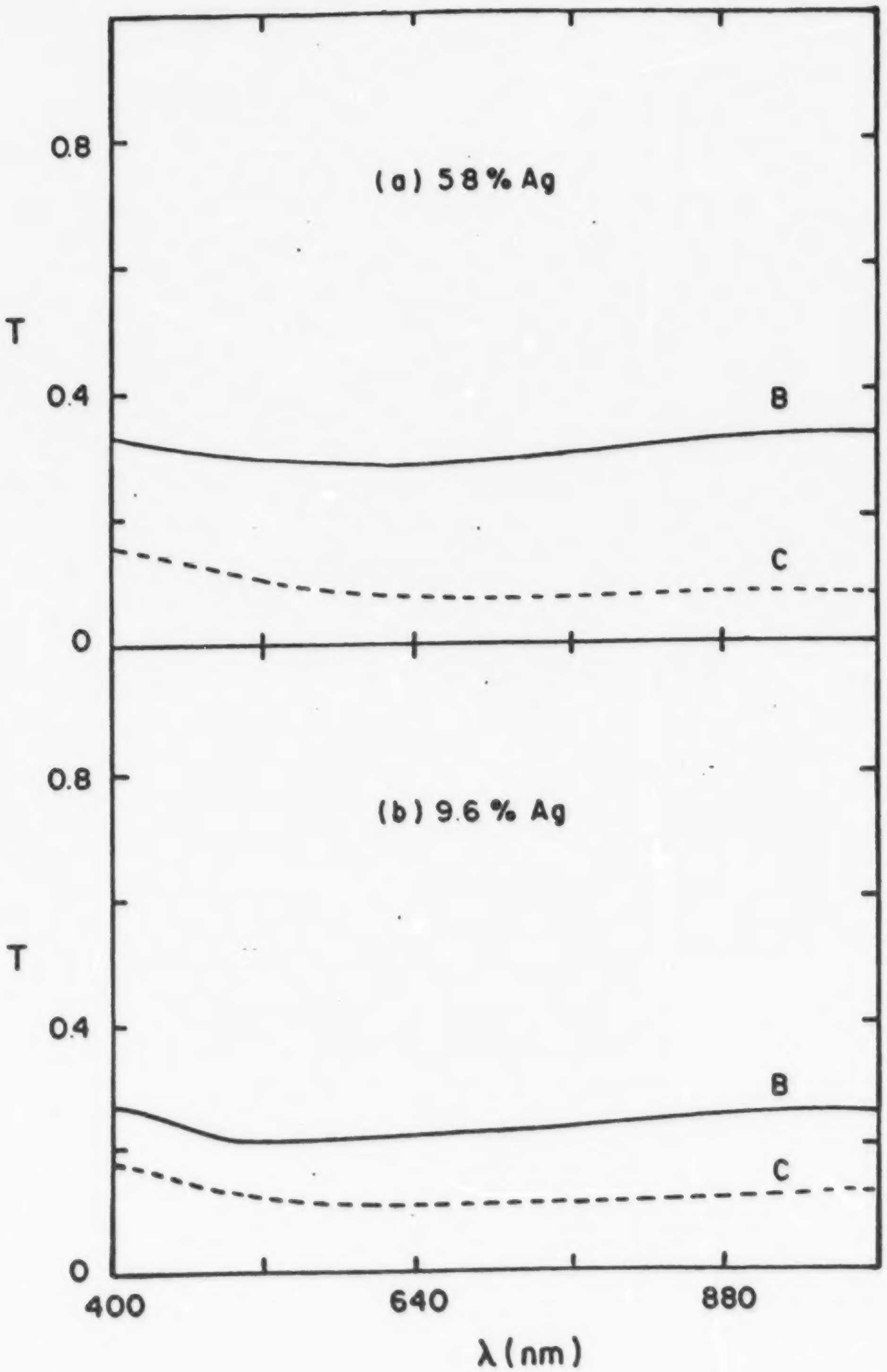

Fig. 7.10: Bleached (B) and colored (C) state transmission of Ag-WO_3 cermets with (a) Q = 5.8% Ag, (b) Q = 9.6% Ag. Applied voltage = 2V.

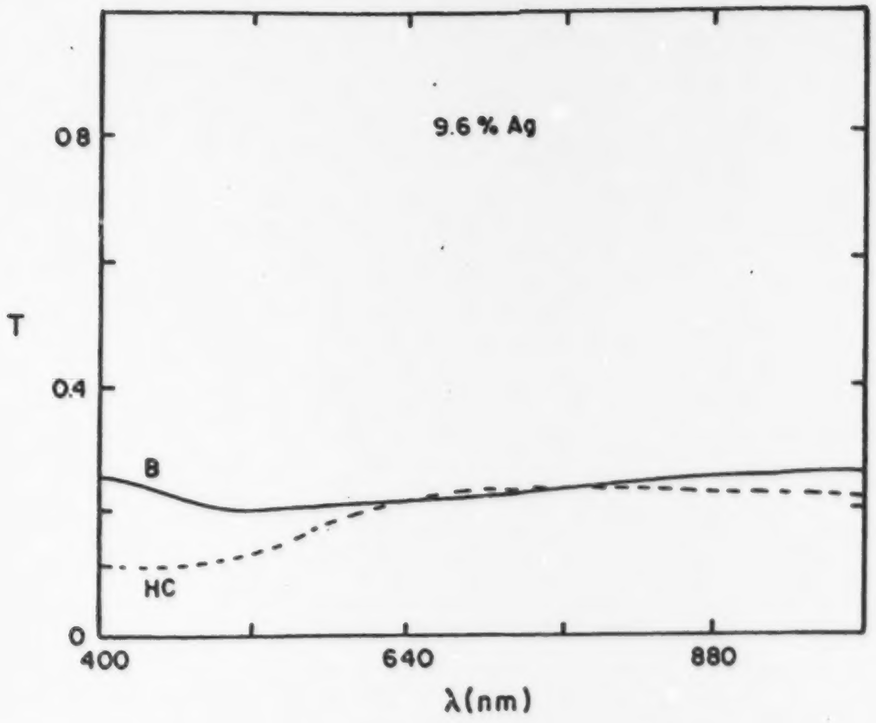

Fig. 7.11: Bleached (B) and heavily injected (HC) state transmission of Ag-WO_3 cermet with Q = 9.6%. Applied voltage = 3V.

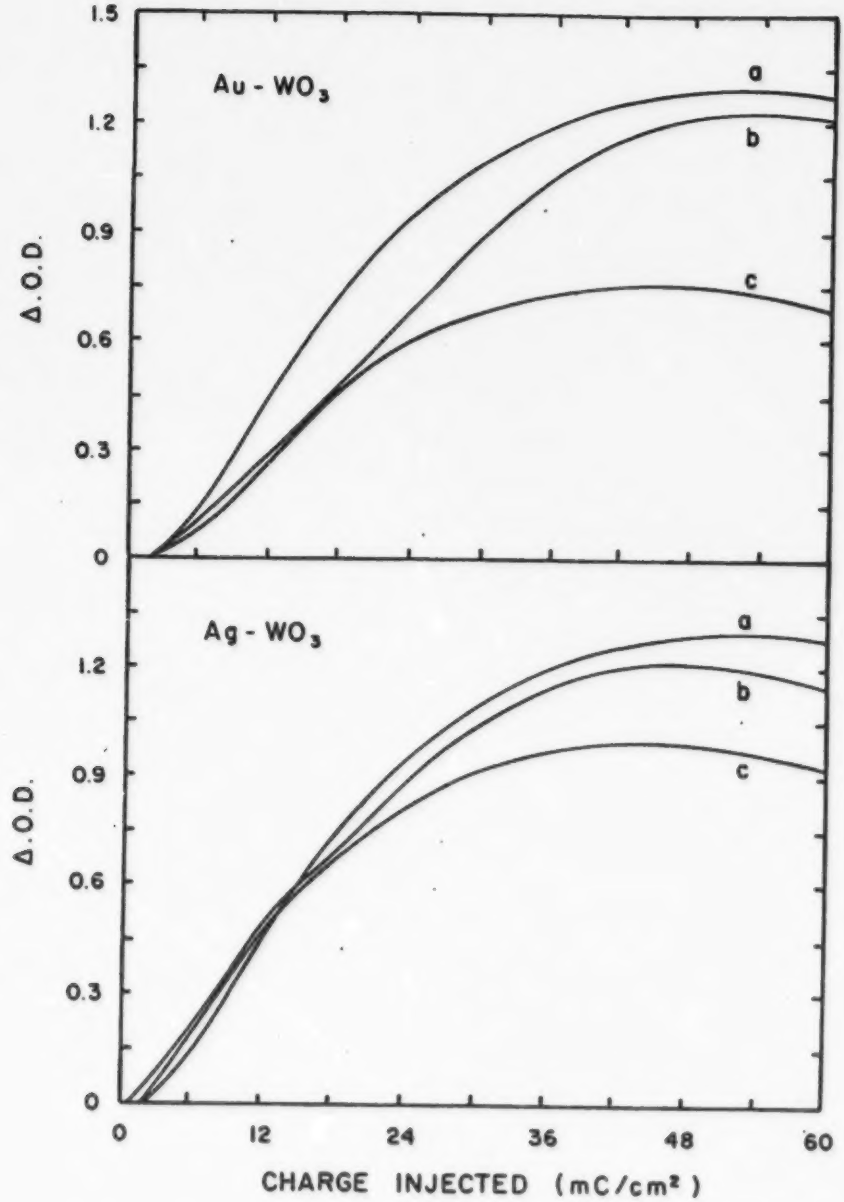

Fig. 7.12: Change in optical density (Δ O.D.) as a function of injected charge for Au:WO$_3$ films with a) Q = 0% Au, b) Q = 2.4% Au, c) Q = 8.7% Au and for Ag:WO$_3$ films with a) Q = 0% Ag, b) Q = 2.4% Ag and c) Q = 9.6% Ag.

cermets is much diminished. With increasing metal composition in WO_3, i) there is a decrease in the maximum ΔO.D achievable before the irreversiblity onsets and ii) the charge density (Q) value at which the maximum ΔO.D is attained decreases. This is due to the fact that for a fixed number of injected charge and film thickness, the ratio of Li^+ to W sites decreases with increasing metal concentration, thus rendering the ionic injection "heavy" in films with higher metallic content.

$Sn:WO_3$

For this study three compositions of Sn in WO_3 were used: 2.4%, 4.8% and 9.1%. For these cermets the optical behavior was different from both $Ag:WO_3$ and $Au:WO_3$ cermets. The substrate temperature used for these depositions was 200°C. The spectral measurements were carried out in the range of 400 nm to 1500 nm. Electrical measurements of these cermets were carried out in-situ using four point method with Au:Cr electrodes. Electrochromic coloration was carried out using an electrochemical cell containing 1M $LiClO_4$ in PC or 10% H_2SO_4 aqueous solution for Li^+ or H^+ injection, respectively. Other conditions are similar to those of $Ag:WO_3$ and $Au:WO_3$.

In Fig. 7.13 are given the transmission spectra of pure WO_3 film and $Sn:WO_3$ cermets deposited on glass substrates in the spectral region between 400 nm and 1500 nm for various Sn filling factor. The pure WO_3 film exhibits a fairly good transmission throughout the spectral region examined and has a very light bluish

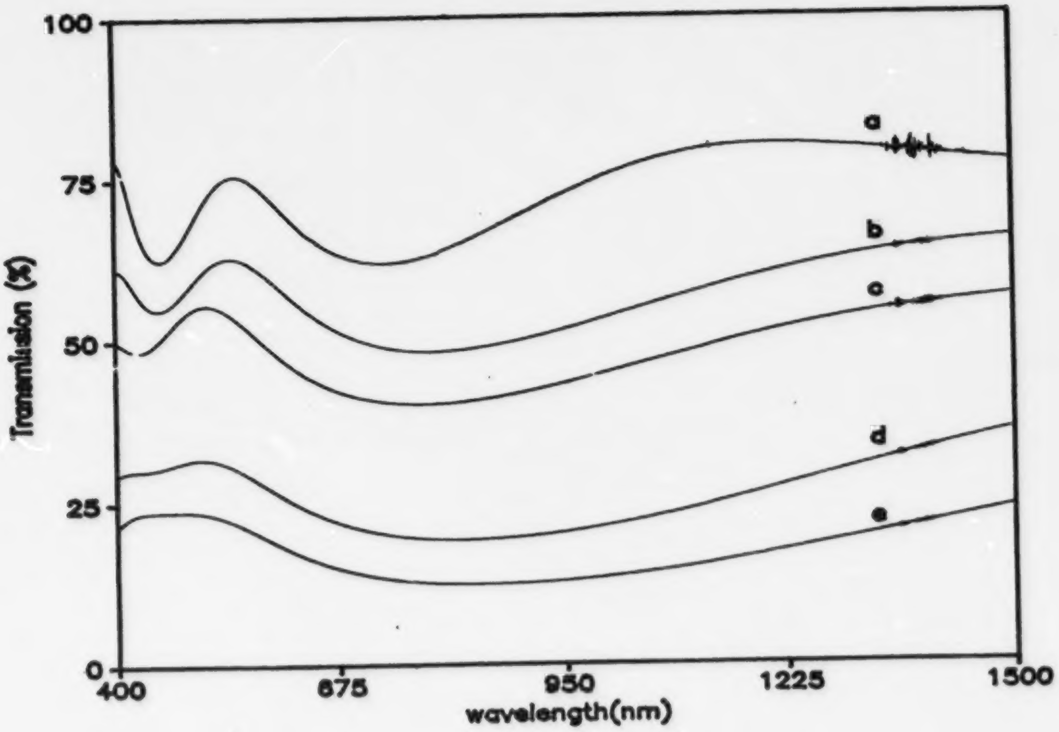

Fig. 7.13: Transmission spectra of Sn:WO$_3$ composites with Sn concentration of (a) 0%, (b) 2.4%, (c) 4.8% and (e) 9.1%.

appearance. With increasing Sn content in the WO_3 matrix, there is a decrease in the overall transmission of these samples. However, unlike other cermets[71,72], there is no absorption structure developing in the visible region. Even in the film with a Sn concentration of 9.1% no such structure appears. Hence, the behavior is not of a system in which optically absorbing metal particles are suspended in a dielectric matrix. The fairly good transparency maintained by these films in the visible region indicates the possible formation of tin oxide in the WO_3 matrix. The results of the in-situ measurement of electrical resistivity of these samples is given in Table 7.1. Our pure WO_3 sample has a resistivity value which is significantly lower than those reported (10^8 - 10^9 Ω-cm) for thermally evaporated amorphous WO_3 samples[60-62]. With the addition of tin in the WO_3 matrix, the resistivity decreases further by several orders as can be seen from the Table. Even the film with 2.4% tin exhibits a rather low resistivity indicating that in addition to the formation of tin oxide, there is possibly a structural change in WO_3, bringing down the resistivity by such a tall order. Such an improved conductivity and the fairly good transparency as exhibited for example by 2.4% Sn film can be of great significance in the fabrication of electrochromic systems. However, an improved electronic conductivity is invariably accompanied by limited electrochromic performance of the systems[62].

TABLE 7.1

Samples	Electrical resistivity (ρ)
WO_3	1.47×10^4 Ω-cm
Sn: WO_3 (2.4% Sn)	0.387 Ω-cm
Sn: WO_3 (4.8% Sn)	0.107 Ω-cm
Sn: WO_3 (9.1% Sn)	0.039 Ω-cm

In order to examine the electrochromic performance of these composites, H^+ and Li^+ ion injections have been carried out in these films, both in the low and high charge density range. As discussed earlier, with both pure and mixed WO_3 films, we have found that there exists a limit to the charge density of Li^+ ions that can be injected into WO_3 matrix. Beyond this limit, irreversible changes occur in the film and an actual decrease in the optical density can be seen. Such an occurence seems to be due to the formation of lithium tungstate ($Li_2 WO_4$). We had proposed that a similar effect must be the origin of the anomalous behavior reported by Sichel and Gittleman under the prolonged injection of protons. To verify this effect, we have carried out heavy injection of lithium and protons in our tungsten oxide film and its composites with tin. In Figs. 7.14 and 7.15 are given the variation of optical density change

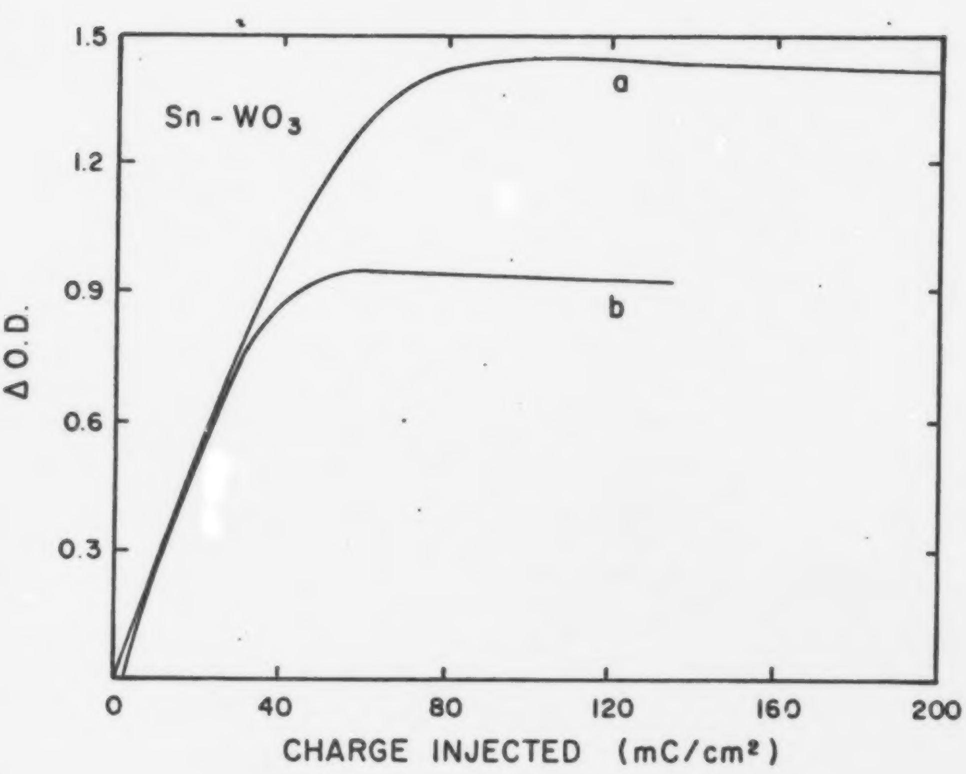

Fig. 7.14: Change in optical density (Δ O.D.) as a function of the injected charge (Q) for proton injection for pure WO_3 composite of 4.8% Sn (b).

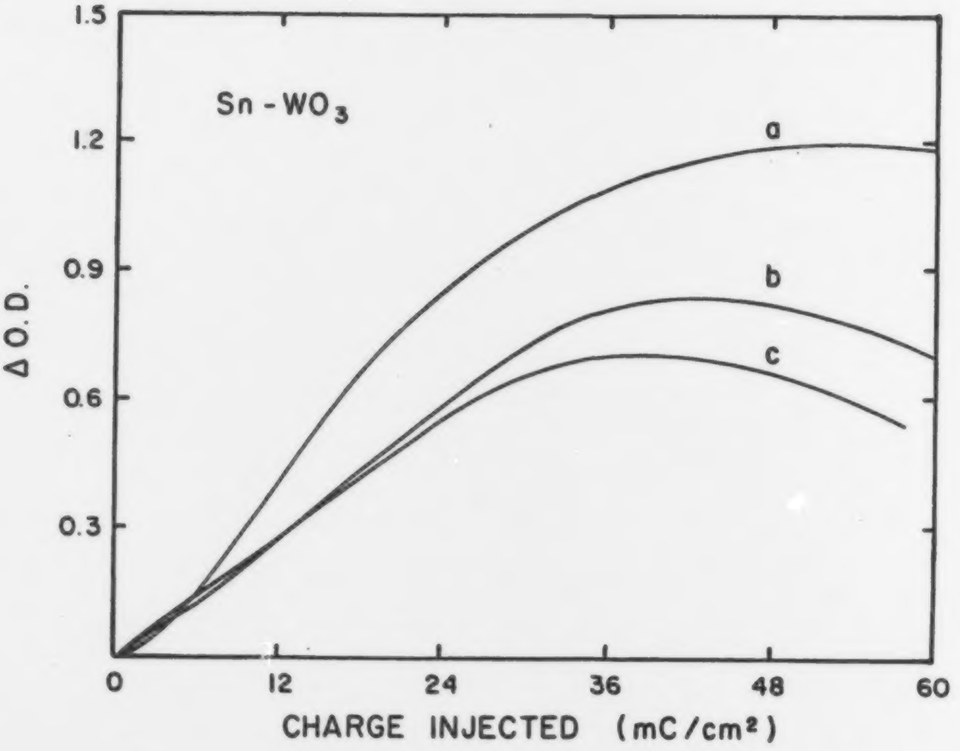

Fig. 7.15: Change in optical density (Δ O.D.) as a function of the injected charge (Q) for lithium ion injection for pure WO_3 film (a) and Sn: WO_3 composites of 2.4% Sn (b) and 4.8% Sn (c).

(ΔO.D.) as a function of injected charge (Q) for proton and lithium ion injection, respectively. For proton injection (Fig. 7.14), there is a linear increase in ΔO.D. initially with injected charge for both WO_3 (a) and Sn composite (b). For the pure WO_3 film this linear variation begins to change around the Q value of 80 mC/cm^2. Under continued injection of protons, there is almost no increase in ΔO.D. beyond this value and eventually, ΔO.D. begins to decrease slightly. Hence, a maximum ΔO.D. value was found in our WO_3 film for a charge density of around 90 mC/cm^2. A similar behavior is also exhibited by the Sn:WO_3 sample with an Sn composition of 4.8%. A reduced maximum ΔO.D. value of about 0.95 is achieved at a charge density as low as 70 mC/cm^2. Further charge injection could not be carried out beyond these values without inducing side reactions in the electrochemical cell. The effect of such a "reversal" of ΔO.D. under high density charge injection is more evident with lithium ions (Fig. 7.15). As described in section 7.2.1, lithium ion insertion in pure WO_3 and Sn:WO_3 composites show similar linear dependence of ΔO.D. on charge injected, initially. However, this linear relationship breaks down at a much lower charge density and ΔO.D. as compared to proton injection. A maximum ΔO.D. value of 1.2 is found for Li^+ injection around a charge density of 50 mC/cm^2. Then, ΔO.D. begins to drop rather steeply leading to a golden yellow appearance of the sample. The effect is even more severe in case of Sn:WO_3 composites as shown in Figs. 7.15(b,c) for samples containing 2.4% and 4.8% of tin. Hence we can clearly see the shift in maximum ΔO.D. which is attained at decreasing charge injected values (Q) and with increasing Sn concentration in WO_3

matrix. It is also found that in all our samples injected with Li^+ beyond the maximum ΔO.D. value, the color change to golden yellow is irreversible. This indicates a possible phase change from $Li_x WO_3$ $(0 < x < 1)$ to Li_2WO_4, hence rendering the films more transparent. Thus, Figs. 7.14 and 7.15 indicate once again clearly that there exists a limit to the charge density that can be injected to achieve reversible electrochromic coloration. The effect of charge injection beyond this limit is more drastic under Li^+ insertion than proton injection. In our pure WO_3 sample, the maximum Li^+ ion density that can be injected without inducing irreversibility of electrochromic process of the system seems to be around 50 mC/cm^2. The same limit for proton injection is around 90 mC/cm^2. This limit is drastically cut down upon the inclusion of tin in the WO_3 matrix. Hence, attention has to be paid to this limiting factor for operating the electrochromic systems reversibly.

In Fig. 7.16 is shown the tranmission spectra of colored (b) and "as deposited" (a) sample of WO_3. This film was colored to a maximum ΔO.D. by proton injection. It can be seen that such a film deposited on ITO coated substrate exhibits good electrochromic coloration change throughout the spectral region examined. In Figs. 7.17 and 7.18 are given similar curves for colored and "as deposited" $Sn:WO_3$ samples with 2.4% Sn under proton and Li^+ ion injection, respectively. In both cases, the coloration was carried out to near maximum ΔO.D. value without rendering the system irreversible. A good change in coloration is obtained in both cases, although the degree of change is higher under proton

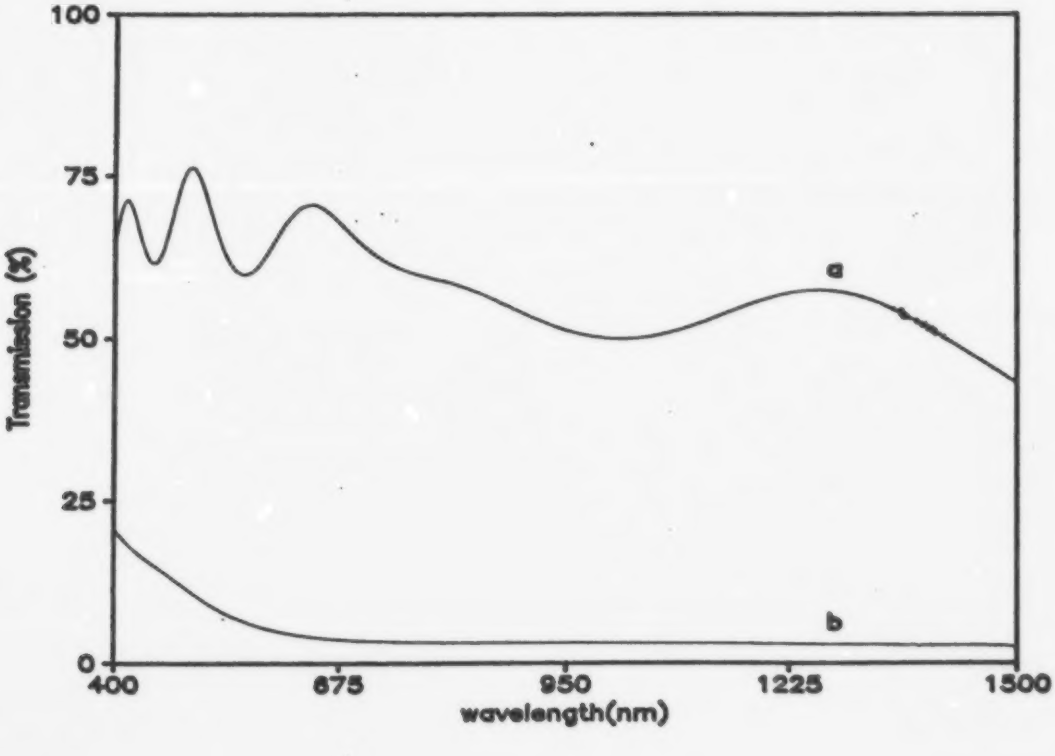

Fig. 7.16: Transmission spectra of "as deposited" (a) and proton injected (b) WO_3 film on ITO coated substrate. The spectra is taken near maximum Δ O.D. value.

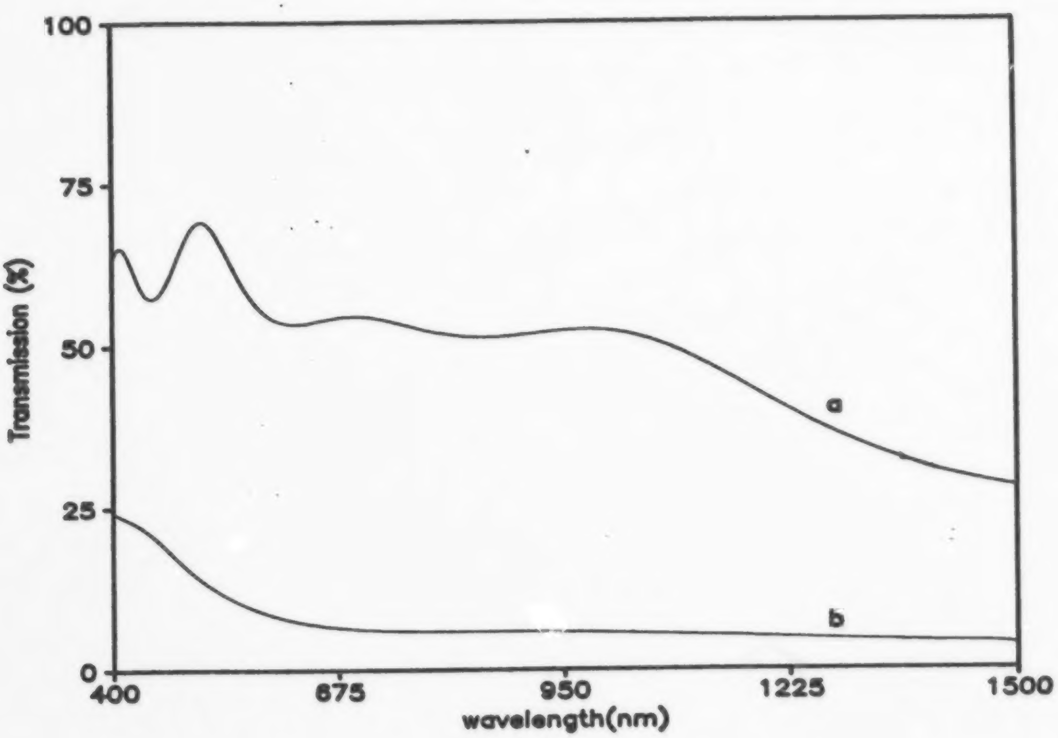

Fig. 7.17: Transmission spectra of "as deposited" (a) and proton injected (b) Sn:WO_3 composite of 2.4% Sn on ITO coated substrate.

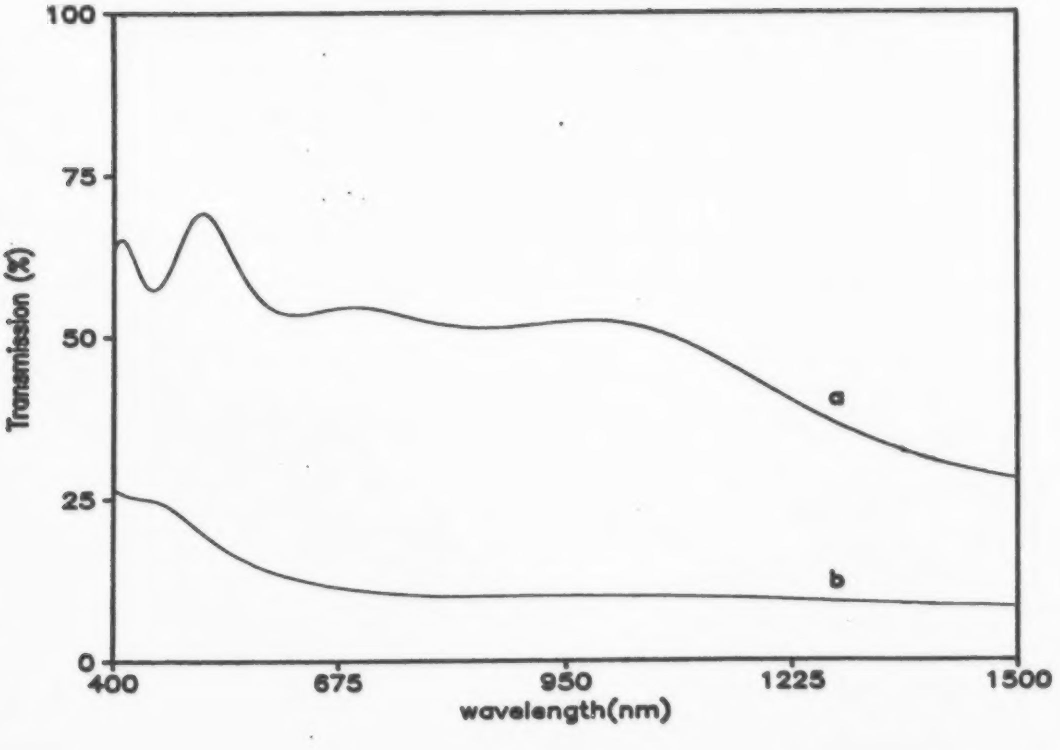

Fig. 7.18: Transmission spectra of "as deposited" (a) and lithium ion injected (b) Sn:WO_3 composite of 2.4% Sn on ITO coated substrate.

injection. The coloration change in the visible region is higher in both cases than in the infrared region due to the lower transmission of the sample in this region in the "as deposited" state. This shows that a fairly acceptable electrochromic performance is exhibited by WO_3 films doped with slight amounts of tin. Such a film not only exhibits a fairly good electrochromic coloration but also a highly enhanced electronic conductivity and good transmission in the "as deposited" state. The employment of such a layer in the dual capacity of the electrochromic (EC) and transparent conductor (TC) would simplify the fabrication of the multilayered electrochromic system. However, further improvements in the overall transmission of such composites may be necessary. Such systems exhibiting mixed ionic and electronic conduction are of importance not only for EC systems but for solid state batteries too.

8. INORGANIC ION CONDUCTORS

Solid state materials exhibiting ion conduction properties are usually referred to as "solid electrolytes", "fast ion conductors (FIC)", "superionic solids" or simply as "ion conductors", depending on the author's preference or the magnitude of electrical conductivity. Since the pioneering work by Yao and Kummer[75] in 1967 on sodium conduction in β-aluminas, a large number of studies have been made on alkali ion conduction in inorganic solids. Applications of these conductors can be found in various areas such as solid state batteries, fuel cells, electronic displays or memory devices. More recently, in the early 80's, suggestion of applying electrochromic (EC) materials to the fabrication of smart windows (SW) has prompted increased interest in ion conductor studies, especially those aiming at finding transparent ion conductors.

Unfortunately, although a large number of works can be found on inorganic ion conductors in the last 20 years, few studies have dealt with optical properties of those conductors. Usually, only a mere observation on the conductor's color or general appearance is made in published works, unless the optical studies have been conducted on the switching device itself, including the electrochromic and other layers composing the smart window. This section is thus more directed toward the electrical properties of ion conductors found to be suitable for EC devices application, with some emphasis on SW.

8.1 General considerations

The following characteristics should be found in ion conductors sought for SW application:

(a) An ion conductivity preferably higher than 10^{-7} S/cm at room temperature. Although for display devices, the ion conductivity should be higher than 10^{-4} S/cm for good response times (at least a fraction of a second), with SW, coloring and bleaching times of several minutes can be allowed;

(b) The transference number t_i should be close to unity

$$t_i = \sigma_i / \sigma \approx 1$$

where $\sigma = \sigma_e + \sigma_i$ is the total conductivity consisting of the electronic σ_e and the ionic σ_i components;

(c) The electrical resistivity should be high, preferably greater than 10^{12} Ω-cm at room temperature;

(d) The ion conductor should be chemically compatible with other layers (WO_3, Nb_2O_5...) used in solid-state devices;

(e) Ideally the ion conductor should be easy to fabricate in thin film form, exhibiting high mechanical strength and high optical transmission properties (e.g., comparable to those of indium-tin oxide used as transparent electrodes in SW).

A large number of conducting solids show transport properties for cations such as H^+, Li^+, Na^+, K^+, Ag^+ and Cu^+. Anions can also be the ionic species but while many ions (F, Cl, Br, I, O^2) can be considered, good anion conductors at room temperature are only found for F. This is partly due to the fact that F has the smallest size of the halide ions, and also, as compared to O^2, a lower electric charge and less covalent bonding.

A perfectly ordered crystalline ionic solid would not allow the transport of ions. Defects are needed and the two types mostly responsible for ion conduction are the Schottky and Frenkel defects. The thermally activated diffusion process involves the free energy required for an ion to jump to a neighbouring, energetically equivalent lattice site. Phenomenologically, the ionic conductivity has the form of an Arrhenius equation[76]

$$\sigma_i = (A/T)\ \exp(-E_a/kT) \qquad (1)$$

where T is the absolute temperature, k the Boltzmann constant, A the pre-exponential factor and E_a the effective activation energy. A and E_a in general do not vary with temperature.

Unless a phase transition is involved, variations of the ionic conductivity with temperature are generally governed by Eq. (1), i.e. when log (σ_i) is plotted against T^{-1}, one will find a straight line with a characteristic slope for each material. Normally, the ionic conductivity would increase with increasing temperature. If an ion conductor is found suitable at room temperature, any heating incurred during the use of SW is expected to enhance the ionic conductivity and hence, the response time of the devices.

Studies of ion conductivity at temperatures lower than room temperature are less common. One such work has been done by Owens *et al.*[77] for $RbAg_4I_5$, investigating the low temperature degradation of the ion conductor. At -15 °C, a significant increase in resistance was observed, suggesting that some of the $RbAg_4I_5$ disproportionated into the more resistive AgI and Rb_2AgI_3 phases.

When the theory of random walk is applicable, the conductivity for an ion conductor is expressed by[76]

$$\sigma_i \approx \gamma \ (Nq^2/kT) \ c \ (1-c) \ \ \ell^2 \ \nu_0 \ \exp(-\Delta H_m/kT) \qquad (2)$$

where c is the concentration of the mobile ions of charge q and per N number of available sites, ℓ the mean jump length, ν_0 the jump frequency, and ΔH_m the motional enthalpy. The factor γ is given by $(f/6) \exp(\Delta S_m/k)$, with (f) a geometrical correlation factor determined by the jump path configuration and ΔS_m is the entropy.

It is argued that for high ionic conductivity, the product c(1-c) should have a reasonable value and ΔH_m should be small. For such conditions to be met, normally the working ion species are monovalent and weakly bound to the solid matrix, and the number of available sites must largely exceed the number of carriers present. Other criteria for high ionic conductivity as well as theoretical approaches for ion conduction in solids, are discussed by many authors[76,78,79].

8.2 H^+ ion conductors

Early studies of all-solid-state devices have used hygroscopic films such as MgF_2 and LiF as a solid electrolyte permitting proton and electron injection into cathodic EC materials. As compared to other cations, protons exhibit the highest mobility in solids, and response times in EC devices are relatively short when H^+ ion conductors are used as electrolytes. Following Deb's pioneering work[80], a solid state device has been proposed by the same author and Shaw[81] utilizing CaF_2 and MgF_2 dielectric thin films as solid electrolytes.

In this type of device, the water in the dielectric layer is dissociated by the voltage, creating protons necessary for the coloration of cathodic EC materials. Deneuville _et_ _al._[33] have studied in detail the operation of a device based on WO_3 and MgF_2. The amorphous WO_3 film and MgF_2 layer were deposited by reactive evaporation at pressures between 5×10^{-6} and 5×10^{-3} torr and a temperature of 50 °C. Yoshimura _et_ _al._[19,82] investigated the gas adsorption at the WO_3-MgF_2 interface and its effects on coloration characteristics of the EC device. The moisture in the ambient atmosphere is believed to contribute to more than half the optical density of the devices. The water would mainly be dissociated near the top semi-transparent Au electrode, providing protons for the coloration cycle. With a relatively high coloration potential (2.5 V), bubbles were observed at this electrode and attributed to O_2 gas generated by the electrolysis of water. This certainly contributed to the shortening of the device life.

Other works have examined the suitability of ZrO_2 (Ref. 83), Ta_2O_5 (Ref. 83), Cr_2O_3 (Ref. 84), $Cr_2O_3 \cdot V_2O_5$ (Ref. 85), SiO (Ref. 16), SiO_x (Ref. 86), SiO_2 (Ref. 87) and LiF (Refs. 12,18) as solid electrolytes. These materials were generally prepared in thin film form with a thickness varying from 0.15 to 0.50 μm. In the case of a device configuration such as

TC / a-WO_3 / a-Cr_2O_3/ TC

as previously mentionned. It is believed that both WO_3 and Cr_2O_3 undergo color changes because Cr_2O_3 is an anodic EC material, coloring with injection of OH^-. Those negative ions are generated by dissociation of water trapped in both WO_3 and Cr_2O_3.

Problems usually associated with devices made with the above dielectric solid electrolytes seem to be the dependence upon humidity in the atmosphere and the rapid deterioration of electrodes[82]. Strong electrical fields were normally needed due to the high electrical resistance at the electrode / electrolyte interface. Nevertheless, devices that could operate without significant deterioration after more than 10^6 cycles have been reported[84].

More conventional proton conductors can be found in Table 8.1. Hydrogen uranyl phosphate tetrahydrate $HUO_2PO_4 \cdot 4H_2O$(HUP) is certainly an excellent proton conductor with a conductivity of about 10^{-3} S/cm, comparable to the conductivity of acidic solutions of approximate pH 2-3. It has been used to fabricate an all-solid-state device by Howe et al.[96] and Takahashi et al.[97]. The

HUP layer was reported to be pale yellow[97] or opaque[96] depending on the preparation conditions. Interestingly, clear HUP layers of 100 μm thickness could be prepared on relatively large surfaces, exhibiting greater than 70% light transmission in the range 530-850 nm (Ref. 96). A device using HUP clear films operated for six months through 5×10^5 cycles, exceeding the lifetime of the acid solution /WO_3 cells. However, the problem of an apparent electrochemical decomposition of HUP with time has to be addressed in order to improve device durability.

Devices using phosphotungstic acid, $H_3PO_4(WO_3)_{12} \cdot 29H_2O$ (PWA), and zirconium phosphate, $ZrO(H_2PO_4)_2 \cdot 16H_2O$ (ZP), have been reported by Mohapatra et al.[98]. They had the configuration In_2O_3/ H_xWO_3/ solid electrolyte / WO_3 / In_2O_3, with the solid electrolyte being either PWA or ZP. Despite their high proton conductivity, PWA and ZP are not considered very good solid electrolytes. When in contact with H_xWO_3, reduction of PWA was observed, resulting in loss of contrast in the EC device. The dissolution rate of the WO_3 film in ZP was about 10 nm/day, comparable to that found with pure water[98]. Such dissolution rate was even higher than the one observed in some liquid electrolytes[99] (e.g. glycerin - H_2SO_4). Electrochromic effects can also be found in solid phosphotungstic and phosphomolybdic acids, and EC devices based on these materials were fabricated by Tell and Wagner[100].

The search for a proton conductor having more stable performance has led to the realization of a device consisting of indium tin oxide (ITO) / WO_3 / SPA / counter electrode, where SPA stands for $Sn(HPO_4)_2 \cdot H_2O$ prepared by the spraying method in thin film form and the counterelectrode was either metal or graphite[94]. The proton conductivity of SPA did not seem to be affected by temperature or humidity in the atmosphere. The response time of the device, although not very quick for an EC display, should be adequate for smart windows. The white color of SPA is however a limiting factor for any transmissive device.

Table 8.1. Proton Conductors

Material	Conductivity (S/cm)	Temperature (°C)	Reference
$HUO_2PO_4 \cdot 4H_2O$	4×10^{-3}	25	88
$H_8UO_2(IO_6) \cdot 4H_2O$	7×10^{-3}	25	89
H_3O^+-β''alumina	5×10^{-3}	25	90
H_3OClO_4	3×10^{-4}	25	91
$(H_3PO_4)(MoO_3)_{12} \cdot nH_2O$	3×10^{-12}	25	92
$(H_3PO_4)(WO_3)_{12} \cdot nH_2O$	3×10^{-12}	25	92
$Sb_2O_5 \cdot 4H_2O$	1×10^{-3}	RT	93
$Sn(HPO_4)_2 \cdot H_2O$	$\sim 10^{-5}$	RT	94
$Ta_2O_5 \cdot 3.92H_2O$	1×10^{-3}	25	95

RT = room temperature

Other potential materials for solid proton electrolytes include screen printed antimonic acid, $Sb_2O_5 \cdot nH_2O + Sb_2O_3$, investigated by Matsudaira _et al_.[101], and hydrous oxides such as $Nb_2O_5 \cdot nH_2O$, $Ta_2O_5 \cdot nH_2O$, $V_2O_5 \cdot nH_2O$ and $CeO_2 \cdot nH_2O$ studied by Slade *et al*.[95]. Ambient temperature conductivity was found to increase with water content and microscopic agglomerate size of the oxide. One of the promising materials is $Ta_2O_5 \cdot 3.92H_2O$ which exhibits a conductivity of 1 × 10^{-3} S/cm at 25 °C. Other conductivity studies on hydrous oxides or related systems can also be found[102-104].

8.3 LI$^+$ ion conductors

Beside proton conductors, lithium ion conductors are of great interest for EC devices. A number of those conductors are listed in Table 8.2, many of which can be prepared in thin film form. Compared to proton conductors, lithium ion conductors exhibit a lower ionic conductivity and a lower diffusion rate of ions, thus increasing the response time of EC devices. The Li^+ conductors have however the advantages of providing higher resistance to oxidation, longer memory effects and independence with respect to humidity in the atmosphere.

One of the early attempts to use lithium ion conductor in an EC device was made by Miyamura *et al.*[116]. Thin films of Li_3N were prepared by vacuum evaporation technique in nitrogen under low pressure. Lithium nitride prepared this way seems to have ionic conductivity of about 10^{-3} S/cm and a negligible electronic conductivity. The EC device performed however only for a limited number of cycles, apparently due to the instability of Li_3N in the presence of moisture in air. Lithium iodide, another good lithium ion conductor, unfortunately is also not stable in air and should be discarded unless a proper way is found to shield it.

Another attempt to find a proper electrolyte was to dope MgF_2 with lithium. This has been done by Yoshimura et al.[117] by heating Li_3N at a temperature above 1000 °C to decompose it into Li and N_2. The Li atoms are thus deposited on MgF_2 and they diffuse into it. The EC device, whose dimensions were not given, had the following configuration

ITO / WO_3 / Li-MgF_2 / Pd(electrode) / MgF_2(protecting layer)

It exhibited excellent coloration and bleaching responses (respectively 100 ms and 200 ms) but after repeated operation spontaneous coloration increased and bleaching was impaired. The disappearance of Li trapping sites in the MgF_2 was assumed responsible for the unstable operation.

Yoshimura et al.[118] also proposed another lithium ion conductor, Li_2WO_4, prepared by vacuum deposition at 10^{-6} torr. The device, of unspecified dimensions, exhibited very quick response (ΔO.D. = 0.3 in 50 ms in coloration, where O.D. stands for optical density) and showed little deterioration after 10^4 cycles. In spite of this, spontaneous coloration was often observed and the authors suggested some ways to suppress this undesirable coloration effect.

Studies by Oi and co-workers provided many good candidates for lithium ion conductors[106,107,110]. One of the first materials proposed was $LiAlF_4$ prepared in thin film form[106]. These amorphous films exhibit an ionic conductivity of 1×10^{-6} S/cm and a very low electronic conductivity ($< 10^{-11}$ S/cm). They are also transparent and non hygroscopic and are thus quite suitable for SW applications. A device using $LiAlF_4$ as a solid electrolyte has been proposed by Oi et al.[119], while another work based on the materials WO_3 / $LiAlF_4$ / $2Li_2O \cdot 4FeO \cdot 7WO_3$ showed fairly rapid coloration time (0.5 s) and performed for 10^6 cycles of coloring and bleaching[120]. Recently however, Seward et al.[112] remarked that such films, if thermally deposited, would have a tendency to crystallize and crack.

Table 8.2. Lithium Ion Conductors

Material	Conductivity (S/cm)	Temperature (^oC)	Reference
$LiAlCl_4$	1.2×10^{-6}	25	105
$LiAlF_4$	$\sim 10^{-6}$	RT	106
$LiF+AlF_3$(5-16%)	$\sim 10^{-6}$	RT	107
$LiF+NiF_2$(0.2-18%)	$\sim 10^{-6}$	RT	107
$LiI+CaF_2$(2%)	1.0×10^{-5}	30	108
$LiI(+CaI_2)$	$1.8\text{-}7.5 \times 10^{-6}$	30	108
$LiI+Al_2O_3$(40%)	1.2×10^{-5}	25	109
Li_2MgAlF_7	7×10^{-7}	RT	110
$LiAlSi_2O_6$	1.4×10^{-5}	25	111
$LiAlSiO_4$	4.7×10^{-5}	25	111
Li_3N(pure)	3.7×10^{-8}	25	105
LiN(96%)	3.0×10^{-7}	25	105
Li_3N(Li-rich)	2×10^{-4}	25	105
$LiNbO_3$	$\sim 10^{-7}$	RT	112
Lithium β-alumina	1.3×10^{-4}	25	113
Lithium sodium β-alumina	5×10^{-3}	25	114
$LI_{3.6}Si_{0.6}P_{0.4}O_4$	$\sim 10^{-6}$	25	115

RT = room temperature

Other materials in thin film form proposed by Oi[107] were obtained by addition to LiF of components such as NiF_2 and AlF_3 which have the effect of increasing considerably the conductivity of LiF. Samples with composition $mLiF \cdot nAlF_3$ and $mLiF \cdot nNiF_2$ with (m/n) between 5/3 and 1/1 can exhibit room temperature conductivity of about 10^{-6} S/cm, i.e. six orders of magnitude larger than that of LiF alone. Compositions such as $Li_5Al_3F_{14}$ and Li_2NiF_4 were cited. Interesting results were also obtained with addition of CrF_3 and ScF_3 to LiF (Ref.121).

Thin films of Li_2O-B_2O_3 have been studied by Ito et al.[122], exhibiting ionic conductivity of 1 × 10^{-7} S/cm at room temperature. The conductivity increased with Li content and reached a maximum value near the composition $3Li_2O \cdot B_2O_3$. The films were prepared by thermal evaporation with mixtures of Li_2O and B_2O_3. They were colorless, transparent and slightly hygroscopic.

Works on RF-sputtered glassy films of $LiNbO_3$ and $LiTaO_3$ have been recently conducted by Seward et al.[112] who reported that the $LiNbO_3$ films were mechanically very strong, exhibiting an ionic conductivity of about 10^{-7} S/cm while the electronic resistivity was quite high. Prototypes of SW have been studied, showing good transmission modulation, acceptable switching time and good open circuit memory. The configurations used were

$$ITO / WO_3 / LiNbO_2 / V_2O_5 / In_2O_3$$

and

$$ITO / WO_3 / LiNbO_2 / In_2O_3 / ITO$$

where all the films were RF-sputtered with the exception of V_2O_5 which was thermally deposited. More works are however needed in order to establish the applicability of such devices in SW fabrication.

Other investigations on lithium-conducting glasses include studies by LeVasseur et al.[123] who prepared thin glassy films by sputtering and evaporation, work by Miyauchi et al.[124] who researched sputtered films of $Li_2O-SiO_2-ZrO_2$ and Boilot et al.'s[125], proposing the gel method to prepare $Li_2O-Al_2O_3-SiO_2-P_2O_5$. In particular, this latter work might form the basis of economical preparation of large area conducting surfaces with most interesting properties.

Ceramic lithium ion conductors[113,114] on the other hand show the most interesting values for ion conductivity but thin film fabrication of these materials is difficult.

8.4 Potassium and sodium ion conductors

Apart from lithium ion conductors which seem to be preferred for EC device development, other useful alkali ion conductors are the sodium and potassium ones. Some of the common conductors are listed in Table 8.3. Green and Kang[130] used sodium β-alumina as a solid electrolyte for their EC cell which consisted of ITO / WO_3 / Na-β-alumina / Na_xWO_3/ ITO. The sodium β-alumina was in the form of a white opaque wafer about 0.8 mm thick. It served as a substrate on which other materials in the EC device were deposited. Care was taken not to expose the sodium ß-alumina for too long in air as it could absorb water in the atmosphere and have its properties altered. When polished to a smaller thickness (0.44 mm) the ceramic wafer can transmit 30% in the visible[131]. The usefulness of both sodium and potassium alumina will however remain limited for SW applications unless successful methods for thin film preparation are found[132].

Another ceramic sodium ion conductor already used for EC display devices is Nasicon or $Na_{1+x}Zr_2Si_xP_{3-x}O_{12}$ (Ref. 127). This material apparently is less sensitive to moisture in air than sodium β-alumina.

Table 8.3. Sodium and Potassium Ion Conductors

Material	Conductivity (S/cm)	Temperature °C	Ion	Reference
$NaAlCl_4$	3.5×10^{-7}	25	Na^+	105
$NaSbO_3$	$\sim 1.4 \times 10^{-5}$	25	Na^+	126
$NaTaWO_6$	$\sim 2 \times 10^{-5}$	25	Na^+	126
$NaTa_2O_5F$	$\sim 4 \times 10^{-5}$	25	Na^+	126
$2Na_{0.3}Nb_2O_5$	$\sim 4 \times 10^{-6}$	25	Na^+	126
$Na_{1+x}Zr_2Si_xP_{3-x}O_{12}$	$\sim 3 \times 10^{-4}$	-	Na^+	127
$Na_{0.5}In_{0.5}Zr_{0.5}S_2$	$\sim 10^{-4}$	27	Na^+	128
$Na_{0.72}In_{0.72}Sn_{0.28}O_2$	10^{-7}	27	Na^+	129
Sodium β-alumina	1.4×10^{-2}	25	Na^+	113
$K_{0.72}Se_{0.72}Hf_{0.28}O_2$	4×10^{-8}	27	K^+	129
$K_{0.72}In_{0.72}Zn_{0.28}O_2$	1×10^{-7}	27	K^+	129
$K_{0.72}In_{0.72}Sn_{0.28}O_2$	5.6×10^{-7}	27	K^+	129

8.5 Silver ion conductors

A solid state EC system using Ag^+ conductor was reported early in 1974 by Green and Richman[133]. The solid electrolyte, hygroscopic $RbAg_4I_5$, was prepared by thermal evaporation, giving a faint milky appearance. The device operated for an unspecified number of cycles but was found to deteriorate with sunlight, water vapour and excessive d.c. potentials. Some of the well-known silver ion conductors and their conductivities at room temperature can be found in Table 8.4.

Table 8.4. Silver Ion Conductors

Material	Conductivity (S/cm)	Temperature (°C)	Reference
KAg_4I_5	0.21	22	134
$RbAg_4I_5$	0.21	22	134
$Ag_{19}I_{15}P_2O_7$	0.91	25	135
$Ag_6I_4WO_4$	0.047	25	136,137
Silver β-alumina	6.4×10^{-3}	25	113

8.6 Fluorine ion conductors

For anodic electrochromic materials such as iridium oxide, rhodium oxide and nickel oxide, a proper material for solid electrolyte would be a fluorine ion conductor. An excellent review of these conductors has been recently made by Reau and Grannec[138] who suggested that fluorides can be considered the best anionic conductors and quite suitable for applications requiring materials with large electronic resistance. In Table 8.5 are shown some of these fluorine ion conductors.

Rice and Bridenbaugh[148] have investigated EC cells of configuration SnO_2 / AIROF / PbF_2 or $PbSnF_4$ / Au, where AIROF stands for an anodic iridium oxide film. PbF_2 and $PbSnF_4$ in this study were evaporated to form polycrystalline films. The devices, of unspecified working area, showed an excellent coloration and bleaching response time of the order of 0.1 s. The electrochemical half-reactions, according to Rice and Bridenbaugh, would be as follows:

$$PbSnF_4 + 2e \rightleftharpoons Pb + SnF_2 + 2F^-$$

$$\text{AIROF (bleached)} + F^- \rightleftharpoons \text{AIROF(colored)}.\,F + e$$

The device performance was however rather unsatisfactory and it operated for only 100 cycles. A possible failure mechanism advanced by the authors is the uneven formation/dissolution of lead deposits at the gold electrode. This might lead to the formation of metal dendrites penetrating the electrolyte layer, thus causing a short circuit. The search for a suitable fluoride-reversible counterelectrode is suggested for solving this problem.

Although iridium oxide is a very interesting EC material, its prohibitive cost prevents its use for large area windows. If fluorine ion conductors are to be used, it would then be preferrable to develop other EC materials such as nickel and rhodium oxides.

Table 8.5. Fluorine Ion Conductors

Material	Conductivity (S/cm)	Temperature (°C)	Reference
$Pb_{0.88}IN_{0.12}F_{2.15}$	$\sim 2 \times 10^{-4}$	25	140
$Pb_{0.75}Sb_{0.25}F_{2.25}$	$\sim 5 \times 10^{-4}$	25	141
$Pb_{0.90}Zr_{0.10}F_{2.20}$	$\sim 10^{-4}$	25	142
$K_{0.50}Bi_{0.50}F_2$	$\sim 2 \times 10^{-4}$	25	143
$Rb_{0.50}Bi_{0.50}F_2$	$\sim 4 \times 10^{-4}$	25	143
α'-$PbSnF_4$	$\sim 10^{-3}$	25	144
$Bi_{0.94}K_{0.06}F_{2.88}$	$\sim 7 \times 10^{-4}$	25	145
$TlSn_2F_5$	$\sim 6 \times 10^{-4}$	25	146
$NH_4Sn_2F_5$	$\sim 5 \times 10^{-4}$	25	147
Tl_2ZrF_6	$\sim 2 \times 10^{-4}$	25	147

8.7 Conclusion

Inorganic ion conductors have been reviewed with some emphasis on SW applications. For transmissive devices it is necessary to explore and develop techniques for preparing thin films of solid electrolytes. Beside resistive heating, sputtering and electron beam evaporation, it would be worthwhile to also consider methods such as the gel and spraying processes. Thanks to recent progress in ion conductor research as attested by the large number of publications during the last decade, especially in the area of lithium ion conductors, the future for all-solid-state SW looks promising. Much remains however to be done in optical, electrical and mechanical characterization of such solid electrolytes, when the ion conducting material is actually integrated into the EC device.

9. ION CONDUCTING AND ION STORAGE LAYERS AND THE PROTOTYPE EC SYSTEM

As already enumerated in the earlier sections, besides the EC layer both the fast ion conducting (FIC) and counter electrode or ion storage (CE) layers are important for the stable operation of an EC device. We have carried out the study of optical and electrical properties of several materials in thin form to test their suitability for application in EC devices as FIC and CE layers.

In this section we have discussed in detail these properties which are suitable for their utilization in EC device. The fabrication and performance characteristics of the prototype EC device are also discussed in this section.

9.1 Ionic conductors

This layer separating the EC layer and the CE should be a very good electrical insulator in addition to being a good ionic conductor to maintain an electric field across the device for EC operation. It should also be a transparent material. For the fabrication of our all solid EC device we have studied two materials deemed suitable for this application. These are lithium aluminum fluoride ($LiAlF_4$) and lithium borate ($LiBO_2$). $LiAlF_4$ is an amorphous film exhibiting an ionic conductivity of $\leq 10^{-11}$ S/cm. It also exhibits a very high transmission. The transmission spectra of a 100 nm thick $LiAlF_4$ film prepared by thermal

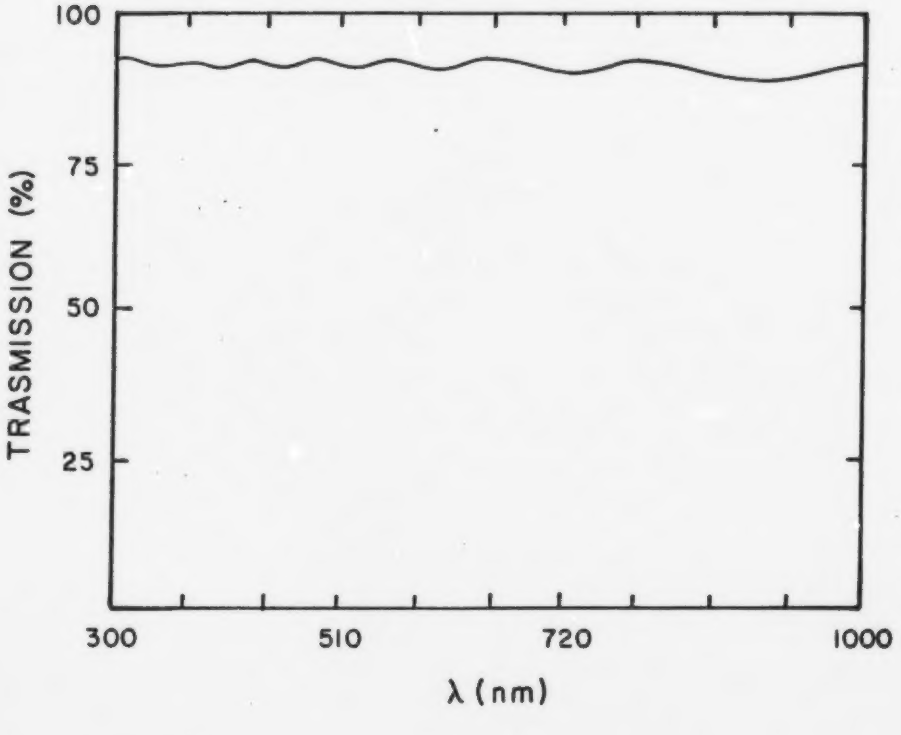

Fig. 9.1: Transmission of 100 nm thick $LiAlF_4$ film deposited on glass.

evaporation on glass substrate is shown in Fig. 9.1. $LiAlF_4$ has been used by several workers in EC devices[119,120]. However, as discussed earlier some problems such as crystallization and cracking of the films deposited thermally are also reported. We also found that the films prepared by mixing 1 to 1 weight ratio of LiF and AlF_3 and by thermal deposition were fairly hygroscopic. Hence, much emphasis was not paid to $LiAlF_4$ films in the fabrication of the EC system. $LiBO_2$ has been recently studied for its ion conducting properties for utilization in solid state batteries[149]. Thermally deposited thin films of $LiBO_2$ have been found to be extremely good ionic conductors. Also, our studies of the optical properties of these films show that they have very high transmission in the visible and NIR regions of the spectrum. The study of the optical constants of our $LiBO_2$ is reported in section 6. In Fig. 9.2 is given the transmission curve for a 100 nm thick $LiBO_2$ film on glass prepared by thermal evaporation, for comparison with $LiAlF_4$ film. Unlike $LiAlF_4$ the film of $LiBO_2$ is found to be very stable even at high humidity conditions. For evaluating the electronic insulation properties of these samples we have used the Arnoldussen technique, as described below briefly. $LiBO_2$ films prepared by thermal evaporation are reported[149] to have an ionic conductivity of the order of 10^{-7} 10^{-8} Ω^{-1} cm^{-1}.

Arnoldussen technique:

This technique used for a qualitative analysis of the ionic conductivity of a film consists of a glass substrate coated with

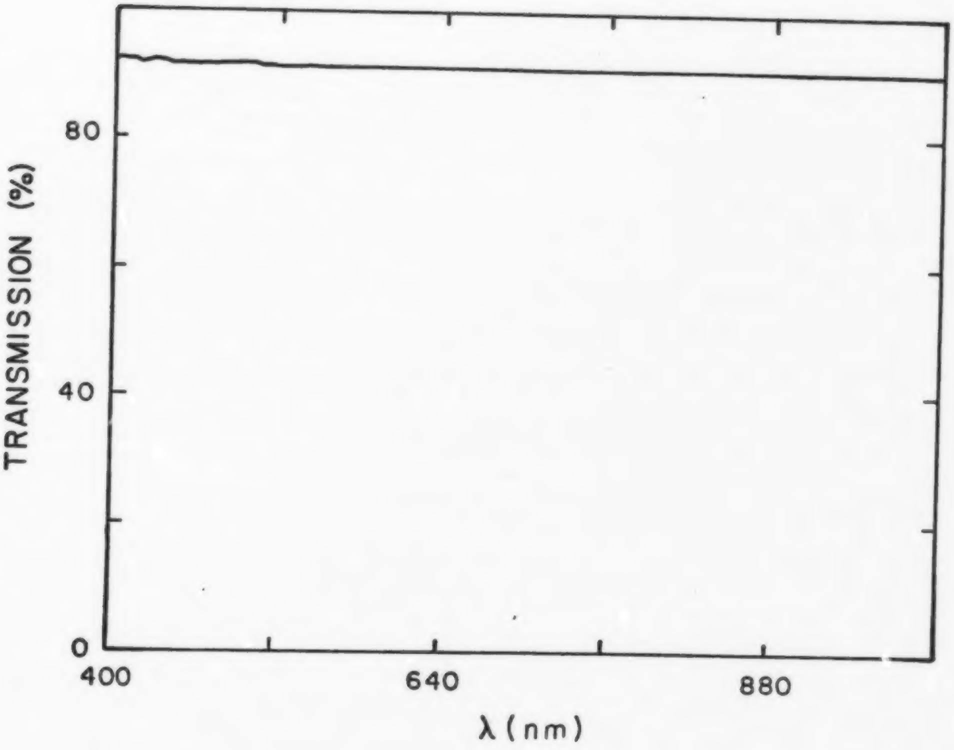

Fig. 9.2: Transmission spectra of 100 nm thick film of $LiBO_2$ deposited on glass.

a thin film of WO_3. This film of WO_3 is then covered partially by the film to be tested for conductivity i.e. $LiAlF_4$ or $LiBO_2$, as shown in the Fig. 9.3. The test is carried out in three steps to determine both the ionic conductivity and the electrical insulation of the film to be tested. In the first test a small area of WO_3 is covered with the $LiClO_4$ electrolyte. Then a zinc rod is held in the middle of this liquid puddle touching the WO_3 film. Due to the reaction at the zinc electrode, $Zn \rightarrow Zn^{2+} + 2\acute{e}$, free electrons are released into WO_3. These electrons are simultaneously charge compensated by the Li^+ ions diffusing into WO_3. Due to the formation of Li_xWO_3 a coloration front appears around the Zn rod. This front extends outward at the rate of diffusion of electrons in WO_3 till it reaches the boundary of the liquid puddle. This first step assures the working of this method.

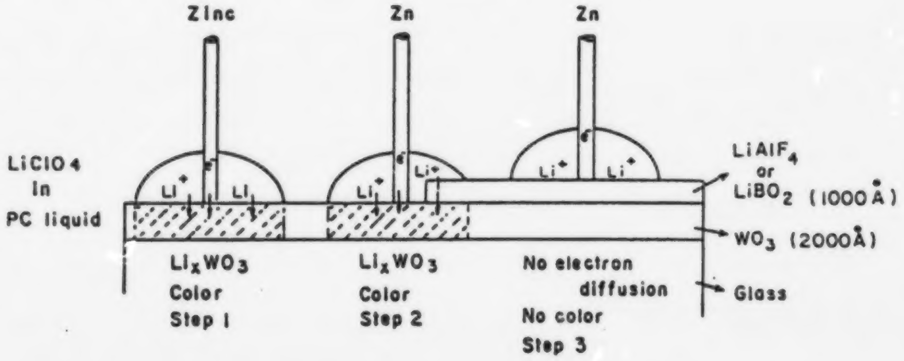

Fig. 9.3: The Arnoldussen technique

In the second step the $LiClO_4$ liquid puddle is placed in such a way that it covers WO_3 on one side and $LiAlF_4$ or $LiBO_2$ on the other as shown in the figure. Then the zinc rod is placed in the middle touching the WO_3 surface. In this case the color front moves outward from the zinc rod as before at the rate of diffusion of the electrons in WO_3. This color front moves through the area under the film to be tested only if the film is an ion conductor. We saw both in the case of $LiAlF_4$ or $LiBO_2$ that the color front moved into the area under these films at the same rate as in WO_3 showing qualitatively that both these films are good lithium conductors.

In the final step the liquid puddle and the zinc rod were placed completely over the $LiAlF_4$ or $LiBO_2$ film so that there was no direct injection of electrons into WO_3. In this case no coloration was observed since neither $LiAlF_4$ nor $LiBO_2$ transport electrons. Thus showing that these films, as required, are electronic insulators. Based on these observations, optical properties and physical stability, $LiBO_2$ was chosen for utilization as FIC in our EC device. To the best of our knowledge $LiBO_2$ films have never been used in EC devices.

9.2 Counter Electrode (CE) or Ion storage

In our proposed configuration of complimentary EC system the CE layer plays as important a role as the EC itself. The functional requirements on this layer are that (i) it be a good mixed (ion & electron) conductor, (ii) it should have a very low coloration efficiency compared to the EC layer, especially in the region of optical modulation required and (iii) it should be exactly reversible in electrochromic reaction with respect to the electrochromic layer, several transition metal oxide (TMO) materials with low coloration efficiency are suitable as CE or ion storage layers. These include TiO_2, Nb_2O_5, Ta_2O_5, V_2O_5, In_2O_3 etc. For the fabrication of our EC sample we have carried out the detailed investigation of Nb_2O_5 film because of (i) the ease with which the film can be prepared, (ii) its low efficiency coloration in the near infrared region and (iii) its chemical stability. Hence, only the details of the study on Nb_2O_5 films are given here.

The films of Nb_2O_5 were prepared by sputtering technique using Nb_2O_5 targets. The films were deposited in different mixtures of oxygen and argon gases. A pressure of 2×10^{-3} Torr was maintained during these depositions and all the Nb_2O_5 samples in this study were deposited to a thickness of 200 nm.

The optical properties of Nb_2O_5 films are quite sensitive to the sputtering conditions. In Fig. 9.4 are shown the transmission spectra of Nb_2O_5 films sputter deposited on glass substrates with different ratio of oxygen and argon gases. As can be seen from this figure a superior transmission is exhibited by these samples only in the presence of oxygen gas. The film deposited in a 100% Argon atmosphere has a much lower transmission throughout the spectral range examined. On the basis of these results only films deposited in 25% O_2 and 75% Ar mixtures have been used in the fabrication of our all solid EC sample.

For examining the capability of Nb_2O_5 films for undergoing reversible lithium ion insertion and extraction the films were deposited on ITO coated substrates. These films were then

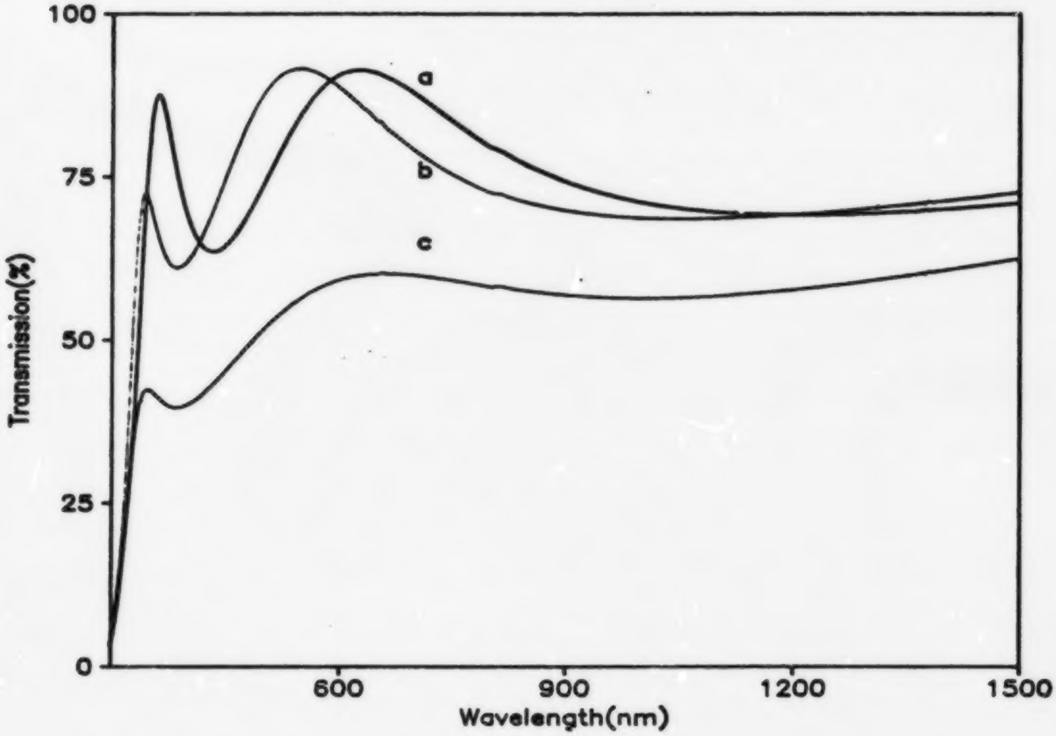

Fig. 9.4: Transmission spectra of sputter deposited Nb_2O_5 film on glass at different oxygen and Argon gas mixtures: a) Ar - 75%, O_2 - 25%, b) Ar - 90%, O_2 - 10% and c) Ar - 100%.

introduced into an electrochemical cell containing $LiClO_4$ in PC and a carbon counter electrode. Lithium ion insertion and extraction was studied by applying a galvanostatic potential between the film and the counter electrode. Cyclic switching was carried out using triangular voltage between -2.5V and +2.5V as shown in Fig. 9.5(a). The injected charge density variation and transmission changes during these cycles are given in Fig. 9.5(b). Similarly the current variation is shown in Fig. 9.5(c).

The variation of ΔO.D. with the injected charge density is given in Fig. 9.6. This variation is also recorded at 632 nm. There is a fairly linear dependence of ΔO.D. on the injected charge (Q). The coloration efficiency which is given by the slope of this plot (Fig. 9.6) gives a value of 11 cm^2/C. Hence, the coloration efficiency of Nb_2O_5 is fairly small as compared to that of WO_3 film. From the ΔO.D. vs. Q plot of WO_3 film (Fig. 7.2, section 7) we can see that the coloration efficiency value is around 37.5 cm^2/C for WO_3 film at the wavelength of 632 nm. However, this difference in the coloration efficiencies of WO_3 and Nb_2O_5 increases towards higher wavelengths. A qualitative comparison of the change in transmission of the two films with lithium insertion is obtained from Fig. 9.7 and Fig. 7.4 (section 7). In Fig. 9.7 is shown the transmission change in sputtered Nb_2O_5 film with insertion of 15 nm, 30 nm and 50 nm of lithium by the Nb_2O_3 evaporation technique described earlier. While there is significant coloration of Nb_2O_5 at lower wavelengths with this addition of lithium, the change at higher wavelengths is quite small. On the contrary, the WO_3 film (Fig. 7.4) exhibits a very large optical modulation at higher

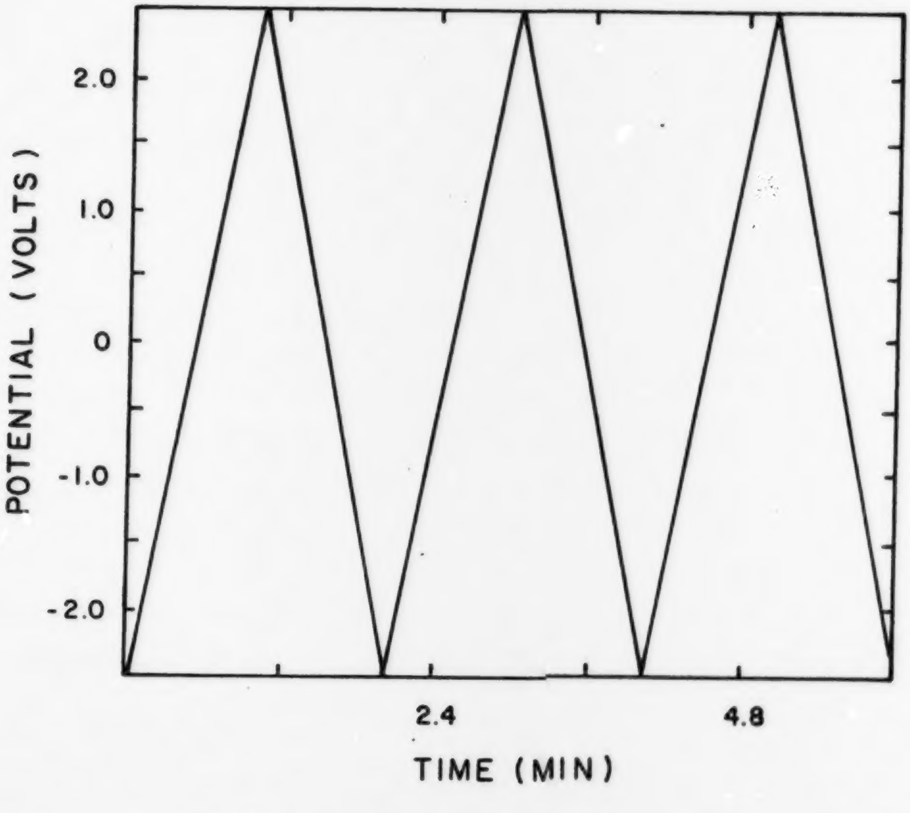

Fig. 9.5(a): Time dependent voltage used for cyclic voltammetry study of Nb_2O_5 film in an electrolyte of $LiClO_4$ in PC.

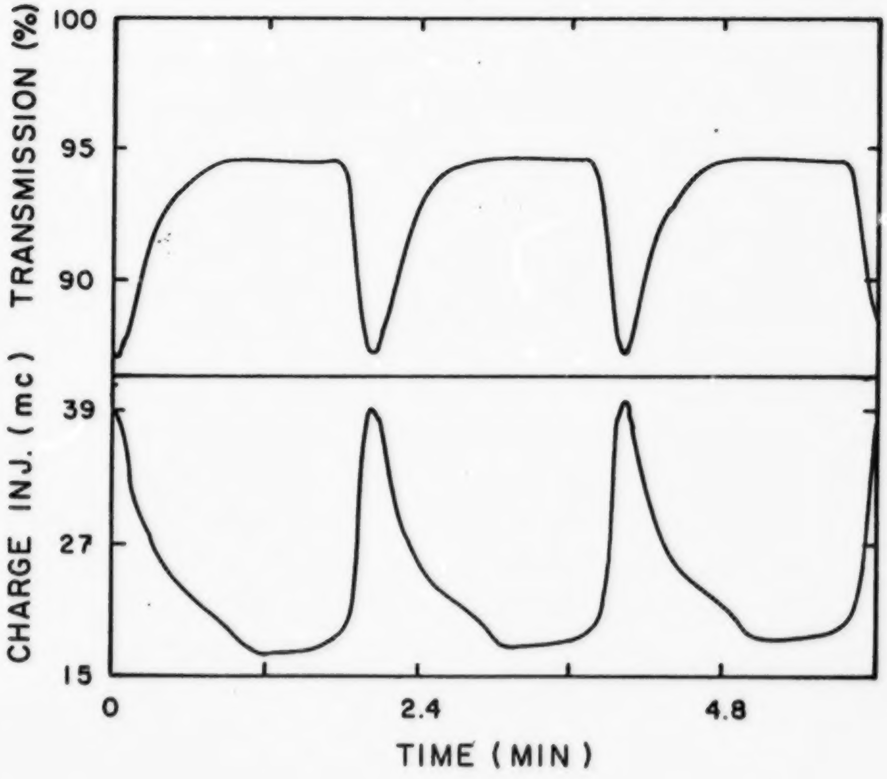

Fig. 9.5(b): Cyclic variation of transmission and charge injected with time for the triangular potential shown in Fig. 8.5 (a) for Nb_2O_5 film.

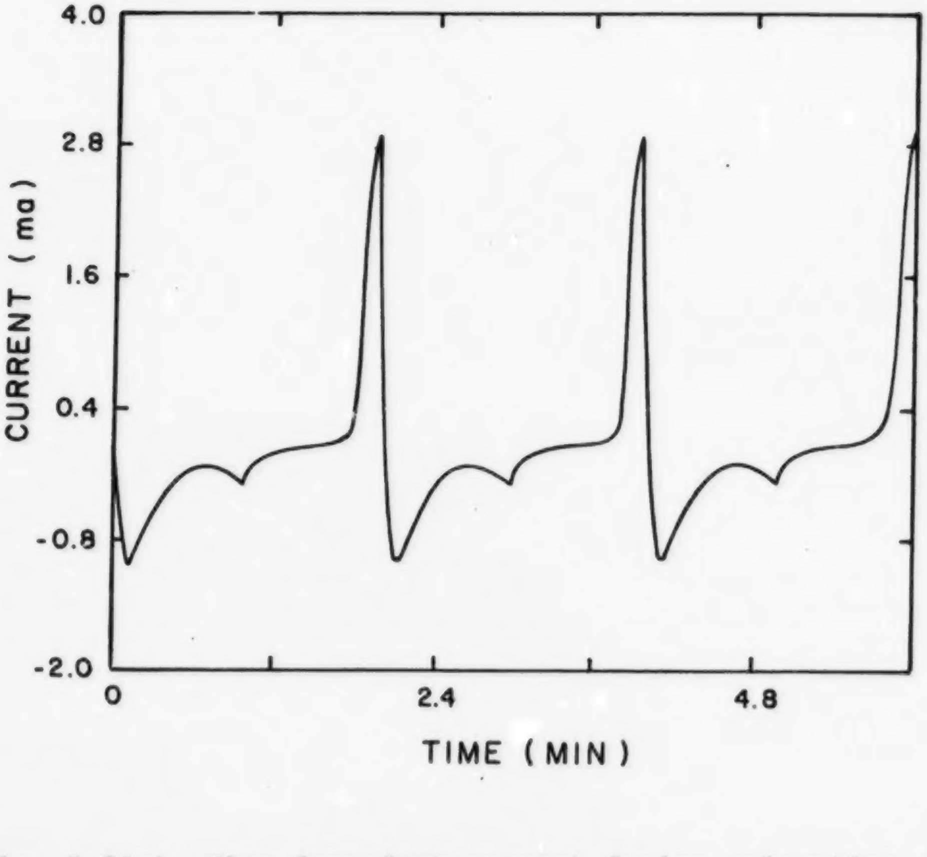

Fig. 9.5(c): Time dependent current during coloration and bleaching of Nb_2O_5 film.

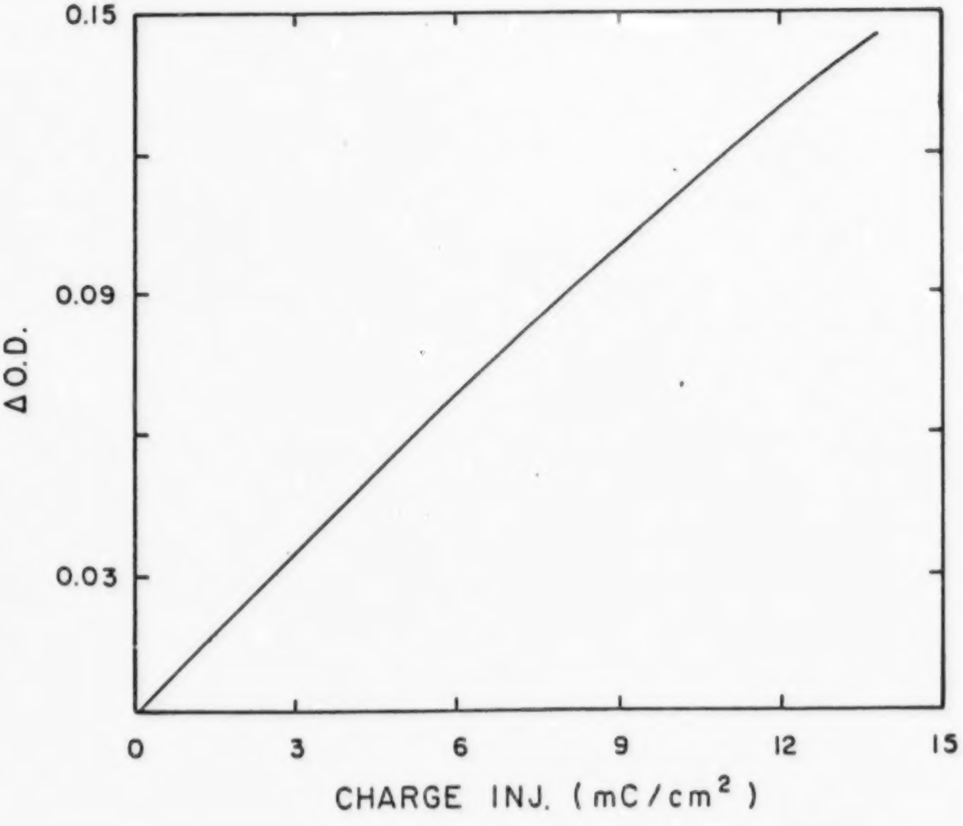

Fig 9.6: Dependence of ΔO.D on the injected charge for 200 nm thick Nb_2O_5 film sputter deposited at 25% O_2.

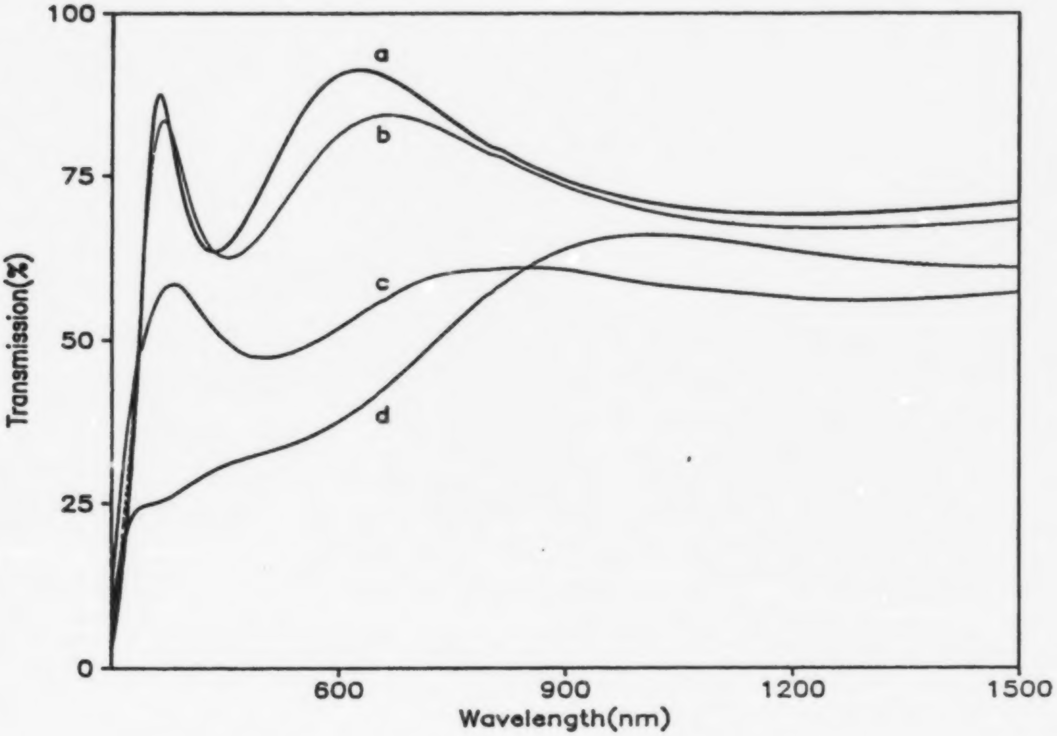

Fig. 9.7: Transmission spectra of sputter deposited (curve a) 200 nm thick Nb_2O_5 film on glass deposited with 15 nm (curve b), 30 nm (curve c) and 50 nm (curve d) of Li mass thickness.

wavelengths upon addition of the same amount of lithium. Hence, it is this significant difference in the coloration efficiencies of the two materials that gives the possiblity of using these materials for the function of EC layer and the ion storage to achieve fairly good optical modulation in the near infrared region, upon shuttling of the lithium ions between the two layers. This is the basis for the fabrication of our all solid complimentary type EC system.

9.3 All solid state prototype EC system and performance characteristics

As discussed in the earlier sections our EC system is based on the combination of $W0_3$ with a high coloration efficiency as EC layer and niobium oxide with low coloration efficiency as the counter electrode or the ion storage layer. Comparing the coloration efficiency of the two layers, especially in the higher wavelength region between 700 and 1500 nm, one can see that such a combination of $W0_3$ as EC and Nb_20_5 as ion storage would lead to ample coloration change electrochromically. The potential optical modulation especially at these higher wavelengths is very suitable for solar energy management applications. For fabricating such a system we have taken into account all the results on the electrical and optical properties of the individual layers described in the earlier sections. In this section are given the optimum parameters and fabrication methods for the fabrication of the prototype system. The EC performance of such a system is also discussed in detail.

Our final all solid state prototype system has the following configuration.

$ITO/Li_xWO_3/LiBO_2/a\text{-}WO_3/Au$

The coating was prepared on a ITO covered glass substrate supplied by Donnelly Corp. with a sheet resistance of 40 Ω/□ . These substrates were first etched in a concentrated Hydrochloric acid solution on one side as shown in the Fig. 9.8. Then the etched samples were cleaned in an ultrasonic detergent bath and then thoroughly rinsed in running distilled water. Then they were immersed in propyl alcohol and dried. These samples were then transferred into the vacuum chamber. The first deposition carried out was Nb_2O_5 film. This film was sputter deposited to a thickness of 200 nm at the rate of 0.1 nm/s covering most of the surface area of the substrate but leaving space for ITO contact. The sputtering of this sample was carried out in an atmosphere of 25% oxygen and 75% Argon.

The lithiation of Nb_2O_5 is carried out in another vacuum coating system to avoid Li contamination in a vacuum of 10^{-5} torr. $LiNbO_3$ was heated in a tungsten boat giving off lithium atoms. Lithiation was carried out to a thickness of 40 nm change on the quartz crystal as described earlier. This thickness is found to be safe for reversible coloration of 200 nm thick WO_3. The film was then deposited with 100 nm of $LiBO_2$ as fast ion conducting layer and 200 nm of WO_3 film both at a substrate temperature of

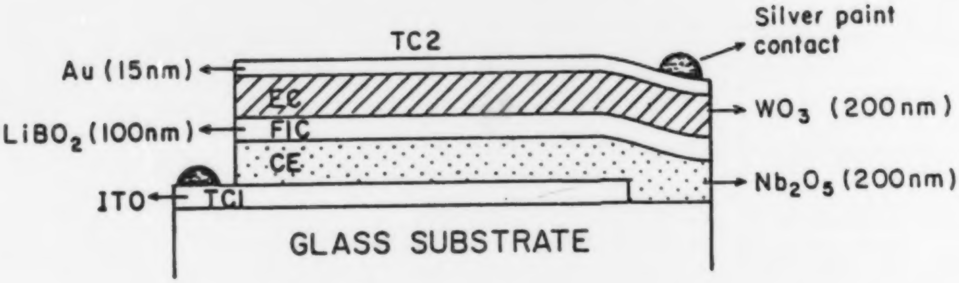

Fig. 9.8: Five layer configuration of our all-solid-state prototype EC system.

200°C, pressure of 5 to 7 × 10^{-6} torr. and deposition rate of 0.2-0.3 nm/s. Both these materials were deposited by thermal evaporation. Finally the top electrode of 15 nm thick gold was evaporated using a mask to avoid the shorting between the top and the bottom electrodes. The active area for EC performance was around 3 cm^2 for these studies. Silver paint contacts were applied on both electrodes at the sides to have better physical contacts on the sample. A heavy loss in transmission and strong interference are found due to the presence of gold film. The reproducible EC performance studies of the sample are carried out only after the initial 10-12 coloration and bleaching cycles.

After these initial studies it was found that our system prepared as described and cycled between colored and bleached state tends to remain in the colored state and not in the bleached state. However, through the application of a small potential it can be held in the bleached state. In Fig. 9.9 is shown the spectra of our solid EC system in the colored and bleached states. These spectra are taken in the transmission mode. For taking the spectra in the bleached state a potential of - 3V was applied (Au electrode + ve and ITO electrode - ve). Similarly a potential of 3V (ITO electrode + ve, Au electrode - ve) was applied for obtaining the colored state. But once the colored state was attained the applied potential was removed. The cycling of this system between the colored and the bleached state with an applied voltage of ±3V is shown in Fig. 9.10. The transmission change with time are measured at the wavelength of 632 nm. About 100 such cycles were carried out and were found to be very reproducible. At this

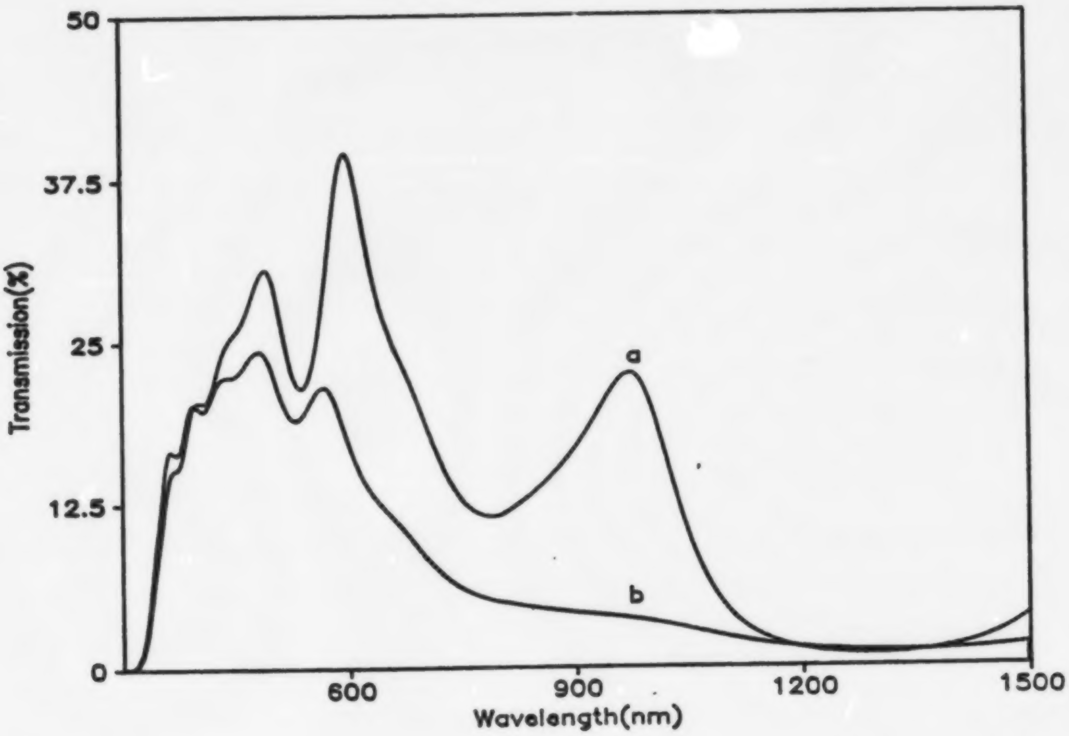

Fig. 9.9: Transmission spectra of the prototype system in bleached (a) and colored state (b). System as deposited is in the colored state. Applied voltage = -3V, for bleached state.

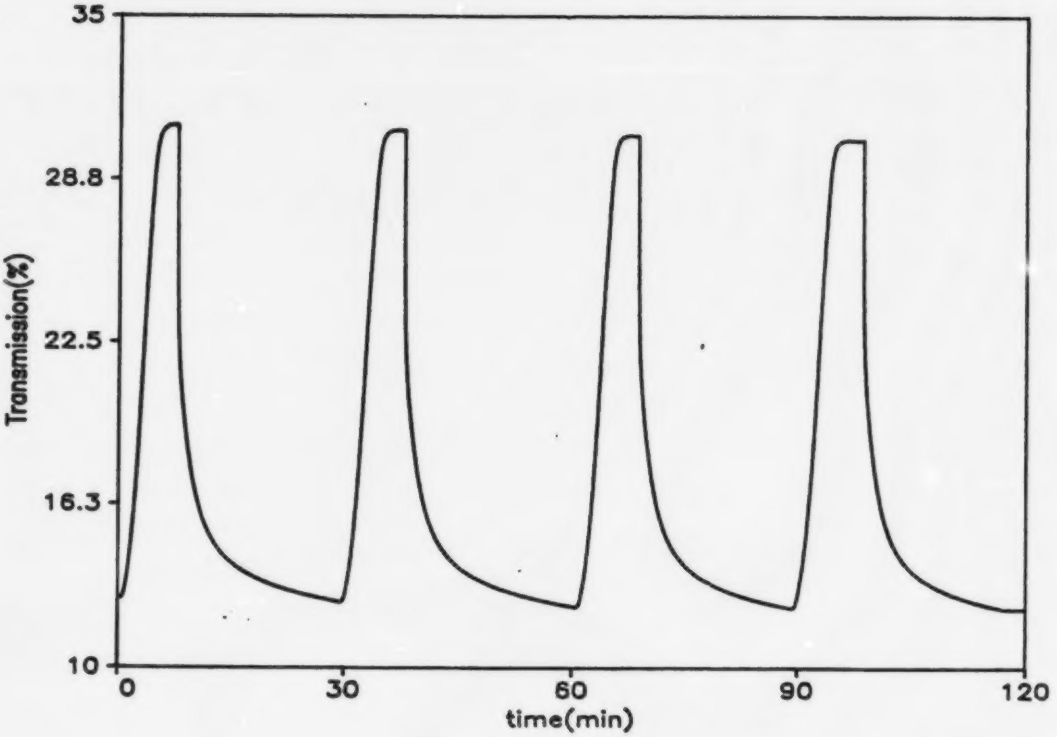

Fig. 9.10: Coloration and bleaching cycles of the prototype system in transmission mode. Applied voltage = ± 3V, cycle time = 30 minutes, wavelength = 632 nm.

wavelength of 632 an optical density change (ΔO.D.) of about 0.4 is found between the colored and bleached states. Further, the time taken by the system for each coloration and bleach cycle is about 30 minutes. This long response time and the ΔO.D. values are not suitable from the application point of view. However, it is also found from Fig. 9.9 that due to the strong interference in the film and the high transmission loss due to the gold film the effect of optical modulation is not completely evident especially in the higher wavelength range between 600 nm and 1500 nm. The optical modulation in this region is of great importance especially in electrochromic systems based on WO_3 films since the absorption band in tungsten bronze (Li_xWO_3) is very predominant in the near infrared region. In an attempt to observe the modulation better reflection measurements from the glass side of the sample was carried out. The reflection spectra was taken in the Cary 2400 spectrophotometer with a Harrick variable angle accessory. The reflection measurement was carried out at 45° and with front coated silver mirror as reference. As shown in Fig. 9.11 there is a very good optical modulation in the form of reflection change between the colored and bleached state at higher wavelengths. Since our sample is based on amorphous tungsten oxide this change occurs from the absorption modulation. Due to the manifestation of bulk of the optical change in the near infrared region, we have carried out detailed study of the EC performance characteristics of our EC system at the wavelength of 850 nm.

After several cycles of coloration and bleaching the optimum values of potential needed to obtain these states were found. The

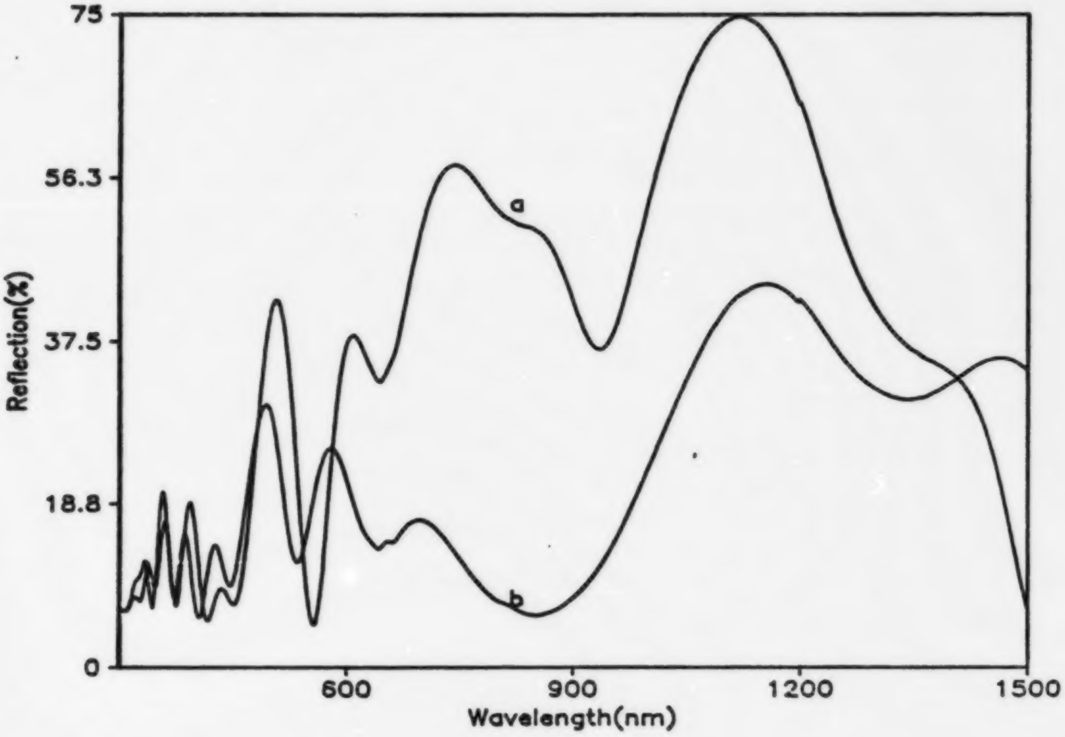

Fig. 9.11: Reflection spectra of the system in colored (b) and bleached (a) states. Measurements at 45° and with silver mirror as reference. Applied voltage = -3V for bleached state.

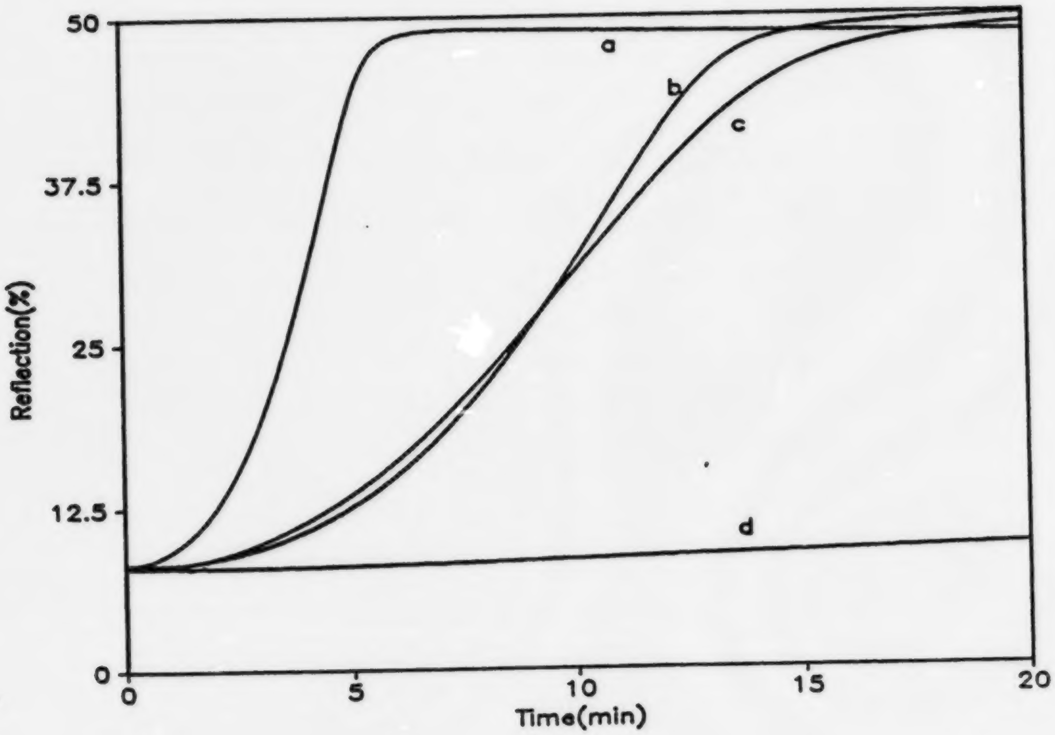

Fig. 9.12: Time dependent bleaching of the system at different applied voltages, V_A: a) $V_A = -3V$, b) $V_A = -2.5V$, c) $V_A = -2.0V$ and d) $V_A = -1V$. Wavelength, 850 nm.

system at its normal state of coloration was applied with different values of potential (-1 to -3V ITO electrode - ve). The system bleached at different rates as shown in Fig. 9.12. At an applied voltage value of 3V, the system reached it's maximum bleached state in about 5 minutes exhibiting an optical density change (ΔO.D.) of 0.8 at 850 nm. It was also found that once the system reached it's maximum bleached state, it could be held in this state permanently with a reduced potential of -2.5V and a current of 1 mA. Hence, the power required to maintain this 3 cm^2 sample in the bleached state is about 2.5 mW. This power requirement is fairly modest from the application point of view. Further, the response time of 5 minutes and ΔO.D. of 0.8 are also acceptable values for switchable window applications.

Similarly, the study of the returning of the system to it's normally colored state was done both under open circuit and with an applied voltage of 1 and 1.5V. The change of reflection with time under these conditions are shown in Fig. 9.13. With an applied voltage of 1.5V the system returns to its complete colored state in about 6 minutes. Using these two optimum values of potential for coloring and bleaching i.e. -3V for bleaching and 1.5V for coloring several reproducible cycles were carried out as shown in Fig. 9.14. In each cycle 6 minutes of coloring and 6 minutes of bleaching was performed to demonstrate reproducible and fairly rapid EC performance of this system. The response time of EC switching is well within the tolerable limit for solar energy management applications.

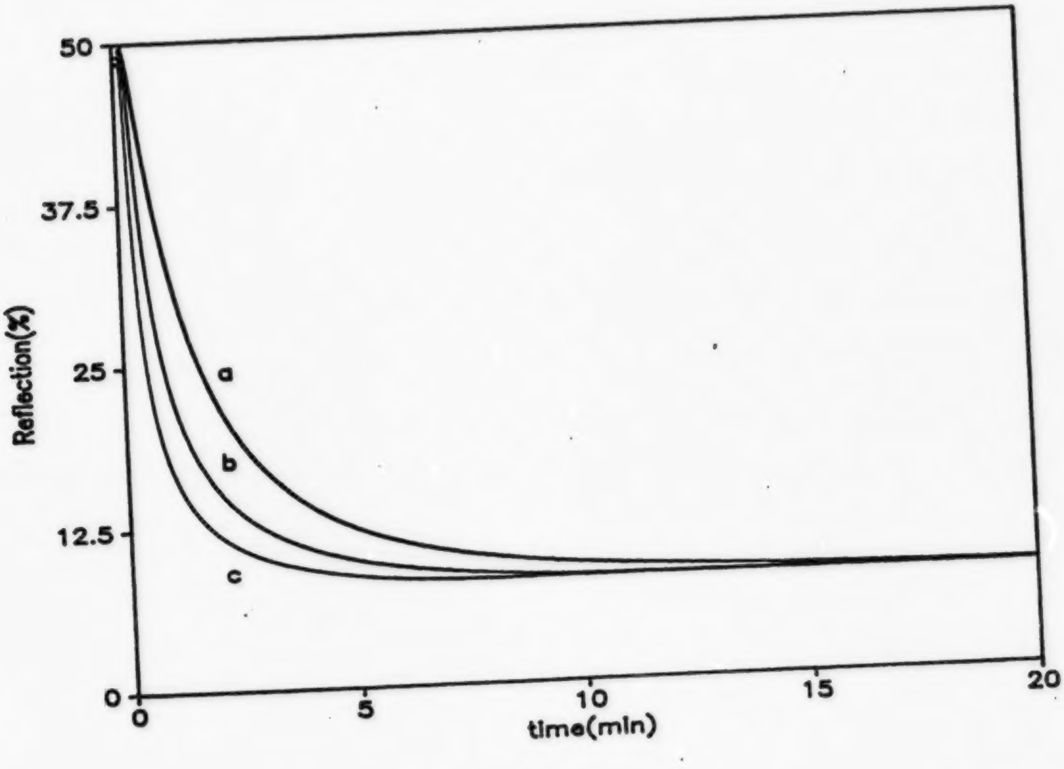

Fig. 9.13: Time dependent coloration (return to normal state) of the EC systems at different V_A: a) open circuit, b) $V_A = 1V$ and c) $V_A = 1.5V$. Wavelength, 850 nm.

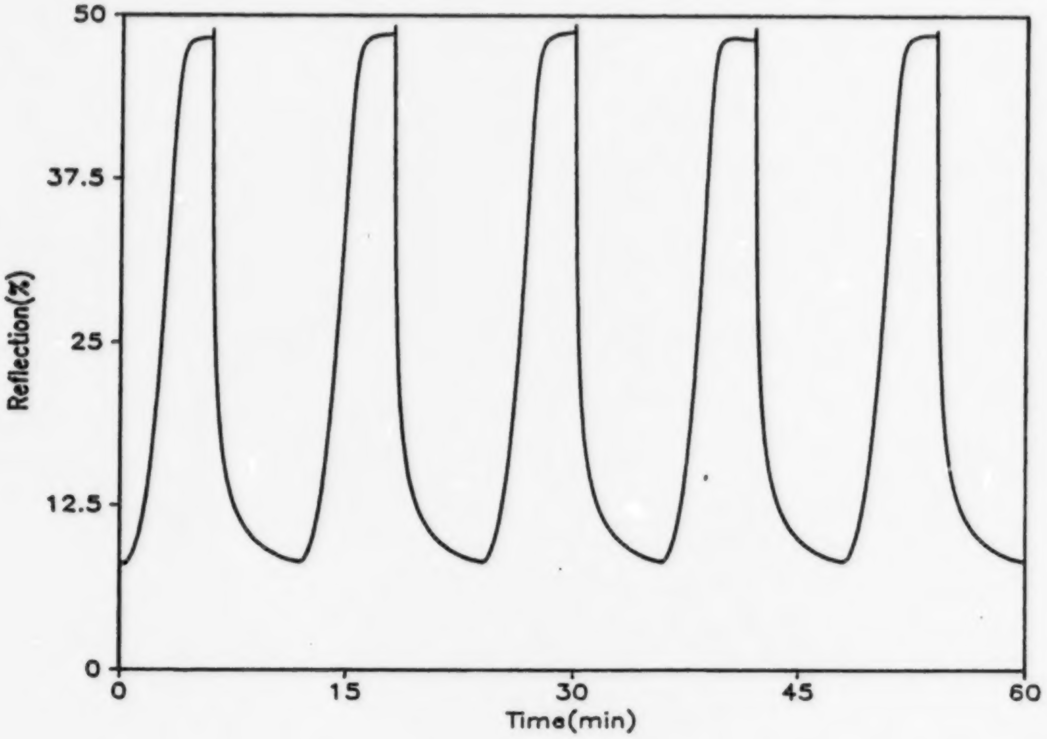

Fig. 9.14: Coloration and bleaching cycles of the prototype system in reflection mode. Cycle time, 12 minutes, V_A = -3V (bleaching) and 1.5V (coloring). Wavelength, 850 nm.

10. CONCLUDING REMARKS

The study of electrochromic materials and devices for switchable windows has been successfully completed. Based on the results of this study several small area, all-solid-state thin film prototype EC systems have been realized. The preliminary study of the EC characteristics of these systems indicate the high application potential of the system as switchable window (SW) device. However, improvements and certain operational modifications have to be made to optimize the EC performance. In this section the EC performance characteristics of one of our EC system which has been studied extensively are given. Advantages and shortcomings of our system and suggestions for future study are also discussed.

Our all-solid-state system with the following components;

$ITO/a\text{-}WO_3/LiBO_2/Nb_2O_5/Au$

has been fabricated and studied. This type of EC system is based on the combination of high coloration efficiency WO_3 as EC layer and low coloration efficiency Nb_2O_5 as CE layer. $LiBO_2$ has been used for the first time as a FIC layer in an EC system. A new technique of lithiation of the system using $LiNbO_3$ has been developed and used extensively for the study and fabrication of the prototype. Along with these new elements of fabrication of the EC system, the deposition conditions of each layer are optimized to achieve the required optical and electrical properties. It is also shown in this work that different types of EC and optical behaviors can be achieved in the EC layer of WO_3 doped with metal particles.

The study of the structure and water absorption behavior have also been carried out. These studies have not only helped us in understanding and choosing the WO_3 with the most suitable characteristics, but have also demonstrated some very useful properties that can be used with advantage in the EC systems. The optical constants of the films used in the EC system are determined with a very high precision using R and T measurements over a wide range of angles. A complete review of inorganic ion conducting materials is also included in this work and the most suitable materials for our work have been selected.

Our five layer prototype EC system fabricated as above is normally in colored state. However, it can be held in the bleached state continuously by the application of a potential. The power consumption for such an operation for our small area prototype is found to be around 2.5 mW. This system demonstrates fairly good optical modulation, especially in the wavelength region between 600 nm and 1500 nm. This absorption modulation is especially interesting for solar energy applications. The study of some of these initial characteristics are tabulated below (Table 10.1).

As per these requirements of an ideal device, our prototype system shows fairly good promise. However, certain improvements need to be addressed for optimizing the EC operation. The currently used outer electrode of Au film cuts down the transmission of the device to a great extent. Hence, in order to optimize the transmission modulation for a SW application this layer has to be replaced with a more transparent electronic conductor. This work is currently in progress in our laboratory

Table 10.1: Desired and realized EC properties

Property	Ideal device	Our prototype
1. Optical modulation (Reflection or transmission)	0 to 100%	Good (Fig. 9.11) especially in NIR region
2. Switching voltage	1-3 volts (small device)	3V (for bleaching)
3. Bleached state transparency in the visible	50-70%	presently not good due to the Au electrode
4. Switching time	Depends on application	About 300 seconds
5. Switching durability	> 10^5 cycles	> 100 cycles (testing still in progress)
6. Power consumption for operation	low	very good
7. Physical durability	withstands environmental and physical durability	robust with respect to physical durability
8. Open circuit memory	> 1 day	Normally in colored state (needs power for maintaining in bleached state)
9. Operating temperatures	-30 to 70°C	not studied

with sputtered indium tin oxide (ITO) coatings. Soon we will be able to replace the top gold electrode with a highly transparent film of ITO. The second problem that has to be overcome in our prototype system concerns the initial colored state of the device. For SW applications it is highly desirable to have the device in the clear state while not operating. The lithium ions injected into the Nb_2O_5 (CE) film diffuse to the WO_3 (EC) side as soon as the EC layer is deposited leading to already colored systems in the as-fabricated state. Hence, for the injected lithium ion density and the given thicknesses of Nb_2O_5 and WO_3 the low energy state seems to be in WO_3. This can however be changed if the proper combination of Li^+ charge injected in the system and the thickness of Nb_2O_5 is achieved. These aspects of the present work need to be investigated further. The study along these lines to establish the bleached state of the as-fabricated system is essential for SW applications. In addition to the discussed modifications required in our systems, further testing will have to be carried out on our prototype system for its switching and physical durability. The EC operation of the system over a wide temperature range will also have to be carried out. Compared to many of the all-solid-state systems cited in the literature using polymer layers as FIC, our system made of all inorganic materials has a better promise of operating over a wide temperature range.

Hence, after these initial studies of EC performance we can optimistically predict that all-solid-state systems such as the one we have fabricated can be transformed into practical devices in the near future. Through this project of study and fabrication of EC system, we have achieved the major elements of operation of such a system. If other peripheral aspects outlined above are successfully addressed, highly efficient and robust EC switching devices will soon become a reality.

Appendix I

XPS studies of WO_3 films

(as described in section 4.2)

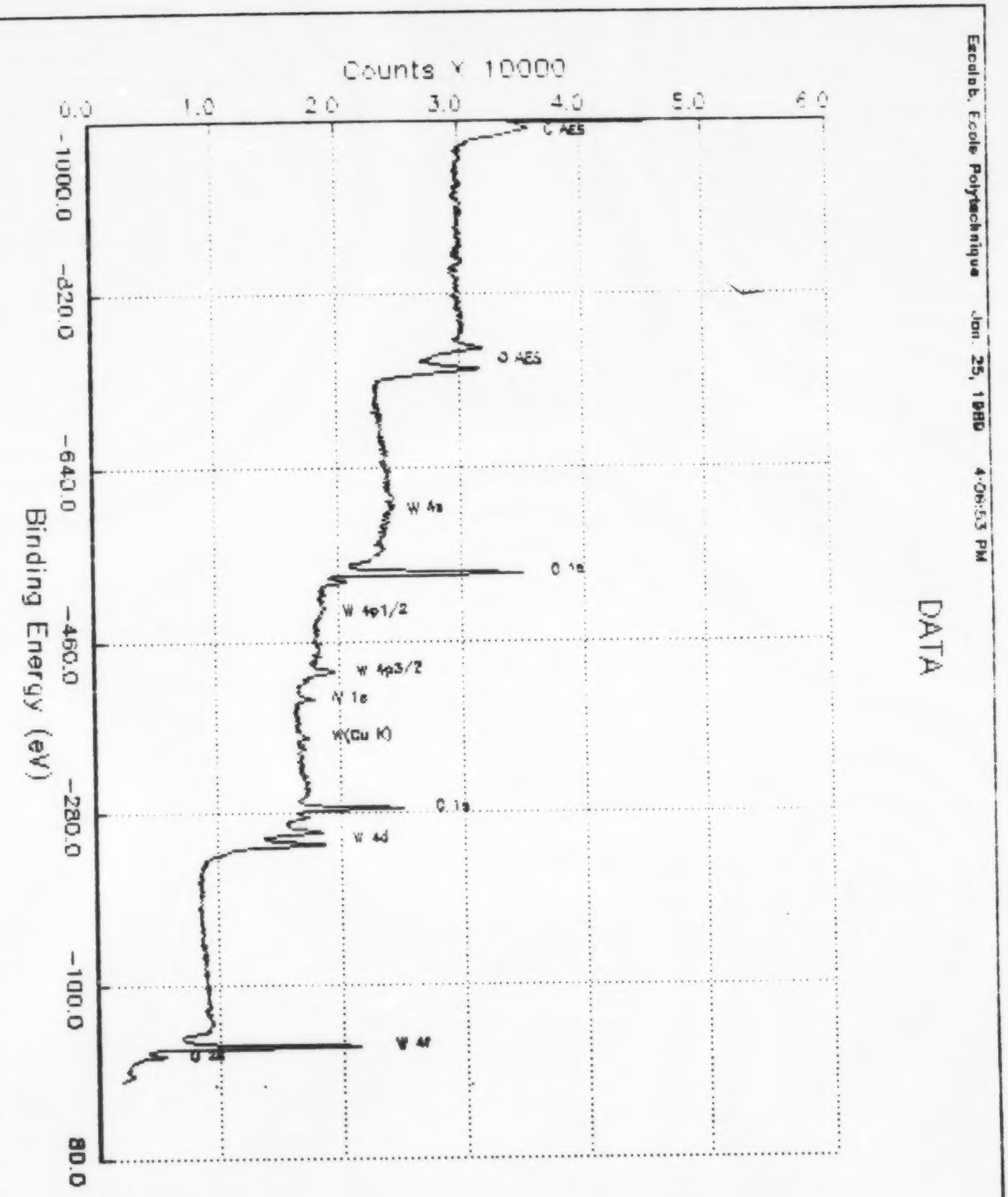

Analysis: 2
Spectrum: 1
Prep.:
Notes:
Exper:
Co: MOncton

Filename: umon7
Technique: Mg BE
SCU : CAE : 50
Cycles: 1
Exp. Type: Survey
Dwell t: 200 ms

Start: -1000.0
Stop: 0.00
Step: 1.00

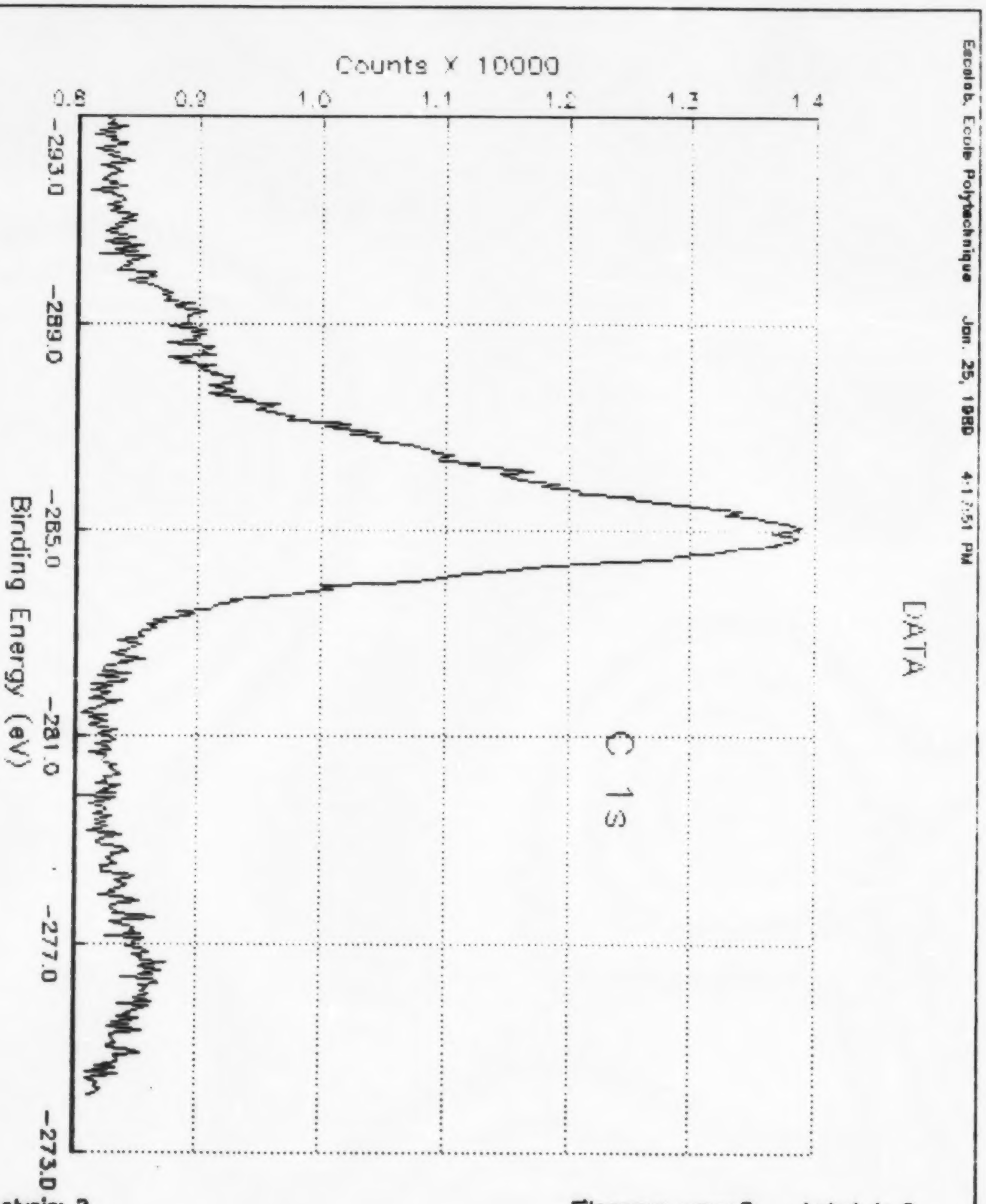

Analysis: 2
Spectrum: 1
Prep.:
Notes:
Exper:
Co: MOncton

Filename: umon8
Technique: Mg BE
SCU : CAE : 20
Cycles: 1
Exp. Type: Multiplex
Dwell t: 400 ms

Label 1: C
Start: -294.00
Stop: -274.00
Step: 0.05
Cycle: 1

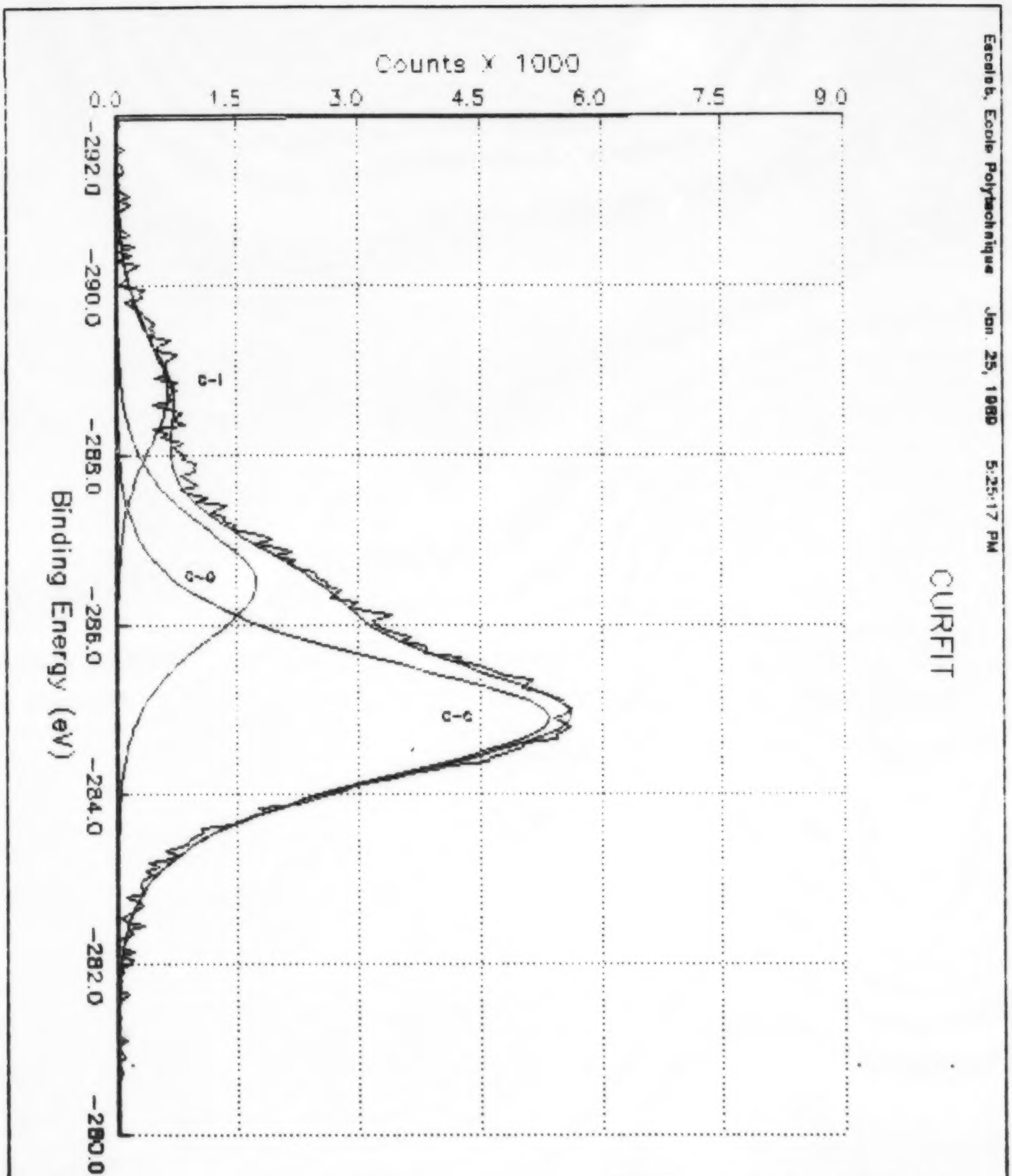

Analysis: 2
Spectrum: 1
Prep.:
Notes:
Exper:
Cie: MOncton

Filename: cumon81
Technique: Mg BE
SCU : CAE : 20
Cycles: 1
Exp. Type: Multiplex
Dwell t: 400 ms

Label 1: C

Start: -294.00
Stop: -274.00
Step: 0.05
Cycle: 1

```
Surface Software Inc.
Curve Fitting Information

Spectra : Filename : cumon81
          Sample   : Liwo
          Label    : C
          Setting  : 1

Peak shape : 35.00 % Gaussian, 65.00 % Lorenztian

Peak          Height    Center        Fwhm          Area    %Area

 # 1          5338.7   -284.94        1.68       10313.4    69.42
 # 2          1738.0   -286.52        1.68        3350.3    22.55
 # 3           631.8   -288.77        1.65        1192.7     8.03
```

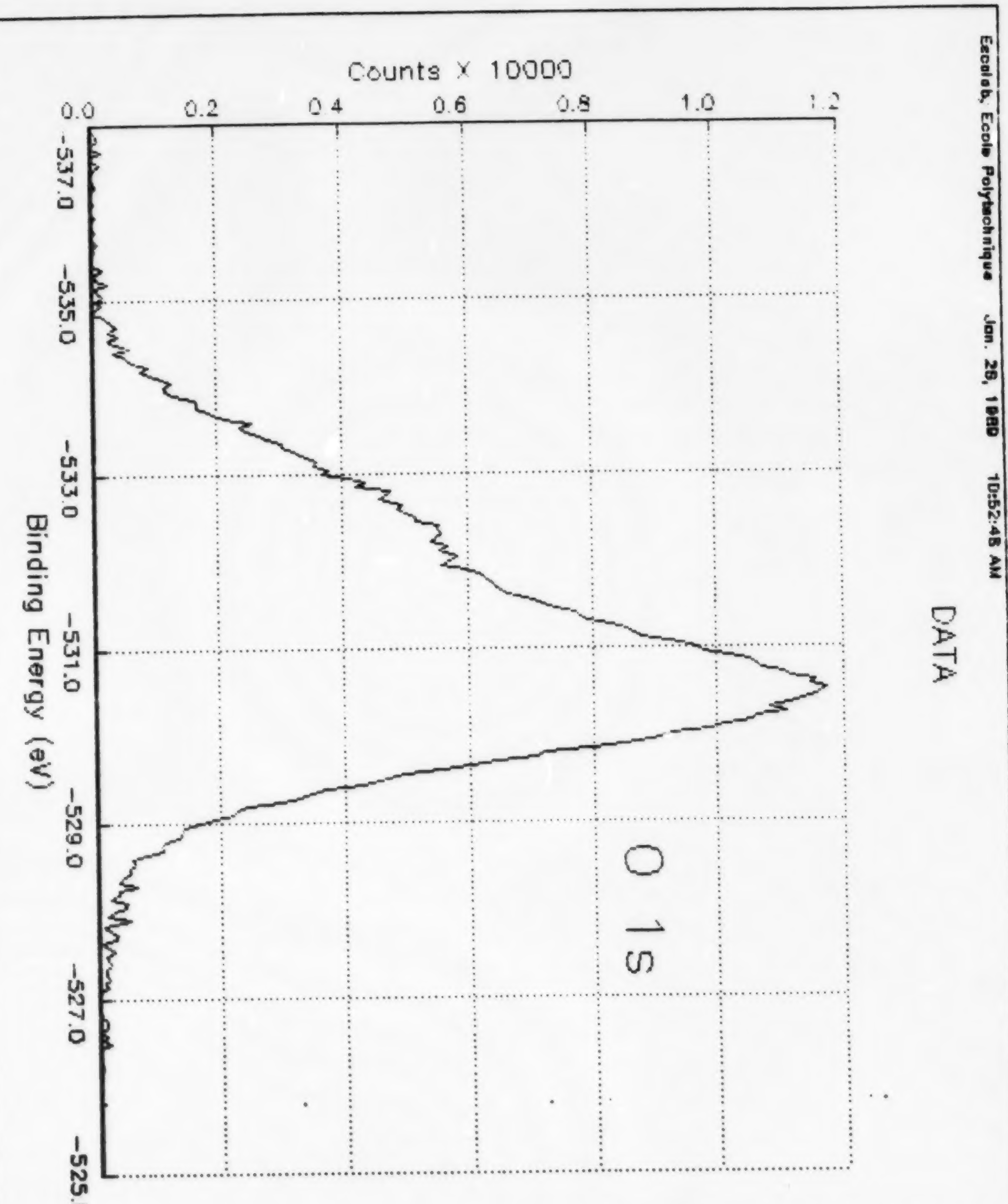

Analysis: 2
Spectrum: 1
Prep.:
Notes:
Exper:
Co: MOncton

Filename: umon8
Technique: Mg BE
SCU : CAE : 20
Cycles: 1
Exp. Type: Multiplex
Dwell t: 400 ms

Label 2: O2

Start: -541.00
Stop: -521.00
Step: 0.05
Cycle: 1

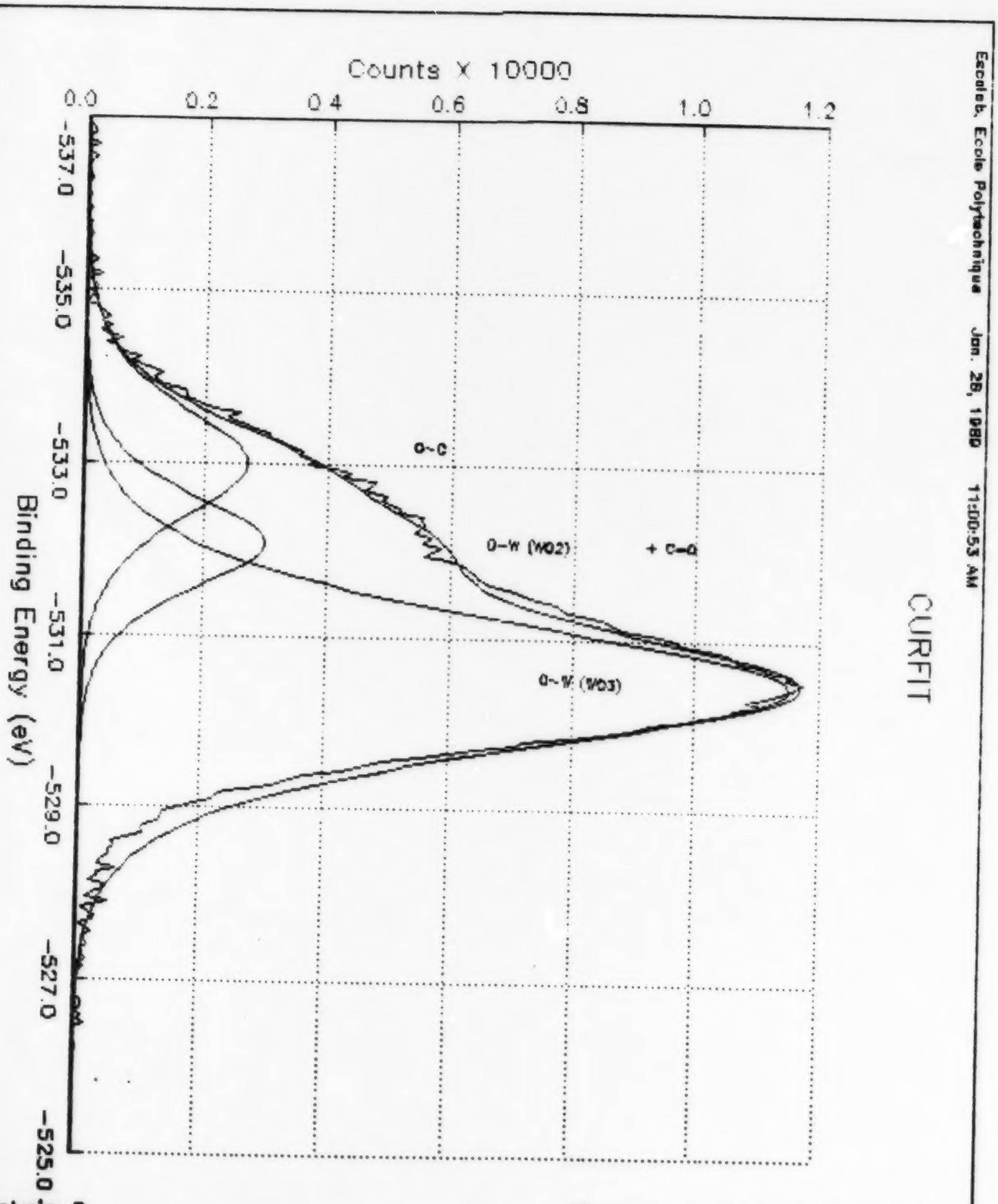

Analysis: 2
Spectrum: 1
Prep.:
Notes:
Exper:
Cie: MOncton

Filename: cumon821 Label 2: O2
Technique: Mg BE
SCU : CAE : 20
Cycles: 1
Exp. Type: Multiplex
Dwell t: 400 ms
Start: -541.00
Stop: -521.00
Step: 0.05
Cycle: 1

Surface Software Inc.
Curve Fitting Information

Spectra : Filename : cumon821
Sample : Liwo
Label : O2
Setting : 2

Peak shape : 35.00 % Gaussian, 65.00 % Lorenztian

Peak	Height	Center	Fwhm	Area	%Area
# 1	11489.4	-530.55	1.79	23660.8	71.85
# 2	2990.8	-532.18	1.31	4496.6	13.65
# 3	2685.8	-533.10	1.55	4774.8	14.50

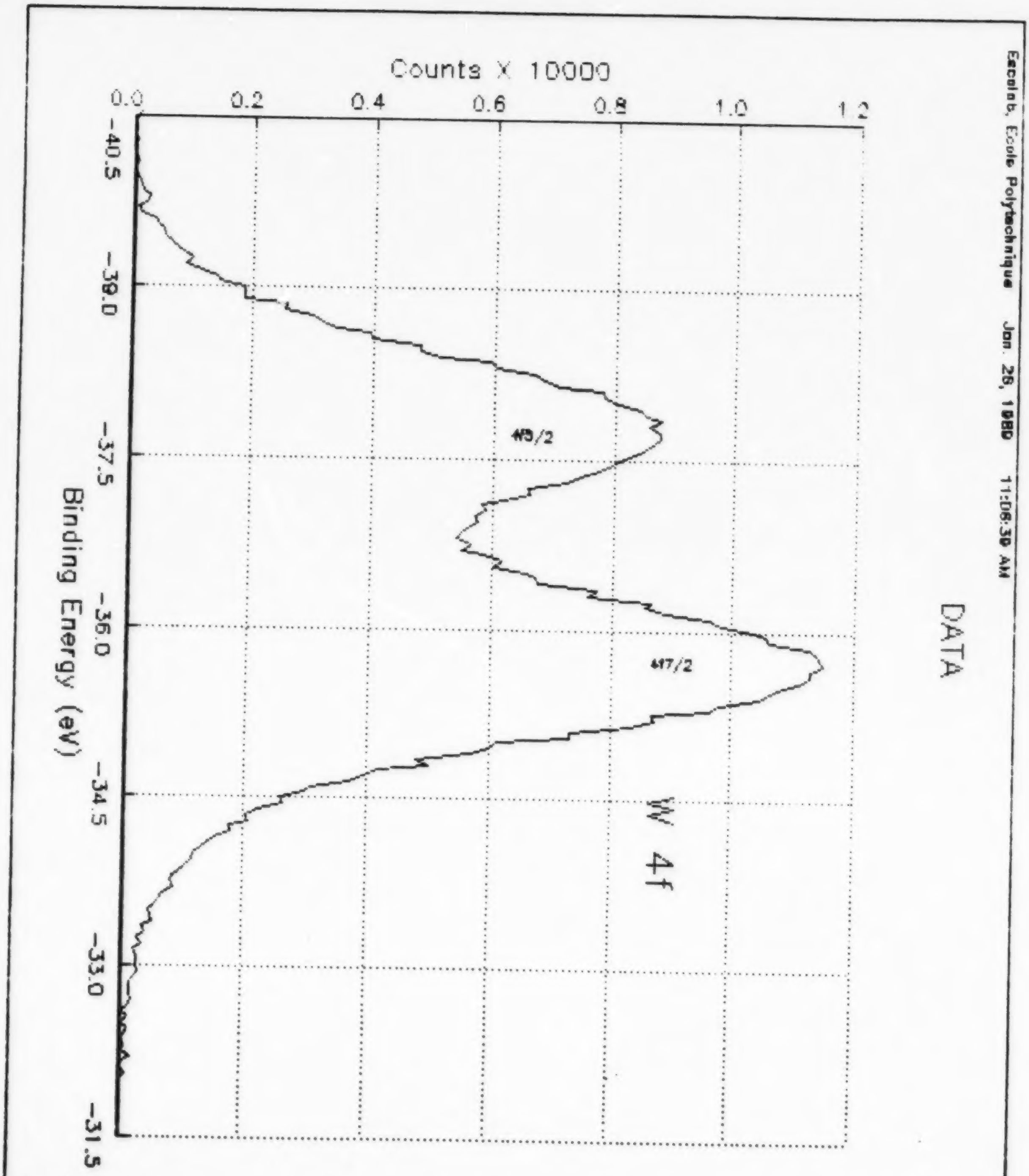

Analysis: 2
Spectrum: 1
Prep.:
Notes:
Exper:
Co: MOncton

Filename: umon8
Technique: Mg BE
SCU : CAE : 20
Cycles: 1
Exp. Type: Multiplex
Dwell t: 400 ms

Label 3: W1

Start: -44.00
Stop: -24.00
Step: 0.05
Cycle: 1

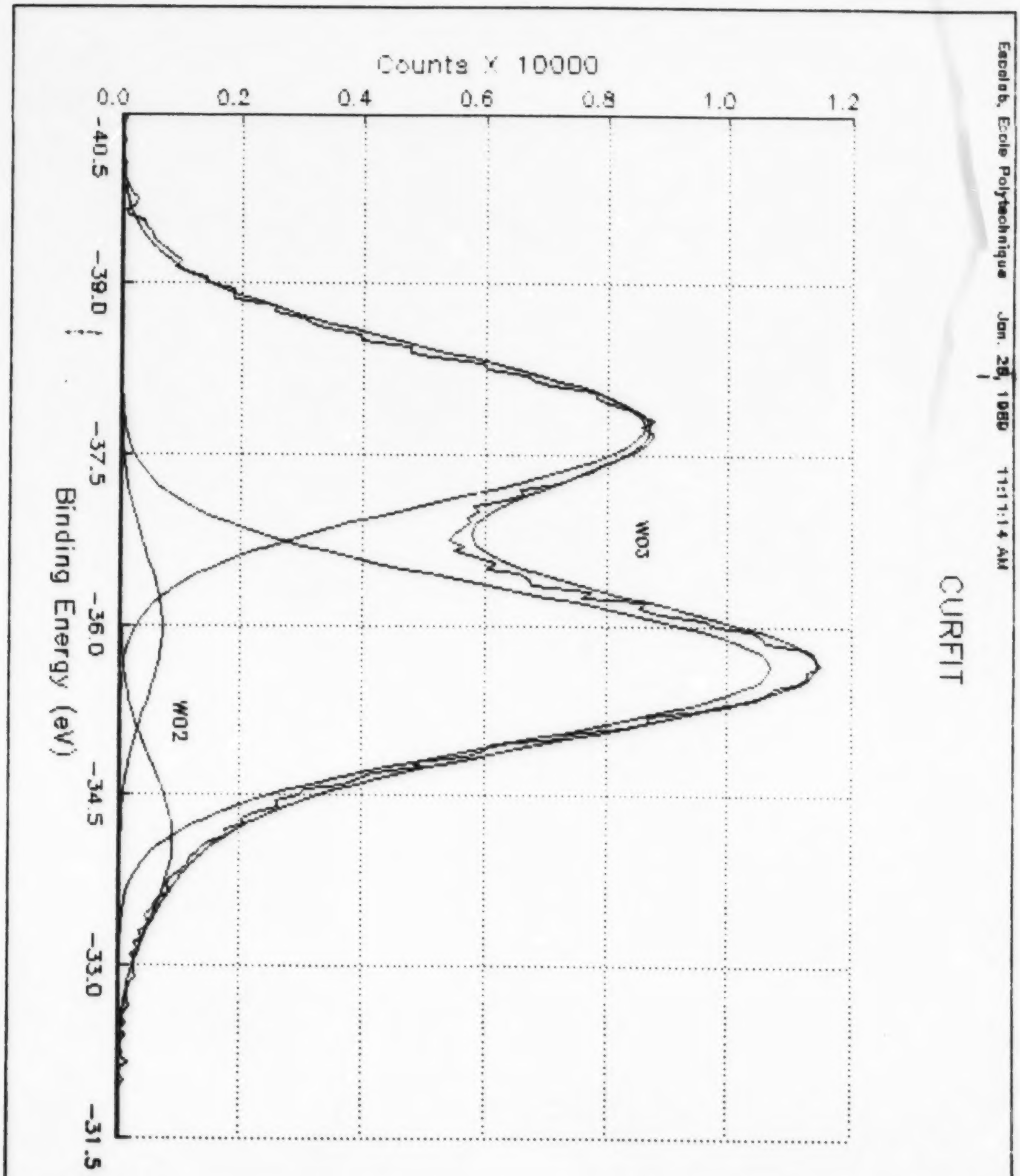

Analysis: 2
Spectrum: 1
Prep.:
Notes:
Exper:
Cie: MOncton

Filename: umon8
Technique: Mg BE
SCU : CAE : 20
Cycles: 1
Exp. Type: Multiplex
Dwell t: 400 ms

Label 3: W1

Start: −44.00
Stop: −24.00
Step: 0.05
Cycle: 1

```
Surface Software Inc.
Curve Fitting Information

Spectra : Filename : umon8
          Sample   : Liwo
          Label    : W1
          Setting  : 3

Peak shape : Gaussian

Peak       Height    Center      Fwhm        Area   %Area

 # 1        877.7    -34.10      1.57      1473.7    4.20
 # 2      10687.0    -35.64      1.57     17952.4   51.17
 # 3        698.3    -35.97      1.57      1173.1    3.34
 # 4       8624.7    -37.75      1.57     14487.9   41.29
```

REFERENCES

1. L. Jones, "Review of The Potential of Passive Solar Strategies For Office Buildings", Solar Energy Program, Report # passive-7, National Research Council, Canada, August 1983.

2. P. Coutier, M. Quattrocchi and W. Place, "A Preliminary Assessment of the Energy Potential of Advanced Materials and Devices for Building Apertures", Lawrence Berkeley Laboratory Technical Note, Berkeley, CA, Oct. 10, 1983.

3. H. Alan Fine and D.L. McElroy, "Assessment of Energy Conservation Potential of Active (Variable Thermal Resistance and Switchable Emittance) Building Thermal Insulation Systems", March 1, 1988.

4. Stephen Selkowitz, "Smart Windows", Glass Magazine, August 1986, pp 86-91.

5. W.C. Dautremont-Smith, Displays 4, 3 (1982); 4, 67 (1982).

6. A.P. Schuster, D. Nguyen and O. Caporaletti, Solar Energy Materials 13, 153 (1986).

7. My T. Nguyen and Lê H. Das, "Poly (N-Benzylaniline)/Poly (Amps)/WO_3 Solid-State Electrochromic Cell", 1989, private communication.

8. J. Guay, M. Leclerc and L.H. Das, J. Electroanal. Chem. 251, 31 (1988).

9. D. Craigen, A. Mackintosh, J. Hickman and K. Colbow, J. Electrochem. Soc., 1529 (1986).

10. A.M. Anderson, C.G. Granqvist and J.R. Stevens, Appl. Opt. 28, 3295 (1989).

11. P.V. Ashrit, D. Pelletier, F.E. Girouard and Vo-Van Truong, J. Appl. Opt. 58, 564 (1985).

12. P.V. Ashrit, F.E. Girouard, Vo-Van Truong and G. Bader, Proc. SPIE 562, 53 (1985).

13. P. Van Konynenburg, Proc. SAE Government and Industry Meeting, Washington, May 2-4 (1989).

14. Vo-Van Truong and M.C. Mehra, "Electrochromic Materials: a Technical Review", Solar Energy Program, National Research Coucnil, Canada, Oct. 1984.

15. C.M. Lampert, Solar Energy Materials 11, 1 (1984).

16. R. Hurditch, A.E. Hughes and P. Lloyd, 19th Electron. Mat. Conf. (Cornell, N.Y., 1977).

17. Y. Hajimoto, M. Matsushima and S. Ogura, J. Electron. Mat. 8, 301 (1979).

18. H.J. Stocker, S. Singh, L.G. Van Uitert and G.J. Zydzik, J. Appl. Phys. 50, 2993 (1979).

19. T. Yoshimura et al., Thin Solid Films 101, 141 (1983).

20. I. Shimiza, M. Shizukuishi and E. Inoue, J. Appl. Phys. 50, 4027 (1979).

21. T. Yoshimura, Personal communication.

22. B. Tell and F. Wadl, J. Appl. Phys. 50, 5944 (1979).

23. S. Ray, R. Banerjee, N. Basu, A.K. Batabyal and A.K. Barna, J. Appl. Phys. 54, 3497 (1983).

24. S. Takaki, K. Matsumoto and K. Suzuki, Appl. Surf. Sci. 33/34, 919 (1988).

25. I. Hamburg and C.G. Granqvist, J. Appl. Phys. 60, R123 (1986).

26. H. Nanto, T. Minami, S. Orito and S. Tanaka, J. Appl. Phys. 63, 2711 (1988).

27. Y. Igasaki, M. Ishikawa and G. Shimaoka, Appl. Surf. Sci 33/34, 926 (1988).

28. M. Labeau, V. Reboux, D. Dhahri and J.C. Joubert, Thin Solid Films 136, 257 (1986).

29. K.H. Guenther and H.K. Pulker, Appl. Opt. 15, 2992 (1976).

30. N. Martensson, in Analytical Techniques for Thin Films, ed. by K.N. Tu and R. Rosenberg, Treatise on Materials Science and Technology, Vol. 27 (Academic Press, 1988), pp. 65-107.

31. R. Hurditch, Electron. Lett. 11, 142 (1975).

32. J. Karouni, Effet des conditions de préparation sur les performances du dispositif électrochrome solide: Au/a-WO_3/MgF_2/Au, Thèse de maîtrise, U. de Moncton (1988).

33. A. Deneuville, P. Gerard and R. Billat, Thin Solid Films 70, 203 (1980).

34. N. Desbiens, Effets de l'atmosphère ambiante sur les propriétés électro-optiques d'un dispositif électrochrome solide, Thèse de maîtrise, U. de Moncton (1988).

35. T. Nishimura, K. Taira and S. Kurita, Appl. Phys. Lett. 36, 585 (1980).

36. N. Yoshiike and S. Kondo, J. Electrochem. Soc. 130, 2283 (1983).

37. H.R. Zeller and H.U. Beyeler, Appl. Phys. 13, 231 (1977).

38. M.R. Goulding and C.B. Thomas, Thin Solid Films 62, 175 (1979).

39. S. Badilescu, P.V. Ashrit and Vo-Van Truong, Appl. Phys. Lett. 52, 1551 (1988).

40. P.V. Ashrit, S. Badilescu, Fernand E. Girouard and Vo-Van Truong, Appl. Opt. 28, 420 (1989).

41. H.R. Wyss and M. Falk, Can. J. Chem. 48, 607 (1970).

42. R.S. Crandall and B.W. Faughnan, Appl. Physics Lett. 26, 120 (1975).

43. A. Harstein, J.R. Kirtley and J.C. Tsang, Phys. Rev. Lett. 45, 201 (1980).

44. Y. Nakao and Y. Yamada, Surf. Sci. 176, 578 (1986).

45. W.P. Griffith, J. Chem. Soc. (A), 286 (1970).

46. V.V. Truong and G.D. Scott, J. Opt. Soc. Am. 67, 502 (1977).

47. P.A. Kilty and W.M.H. Sachtler, Catal. Rev. Sci. Eng. 10, 1 (1974).

48. R.S. Venkatachalam, F.J. Boerio, M.R. Carnevale and P.G. Roth, Appl. Spectrosc. 42, 1207 (1988).

49. Handbook of Optical Constants of Solids, edited by Edward D. Palik (Academic Press, Orlando, 1985), Part I.

50. L. Ward, The Optical Constants of Bulk Materials and Films (Adma Hilger, Bristol and Philadelphis, 1988), Chaps. 2 and 3.

51. F. Abelès in Physics of Thin Films, Georg Hass and Rudolf E. Thun, Eds. (Academic Press, New York and London, 1971), pp. 151-204.

52. Wilford N. Hansen, J. Opt. Soc. Am. 63, 793 (1973).

53. D.W. Juenker, J. Opt. Soc. Am. 55, 295 (1965).

54. J.E. Nestell and R.W. Christy, Appl. Opt. 11, 643 (1972).

55. W.R. Hunter, J. Opt. Soc. Am. 55, 1197 (1965).

56. L. Ward, J. Phys. D: Appl. Phys. 10, 2539 (1977).

57. H.A. MacLeaod, Thin Film Optical Filters (MacMillan, Adam Hilger, 1986).

58. S. Elouatik, Détermination des constantes optiques par les mesures simultanées de R et T, travaux de thèse de maîtrise, Université de Moncton, non publié (1990).

59. W.H. Press, B.P. Flannery, S.A. Teukolsky and W.T. Vetterling, Numerical recipes in Pascal (Cambridge University Press, 1986), Sec. 10.5.

60. S. Benci, M. Manfredi and G.C. Salviati, Solid state communications 33, 107 (1980).

61. K. Miyake, M. Kaneko, M. Sano and N. Suedomi, J. Appl. Phys. 55, 2747 (1984).

62. H. Kaneko, S. Nishimoto, K. Miyake and N. Suedomi, J. Appl. Phys. 59, 2526 (1986).

63. Brian W. Faughnan, Richard S. Crandall and Phillip M. Heyman, RCA Review 36, 177 (1975).

64. O. Bohnke, C. Bohnke, G. Robert and B. Cardville, Solid State Ionics 6, 12 (1982).

65. F. Kanai, S. Kurita, S. Sugioka, H. Li and Y. Mita, J. Electrochem. Soc. 129, 2633 (1982).

66. O. Bonke, C. Bohnke and S. Amal, Materials Science and Engineering B3, 197 (1989).

67. Kenzi Matsuhiro and Yasushi Masuda, Proceedings of the Society for information display (SID) 21, 101 (1980).

68. Shoji Yamada et al, Jap. J. Appl. Phys. 24, 142 (1985).

69. B.J. Molnar, A.R. Haranahalli and D.B. Dove, J. Vac. Sci. Technol. 15, 161 (1978).

70. E.K. Sichel and J.I. Gittleman, J. Electronic Materials 8, 1 (1979).

71. E.K. Sichel and J.I. Gittleman, Appl. Phys. Lett. 33, 564 (1978).

72. R.W. Cohen, G.D. Cody, M.D. Coutts and B. Abeles, Physical Review B 8, 3689 (1973).

73. T. Yamaguchi, M. Sakai and N. Saito, Physical Review B 32, 2126 (1985).

74. E.K. Sichel, J.I. Gittleman and J. Zelez, Appl. Phys. Lett. 31, 109 (1977).

75. Y.F.Y. Yao and J.T. Kummer, J. Inorg. Nucl. Chem. 29 (1967) 2453.

76. J.B. Goodeneough, Proc. R. Soc. Lond. A 393 (1984) 215.

77. B.B. Owens, D.F. Untereker, and P.M. Skarstad, in Fast Ion Transport in Solids, eds. P. Vashishta, J.N. Mundy, G.K. Shenoy (North-Holland, Amsterdam, 1979), p.105.

78. H. Sato, in Solid Electrolytes, ed. S. Geller (Springler-Verlag, N.Y., 1977), p.3.

79. S. Chandra, Superionic Solids (North-Holland, Amsterdam, 1981), and the references herein.

80. S.K. Deb, Proc. Roy. Soc. A304 (1968) 211.

81. S.K. Deb, and R.F. Shaw, US Patent No. 3, 521, 941 (1970).

82. T. Yoshimura, M. Watanabe, K. Kiyota, and M. Tanaka, Jpn. J. Appl. Phys. 21 (1982) 128.

83. Y. Hajimoto, M. Matsushima, and S. Ogura, J. Electron. Mater. 8 (1979) 301.

84. E. Inoue, K. Kawaziri, and A. Iwaza, Jpn. J. Appl. Phys. 16 (1977) 2065.

85. Y. Sato, R. Fujiwara, I. Shimizu, and E. Inoue, Jpn. J. Appl. Phys. 21 (1982) 1642.

86. A.A. Brishka, T.V. Zamozdik, Ya Ya Kleperis, A.R. Lusis, and O.A. Rode, Sov. Phys. Tech. Phys. 26 (1981) 583 [Zh. Tekh. Fiz. 51 (1981) 976].

87. A.R. Lusis, J.J. Kleperis, A.A. Brishka, and E.V. Pentyush, Solid State Ionics 13 (1984) 319.

88. M.G. Shilton and A.T. Howe, Mat. Res. Bull. 12 (1977) 701.

89. M.G. Shilton and A.T. Howe, in Fast Ion Transport in Solids, eds. P. Vashishta, J.N. Mundy, G.K. Shenoy (North-Holland, Amsterdam, 1979), p.727.

90. G.C. Farrington and J.L. Briant, Mat. Res. Bull. 13 (1978) 763.

91. T. Takahashi, in Superionic Conductors, eds. G.D. Mahan and W.L. Roth (Plenum Press, New York, 1976), p.379.

92. O. Nakamura, T. Kodama, I. Ogino and Y. Miyake, Jap. Patent 76/106, 683 (1976).

93. O. Yamamoto, Y. Takeda, R. Kanno, and K. Tone, in Materials for Solid State Batteries, eds. B.V.R. Chowdari and S. Radhakrishna (World Scientific, Singapore, 1986), p.475.

94. K. Kuwabara, S. Ichikawa, and K. Sugiyama, Bull. Chem. Soc. Jpn. 60 (1987) 747.

95. R.C.T. Slade, J. Barker, and T.K. Halstead, Solid State Ionics 24 (1987) 147.

96. A.T. Howe, S.H. Shefffield, P.E. Childs and M.G. Shilton, Thin Solid Films 67 (1980) 365.

97. T. Takahashi, S. Tanase, and O. Yamamoto, J. Appl. Electrochem. 10 (1980) 415.

98. S.K. Mohapatra, G.D. Boyd, F.G. Storz, S. Wagner, and F. Wudl, J. Electrochem. Soc. 126 (1979) 805.

99. J.P. Randin, J. Electron. Mat. 7 (1978) 47.

100. B. Tell and S. Wagner, Appl. Phys. Lett. 33 (1978) 847; B. Tell, J. Electrochem. Soc. 127 (1980)2451.

101. N. Matsudaira, K. Fukuyoshi, Y. Yorimoto, Y. Ikeda, and K. Yoshida, Proc. 3rd Int. Display Res. Conf., Kobe, Japan (1983), p.54.

102. W.A. England, M.G. Cross, A. Hamnett, P.J. Wiseman, and J.B. Goodenough, Solid State Ionics 1 (1980) 231.

103. P. Barboux, N. Baffier, R. Morineau, and J. Livage, Solid State Ionics 9/10 (1983) 1073.

104. D.Z. Dzimitrovicz, J.B. Goodenough, and P.J. Wiseman, Mat. Res. Bull. 17 (1982) 971.

105. R.A. Huggins, Electrochem. Acta 22 (1977) 773.

106. T. Oi and K. Miyauchi, Mat. Res. Bull. 16 (1981) 1281.

107. T. Oi, Mat. Res. Bull. 19 (1984) 451.

108. C.R. Schlaikjer and C.C. Liang, in Fast Ion Transport in Solids, ed. W. van Gool (North Holland, Amsterdam, 1973), p.685.

109. C.C. Liang, in Fast Ion Transport in Solids, ed. W. van Gool (North Holland, Amsterdam, 1973), p.19.

110. T. Oi, Mat. Res. Bull 19 (1984) 1077.

111. I.D. Raistrick, C. Ho, and R.A. Huggins, Mat. Res. Bull. 11 (1976) 953.

112. G. Seward, R.B. Goldner, K. Wong, T. Haas, G.H. Foley, R. Chapman and S. Schulz, Proc. SPIE 829 (1987) 90.

113. J.H. Kennedy, in Solid Electrolytes, ed. S. Geller (Springer-Verlag, NY, 1977), p.105.

114. W.L. Roth and G.C. Farrington, Science 196 (1977) 1332.

115. K. Miyauchi, K. Matsumoto, K. Kanehori, and T. Kudo, Solid State Ionics 9/10 Pt II (1983) 1469.

116. M. Miyamura, S. Tomura, A. Imai, and S. Inomata, Solid State Ionics 3/4 (1981) 149.

117. T. Yoshimura, M. Watanabe, Y. Koike, K. Kiyota and M. Tanaka, Jpn. J. Appl. Phys. 42 (1983) 157.

118. T. Yoshimura, M. Watanabe, Y. Koike, K. Kiyota, and M. Tanaka, Jpn. J. Appl. Phys. 22 (1983) 152.

119. T. Oi, K. Miyauchi and K. Uchera, J. Appl. Phys. 53 (1982) 1823.

120. K. Uchara, T. Oi, and T. Kudo, Abstr. 44th Jpn. Appl. Phys. Meet.(1983).

121. T. Oi, Mat. Res. Bull. 19 (1984) 1343.

122. Y. Ito, K. Miyauchi, and T. Oi, J. Non-Cryst. Solids 57 (1983) 389.

123. A. Levasseur, M. Kbala, P. Hagenmuller, G. Couturier and Y. Danto, Solid State Ionics 9/10, 1439 (1983); A. Levasseur, in Materials for Solid State Batteries, eds. B.V.R. Chowdari and S. Radhakrishna (World Scientific, Singapore, 1986), p.119.

124. M. Miyauchi, K. Matsumoto, K. Kanehori, and T. Kudo, Solid State Ionics 9/10 (1983) 1469.

125. J.P. Boilot, Ph. Colomban, and N. Blanchard, Solid State Ionics 9/10 (1983) 639.

126. J. Singer, W.L. Fielder, H.E. Kautz, and J.S. Fordyca, J. Electrochem. Soc. 123 (1976) 614.

127. G.G. Barna, J. Electron. Mat. 8 (1979) 153.

128. L. Trichet and J. Rouxel, Mat. Res. Bull. 12 (1977) 345.

129. C. Delmas, C. Fouassier, J.M. Reau, and P. Hagenmuller, Mat. Res. Bull. 11 (1976) 1081.

130. M. Green and K. Kang, Solid State Ionics 8 (1983) 281.

131. K. Kang and M. Green, Thin Solid Films 113 (1984) 629.

132. M. Green, and K. Kang, Thin Solid Films 40 (1977) L19.

133. M. Green and D. Richman, Thin Solid Films 24 (1974) 545.

134. B.B. Owens, in Advances in Electrochemistry and Electrochemical Engineering, Vol. 8, ed. C.W. Tobias (John Wiley, New York, 1971), p.1.

135. T. Takahashi, S. Ikeda, and O. Yamamoto, J. Electrochem. Soc. 119 (1972) 477.

136. T. Takahashi, S. Ikeda, and O. Yamamoto, J. Electrochem. Soc. 120 (1973) 647.

137. K. Shahi and S. Chandra, Phys. Stat. Solidi (a) 28 (1975) 653.

138. J.M. Reau and J. Grannec, in Inorganic Solid Fluorides (Academic Press, N. Y., 1985).

139. J.M. Reau, S. Matar, S. Kacim, J.C. Champarnaud-Mesjard, and B. Frit, Solid State Ionics 7 (1982) 165.

140. P. Darbon, J.M. Reau, and P. Hagenmuller, Mat. Res. Bull. 16 (1981) 273.

141. P. Darbon, J.M. Reau, P. Hagenmuller, C. Depierrefixe, J.P. Laval, and B. Frit, Mat. Res. Bull. 16 (1981) 389.

142. S.F. Matar, J.M. Reau, C. Lucat, J. Grannec, and P. Hagenmuller, Mat. Res. Bull. 15 (1980) 1295.

143. J.M. Reau, C. Lucat, J. Portier, P. Hagenmuller, L. Cot and S. Vilminot, Mat. Res. Bull. 137 (1978) 877.

144. M.W. Shafer, G.V. Chandrashekhar, and R.A. Figat, Solid State Ionics 5 (1981) 633.

145. S. Vilminot, G. Perez, W. Granier, and L. Cot, Rev. Chim. Miner. 17 (1980) 397.

146. D. Avignant, I. Mansouri, and J.C. Cousseins, C.R. Hebd. Seances Acad. Sci., Ser. C 291 (1980) 203.

147. C.E. Rice and P.M. Bridenbaugh, Appl. Phys. Lett. 38 (1981) 59.

148. P. Dzwonskowski, C. Julien and M. Balanski, Appl. Surface Science 33/34 (1988) 838.